UNIVERSITY OF CALIFORNIA
RIVERSIDE

Thermal and Electrical Performance Control and Lifespan Progression of Graphene-based Polymer Composites

A Dissertation submitted in partial satisfaction
of the requirements for the degree of

Doctor of Philosophy

in

Materials Science and Engineering

by

Jacob S. Lewis

September 2020

Dissertation Committee:
Dr. Alexander Balandin, Chairperson
Dr. Fariborz Kargar
Dr. Alexander Khitun

The Dissertation of Jacob S. Lewis is approved:

_____

_____

_____

Committee Chairperson

University of California, Riverside

Acknowledgments

I would like to thank my advisor Dr. Alexander Balandin. Throughout my time in his lab he has shown flexibility, particularly evident in his quick appreciation for the unique ideas I occasionally had of solving a particular problem. He cultivates an environment that embraces different perspectives and the end result is a distinctively productive research group. His vision in research often borders on prescience, guided by his deep understanding and consideration of all relevant underlying physical phenomena. My affiliation with his lab even provided the opportunity for a funded stay in Germany in 2018. Similarly, I am grateful to Dr. Fariborz Kargar who often provided close and time-consuming assistance in my research. I can personally attest to his experience reading an endless manuscript. I want to thank every NDL/POEM member I have met. Each have contributed to my work and personal enrichment in their own way. Every one of them had to endure my humor. Individuals who were *particularly* important to my education include Dr. Ruben Salgado who helped integrate me into the lab, Timothy Perrier, Zahra Barani, Dr. Sahar Naghibi, Dr. Tammy Huang, Amirmahdi Mohamadzadeh, and Sriharsha Sudhindra. I would like to thank Dr. Alexander Khitun for serving on my dissertation committee. I am very thankful for the Graduate Assistance in Areas of National Need (GAANN) fellowship for supporting my studies.

My family has remained a continual source of support throughout my life and this endeavor. My mother Lori provided an open and understanding upbringing that didn't stifle my curiosity. I want to thank my two sisters, McKenzie and Erin, who provided an important influence on the direction of my life. My good friends Chad and Kyle played similar roles in my study and life at large and are appreci-

ated. My nephew Desmond never failed to put a smile on my face no matter the circumstances.

Parts of this dissertation are concerned with topics presented in or reprinted from the following journal and pre-print articles:

J. S. Lewis, Z. Barani, A. S. Magana, F. Kargar, and A. A. Balandin, "Thermal and electrical conductivity control in hybrid composites with graphene and boron nitride fillers" *Materials Research Express*, vol. 6, no. 8, p. 085325, May 2019.

J. S. Lewis, T. Perrier, A. Mohammadzadeh, F. Kargar, and A. A. Balandin, "Power cycling and reliability testing of epoxy-based graphene thermal interface materials," *C — Journal of Carbon Research*, vol. 6, no. 2, 2020.

J. S. Lewis, T. Perrier, Z. Barani, F. Kargar, and A. A. Balandin, "Review of graphene-based thermal polymer nanocomposites: Current state of the art and future prospects," 2020. [Online]. Available: https://arxiv.org/abs/2008.10752.

Aut inveniam viam aut faciam

ABSTRACT OF THE DISSERTATION

Thermal and Electrical Performance Control and Lifespan Progression of Graphene-based Polymer Composites

by

Jacob S. Lewis

Doctor of Philosophy, Graduate Program in Materials Science and Engineering
University of California, Riverside, September 2020
Dr. Alexander Balandin, Chairperson

Power dissipation rates of modern semiconductor devices continually increases year after year. Despite this, safe operating temperatures of these devices remain moderately low, typically below 90 °C, after which point devices performance deviates from design and lifespan significantly diminishes. As a result, ever-increasing thermal dissipation capacity is required to achieve acceptable operating temperature. Polymer composites are often applied between two imperfect surfaces to replace air gaps and act as a better thermal bridge to facilitate heat flow between solids or as chip encapsulants to protect from environmental contamination. In each application, the overall thermal dissipation, and thus operating temperature, can be improved by using more thermally conductive polymers. The thermal conductivity of most polymers, certainly all of those in common general use in industry are quite low, below 0.3 W/mK. It is a common tactic to composite the polymers with other, highly thermally conductive materials to then raise the overall composite thermal conductivity. The extraordinary thermal conductivity of graphene has prompted significant study into composites composed of it for these applications. However, since graphene is also electrically conductive, composites

filled to a sufficient level exhibit substantial electrical conductivity, which can be problematic in the electronics industry. The composite may make immediate contact or over the course of a realistic lifespan may make unavoidable, inadvertent contact with active circuit elements resulting from migration phenomena, which may threaten circuit stability depending on the composite's electrical conductivity. This dissertation research developed a methodology for the independent control of thermal and electrical conductivity of graphene composites through hybridization by finely controlling filler levels of graphene and electrically insulating hexagonal boron nitride. Additionally, the lifespan performance of graphene polymer composites was studied in a custom-built accelerated aging instrument which revealed an unexpected enhancement of thermal conductivity in up to 500 power cycling treatments. The improved performance was attributed to an increased coupling between graphene and epoxy polymer resultant from increased cross-linking density, resulting in more firm contact and lower Kapitza resistance. The obtained results are important for future thermal management technologies that leverage the unique heat conduction properties of graphene.

Contents

List of Figures

List of Tables

Chapter 1

Introduction

The development of the solid state transistor by Bardeen, Shockley, and Brattain in 1947 revolutionized the world in ways that they almost assuredly could have not imagined [1]. For instance, in the 2nd quarter of 2020 the seven largest companies in the world by market capitalization were enterprises that either primarily develop software or operate a primarily Internet-based service or commerce infrastructure. None of these companies could exist without powerful re-programmable computing driven by . The development of this device soon sparked an unprecedentedly rapid and consistent progression of transistor surface densification that resulted in a doubling of the number of transistors in semiconductor chips in two years' time, as famously observed by Gordon Moore, that has been the central contributor to technological progress of the past half century. This incredible surface densification is driven by the miniaturization of all circuit components, principally the transistors themselves. Though the miniaturization improves individual transistor's efficiency, the gains in efficiency do not in general offset the circuit's implementation of a greater number of total transistors, resulting in an ever-increasing thermal design power for high-performance computing chips. Very Large Scale Integration (VLSI) devices suffer from unintended behavior alterations

at high temperature caused by factors such as hot carrier degradation and bias temperature instability [2–4]. Semiconductor devices also experience a reduced lifespan resultant from continual use at high operating temperatures. High power GaN amplifiers' duration of lifespan is strongly by the temperatures at which it operates [5].

The scale of VLSI waste heat is monumental and often not fully intuitively grasped even by researchers in the field. Figure 1.1 shows VLSI products' average and "hot spot" heat density with other well-known objects and devices for comparison [6–8]. The low operating temperature of VLSI products relative to the other considered objects shows how phenomenally these devices' heat sink solutions perform. The fact that the planet Mercury receives a bit over 1/100 of the power density from the sun that a modern central processing unit produces but has a daytime temperature roughly six times that of the latter's operating temperature shows the order-of-magnitude superiority of its engineered dissipation solution to the former's radiative cooling.

It is a common practice in industry to place a heat-producing component in contact with an element whose sole purpose is to exchange the developed heat with the environment, cooling down the heat-producing component in the process [9]. For larger machinery, this heat exchanging element is often a radiator that places a fluid in close contact with a heat-producing component such as an internal combustion engine where it will absorb some of the generated heat and then it is moved to a thin, hollow mesh structure so passing air can quickly cool the heated fluid, which will finally return to the heat-producing component forming a heat-exchanging loop. Though this system is very effective at removing large sums of generated heat, they are in general bulky, complex, and expensive solutions that require substantial chassis volume and very large total energies to justify

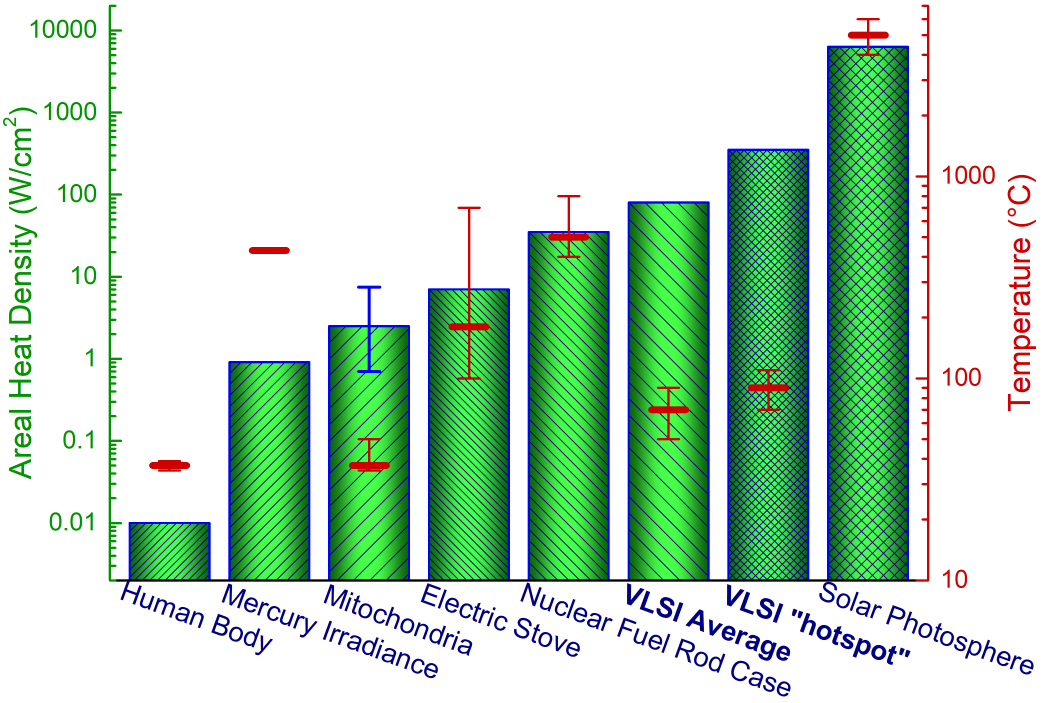

Figure 1.1: Areal heat density of enclosing surfaces and planar surfaces of different objects and devices with their corresponding temperatures. The ratio of the areal heat density to the operating temperature gives an idea as to the relative ability of each object to shed heat. VLSI devices' high heat density and relatively low operating temperature show the quality of the heat sink solution used.

implementation. This fact renders radiator-style heat solutions impractical for most semiconductor-reliant products, though solutions of this type are employed by enthusiasts.

Most devices with a central processing unit or similar VLSI chips are cooled via an intimate contact with a metallic heat sink, allowing the direct conduction of heat between the two surfaces then diffusion throughout. Additionally, depending on various factors chiefly being the thermal design power of the chip, there is often a fan to force a flow of air through the heat sink's designed fins, known as active cooling. This method of waste-heat removal is both easier to apply on a smaller scale and is a much simpler system than those involving radiators. However, due to

limitations in polishing at the solid surface interfaces, the total fraction of the two surfaces that make direct contact with one another is negligible [10]. This results in the presence of a catastrophically disadvantageous thermal insulation between any two solid surfaces caused by trapped air. It has long been the primary strategy of industry to alleviate this problem by introducing a typically viscous liquid between the two mated surfaces to take the place of air in the inevitable gaps between surfaces. Though these liquids often are much less thermally conductive than the metals of either opposing surface, they are dramatically more conductive than the interstitial air that it replaces, greatly reducing the overall thermal resistance from the heat generator to drain. These materials are often referred to as non-curing Thermal Interface Materials (TIMs).

Figure 1.2 (top) shows an interface of two solid surfaces with air gaps between the surface protrusions making contact. Because a very small portion of the two surfaces are making contact, the total heat flow between the heat-producing surface and heat-diffusing surface is quite low, resulting in a large temperature difference between the two materials. In Figure 1.2 (below), a junction with a TIM applied replaces the air gaps with substantially more thermally conductive material [9]. Doing this decreases the corresponding temperature difference between the surfaces, qualitatively represented by closer colors, as one would expect for a decrease in thermal resistance.

Though the surface thermal contact resistance is lowered through the inclusion of TIMs, there remains great room for progress in these materials because they typically have thermal conductivities of 0.5 to 7.0 W/mK, while the materials at either side of the junction are often as high as 400 W/mK [11, 12]. The ultimate goal of TIMs is to achieve a nearly nonexistent thermal interface resistance between any two solid surfaces. The expression for thermal interface resistance is below:

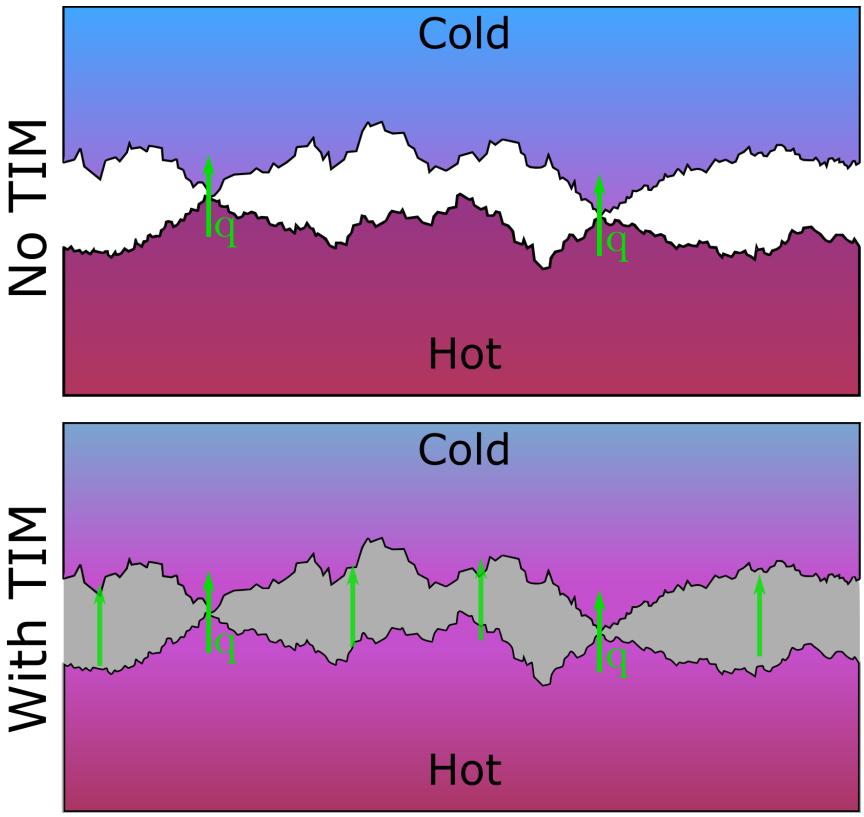

Figure 1.2: Schematic showing a thermal interface without paste (top) and a thermal interface with TIM with a resultant increase of heat flow between hot and cold surfaces, with a closer color profile to illustrate better thermal coupling between the two surfaces (bottom).

$$R_{th} = \frac{BLT}{K} + R_{C1} + R_{C2} \tag{1.1}$$

Where BLT is known as the Bond Line Thickness and is the average thickness of the TIM layer, K is the thermal conductivity of the TIM material, R_{C1} is the contact resistance between the TIM and a surface of interest, and finally R_{C2} is the contact resistance of the other surface and TIM. Due to TIM materials' effectiveness of conforming well to imperfect surfaces outpaces its intrinsic thermal conductivity performance at most applicable thicknesses, the majority of the thermal resistance at the surface mating comes from the quotient of the BLT and the thermal conductivity of the TIM.

It is a very common strategy to decrease the overall thermal interface resistance by focusing on increasing the thermal conductivity of TIMs. Frequently, researchers pursue this by filling base polymers with highly conductive fillers such as copper particles, colloidal silver, carbon nanotubes, few-layer graphene, Boron Nitride, Al_2O_3, microscopic diamonds, and many others in order to improve the overall thermal performance of the polymeric composite [13–24]. Each type of filler endows the composite composed of it with alterations in the eminently salient parameters of thermal and electrical conductivity, heat capacity, coefficient of thermal expansion, and viscosity. Not only is the intrinsic material parameters of both polymer matrix and filler of importance, but the morphology of the fillers can substantially alter the way it interacts within the matrix.

In much the same manner of non-curing TIMs, there is great interest in curing TIMs that has many similar challenges and property considerations. Thermosetting plastics are often used in the encapsulation of chips in an integrated circuit to protect it from environmental contaminants such as moisture and dust. Some such chips encapsulated in this manner are high power and thus high heat-producing, making improvements to the thermal conductivity of encapsulating material desirable to decrease the operating temperature for a given rate of heat production [25]. Figure 1.3a shows a typical dual in-line package with a poorly thermally conductive encapsulant restricting radiative and convective heat flow from its surface due to the fact that heat struggles to permeate the polymer. In contrast, Figure 1.3b shows the same package with a more thermally conductive polymer that allows better heat penetration and a broader region of elevated temperature and greater maximum temperature reached. Due to the fact that these encapsulating TIMs make direct contact with active circuit components, it is often crucial that TIMs in this application remain electrically insulating. This, however, can prove

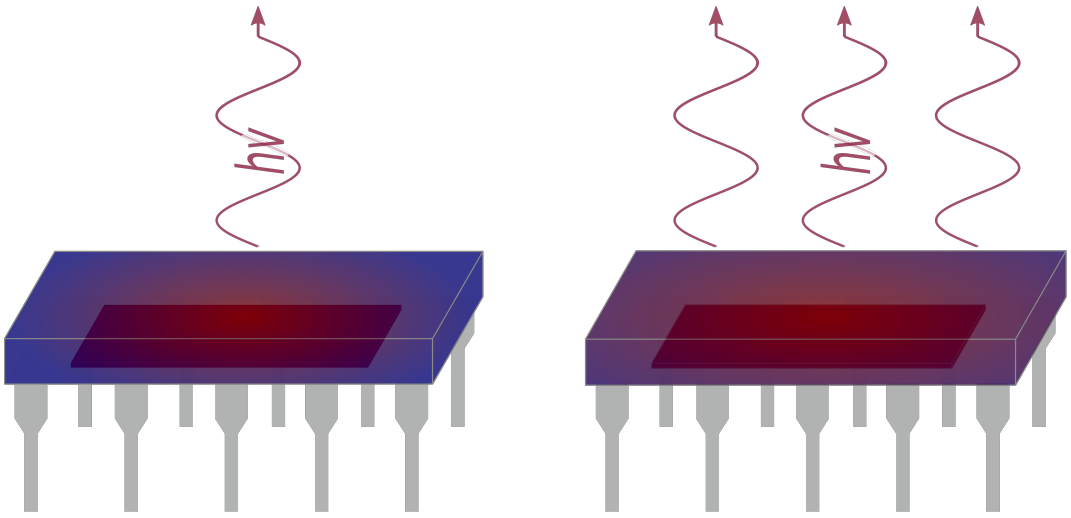

Figure 1.3: a) Dual in-line package a low thermal conductivity encapsulating polymer that does not spread heat well within itself, resulting in hotter chip operating temperatures. b) The same package with relatively higher thermal conductivity polymer that easier spreads heat to the edges and then into the environment by convection, radiation, and conduction through device electrical leads. High heat devices of this type are also often accompanied by a heat sink.

challenging because the majority of the high-performing filler materials are also electrically conductive. Curing TIMs are also frequently studied as an analog for non-curing TIMs due to its relative ease of study and comparability.

To date, TIM composites prepared with mixtures of single-layer and few-layer graphene have proven to be the most effective in curing polymer matrix-based TIMs, primarily due to the extraordinarily high intrinsic thermal conductivity of graphene [26–30]. Works on these composite materials have demonstrated thermal conductivities up to ≈12 W/mK, compared to up to 5 W/mK for commercial TIMs at very high load levels of up to 80 *vol. %* [31]. Furthermore, this performance has proven to be stable, even with a report of improved performance, over the course of a realistic composite lifespan [32].

There has been considerable research into TIMs of multiple filler materials [19,23,33–48]. Figure 1.4 shows common strategies for using multiple fillers to form

a hybrid composite as well as the approach employed in the present dissertation research [42, 49–51]. In the case of thermal conductivity, pairing a larger and smaller filler particle can result in an enhancement in thermal conductivity that is greater than just using the same fraction of either individual particle size. This fact can be explained by increases of packing density and the ability of the smaller particles to fit between the larger particles, both of which can lead to less large-filler agglomeration, offering another mechanism of composite enhancement. Indeed, in ideal circumstances the smaller particle may make direct contact between two large fillers, thus creating a microscopic percolation region. If this microscopic percolation region occurs inside of the polymer composite with a great enough density, large pathways of low thermal resistance forms and the overall thermal conductivity of the composite rises precipitously, the point at which the composite is said to have reached the percolation threshold [30].

It was hypothesized that switching to fillers of comparable form factors and varying the constituent concentrations of each filler in a composite would allow for fine-tuning the electrical conductivity of the composites [52]. Previous works focused on achieving thermal but not electrical percolation in graphene and *h*-BN hybrid composites either did not report the geometries of all fillers used or did use dramatically disparate filler sizes and reported the extraordinary and immediate inhibition of electrical conductivity [53, 54]. Because the *h*-BN geometry was spheres of approximately 120 nanometers in diameter, the particle size is well below the phonon mean free path, significantly hindering the thermal conductivity contribution of this primary heat carrier of *h*-BN [55]. If larger *h*-BN particles were used, one could still control the electrical conductivity of the composites, perhaps with even greater control, and reach a higher maximum thermal conductivity enhancement due to the lack of *h*-BN phonon inhibition that should be present in

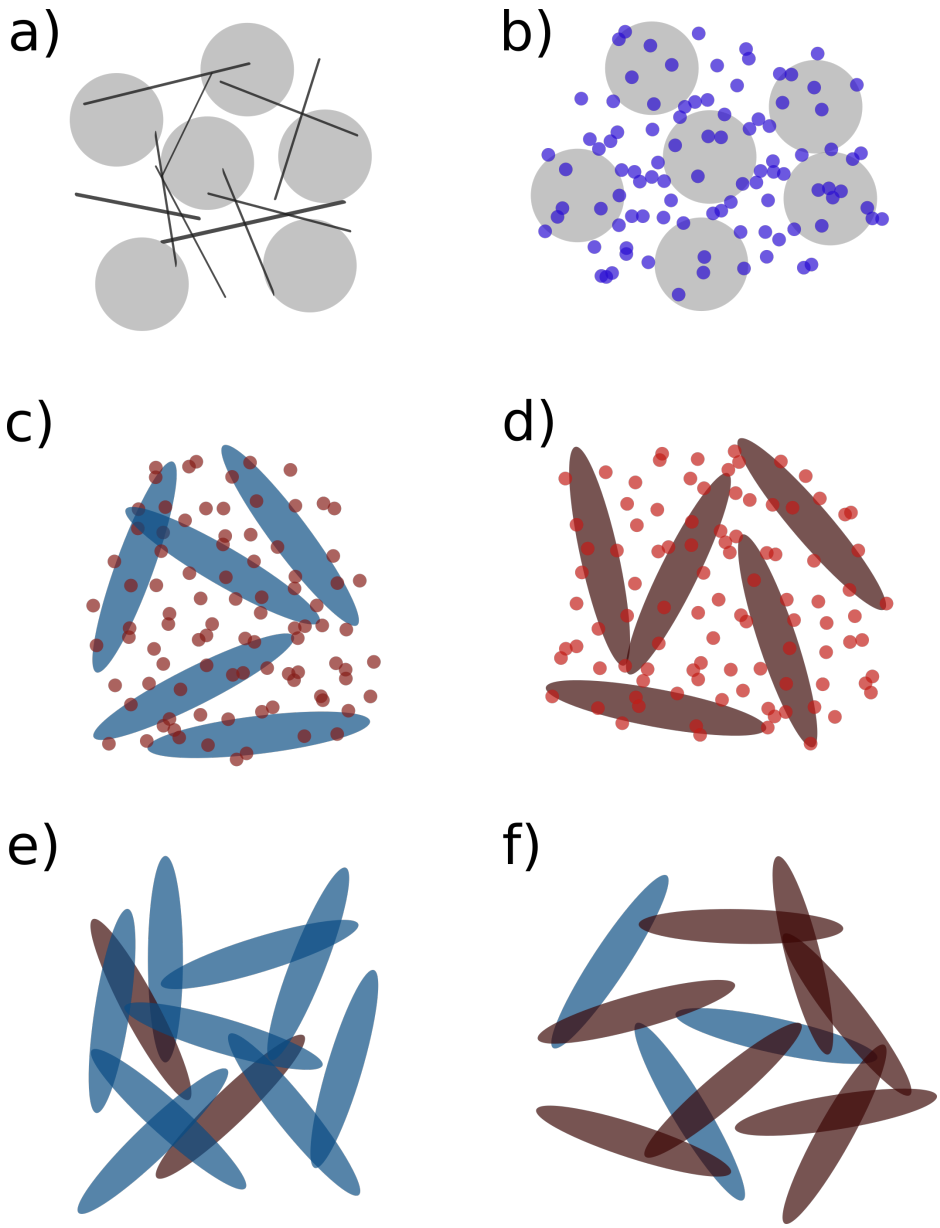

Figure 1.4: Schematic figure of common binary (hybrid) composite filler strategies. a) quasi 1-D materials and another spherical filler b) different-sized spherical fillers. c) quasi-2D flake geometry filler and a much smaller spherical filler of a dissimilar material d) quasi-2D flake geometry filler and a much smaller spherical filler the same material e) hybrid composite of focus in this dissertation, with majority graphene and minority *h*-BN of comparable geometry. f) similar to panel e, with majority *h*-BN and minority graphene. Reprinted with permission from the publication J. S. Lewis, Z. Barani, A. S. Magana, F. Kargar, and A. A. Balandin, "Thermal and electrical conductivity control in hybrid composites with graphene and boron nitride fillers" *Materials Research Express*, vol. 6, no. 8, p. 085325, May 2019. Copyright © Institute of Physics.

prior works.

1.1 Basics of Crystalline Thermal Transport

Crystalline materials conduct heat primarily through the passage of atomic lattice vibrations – phonons – and electrons, the sum of whose contributions to thermal conductivity equals the material's total thermal conductivity; that is $K_T = K_e + K_p$, where K_T is the total thermal conductivity while K_e and K_p correspond to the electron and phonon contributions to thermal conductivity, respectively [56]. In metals with many electrons existing in a free electron gas, the electrical contribution to overall thermal conductivity is dominant. In the case of solid elemental copper, as little as 2% of K_T comes from K_p. K_e can be calculated directly from measurement of the electrical conductivity in accordance with the Wiedemann-Franz law:

$$\frac{K_e}{\sigma T} = \frac{\pi^2 k_B^2}{3e^2} \tag{1.2}$$

where σ is the electrical conductivity, T is temperature, k_B is the Boltzmann constant, and e is the fundamental charge [57, 58]. The thermal conductivity contribution of phonons is

$$K_p = \sum_j \int C_j(\omega) v_j^2(\omega) \tau_j(\omega) \mathrm{d}\omega \tag{1.3}$$

where j corresponds to each salient phonon branch, one longitudinal acoustic and two transverse acoustics, v is the phonon group velocity, and τ is the phonon relaxation time, C is the heat capacity, and ω is the frequency, which each branch parameter is a function of [56]. In much the same way that $d = vt$ from classical mechanics, the phonon mean-free path is related to the group velocity and relax-

ation time by $\Lambda = v\tau$. When the dimensions of a crystal grain or nanomaterial is much larger than the mean-free path then the thermal transport is diffusive and phonons have the distance to undergo multiple scattering events prior to reaching the physical boundaries of the material. If in addition, the material is without impurities or other forms of defects, the phonons are scattered entirely by other phonons resultant from anharmonicity – that is cubic and higher order terms in the potential energy of ion core position – leading to a particular crystal's characteristic intrinsic lattice thermal conductivity, limited solely by Umklapp scattering [59]. In this situation, maximal thermal transport for a given material can be achieved. Should the physical dimensions of a material drop below the acoustic phonon mean-free path, its transport is described as ballistic and its ability to transport heat is more strongly inhibited by boundary scattering [56]. Scattering from boundaries serves to increase the phonon scattering rate, $1/\tau_B$, as

$$\frac{1}{\tau_B} = \frac{v(1-p)}{D(1+p)} \tag{1.4}$$

where D is the overall size of the nano-scale material or the grain size and p is the specularity parameter that is a probability between zero and unity of scattering at the boundary. When $p = 1$, that is to say that phonons are always neatly reflected from a surface, the thermal conductivity is not diminished by interactions at the boundary. As the surface is increasingly roughened at the appropriate scale the thermal conductivity is reduced. When $p \to 0$ in intrinsically thermally conductive materials, the lattice thermal conductivity behaves as $K_p = CvD$. Due to the realistic requirements of polymer composite preparation, special care should be given to the lateral dimensions and surface roughness of filler materials whose heat is primarily carried by phonons. A similar mechanism governs K_e for metallic materials, however the electron mean-free path is much smaller on the order of

tens of nanometers and thus boundary scattering is much less of a concern in metallic fillers at currently mass-producible sizes [60].

Bibliography

[1] J. Bardeen and W. H. Brattain, "The transistor, a semi-conductor triode," *Phys. Rev.*, vol. 74, pp. 230–231, July 1948.

[2] A. Guo and J. A. Del Alamo, "Unified mechanism for positive-a nd negative-bias temperature instability in GaN MOSFETs," *IEEE Transactions on Electron Devices*, vol. 64, pp. 2142–2147, May 2017.

[3] Z. Yu, R. Wang, P. Hao, S. Guo, P. Ren, and R. Huang, "Non-universal temperature dependence of hot carrier degradation (HCD) in finFET: New observations and physical understandings," in *2018 IEEE Electron Devices Technology and Manufacturing Conference, EDTM 2018 - Proceedings*, pp. 34–36, Institute of Electrical and Electronics Engineers Inc., July 2018.

[4] E. Bury, A. Chasin, B. Kaczer, K. H. Chuang, J. Franco, M. Simicic, P. Weckx, and D. Linten, "Self-heating-aware CMOS reliability characterization using degradation maps," in *IEEE International Reliability Physics Symposium Proceedings*, vol. 2018-March, pp. 2A.31–2A.36, Institute of Electrical and Electronics Engineers Inc., May 2018.

[5] R. J. Trew, D. S. Green, and J. B. Shealy, "AlGaN/GaN HFET reliability," *IEEE Microwave Magazine*, vol. 10, no. 4, pp. 116–127, 2009.

[6] K. Schwerzmann, L. M. Cruz-Orive, R. Eggman, A. Sänger, and E. R. Weibel, "Molecular architecture of the inner membrane of mitochondria from rat liver: a combined biochemical and stereological study.," *Journal of Cell Biology*, vol. 102, pp. 97–103, Jan. 1986.

[7] D. Chrétien, P. Bénit, H.-H. Ha, S. Keipert, R. El-Khoury, Y.-T. Chang, M. Jastroch, H. T. Jacobs, P. Rustin, and M. Rak, "Mitochondria are physiologically maintained at close to 50 °C," *PLOS Biology*, vol. 16, pp. 1–17, Jan. 2018.

[8] J. Ramirez, M. Stan, and P. Cristea, "Simulations of heat and oxygen diffusion in UO_2 nuclear fuel rods," *Journal of Nuclear Materials*, vol. 359, no. 3, pp. 174 – 184, 2006.

[9] J. S. Lewis, T. Perrier, Z. Barani, F. Kargar, and A. A. Balandin, "Review of graphene-based thermal polymer nanocomposites: Current state of the art and future prospects," 2020. [Online]. Available: https://arxiv.org/abs/2008.10752.

[10] M. Cooper, B. Mikic, and M. Yovanovich, "Thermal contact conductance," *International Journal of Heat and Mass Transfer*, vol. 12, pp. 279–300, Mar. 1969.

[11] J. P. Gwinn and R. L. Webb, "Performance and testing of thermal interface materials," *Microelectronics Journal*, vol. 34, pp. 215–222, Mar. 2003.

[12] A. Bar-Cohen, K. Matin, and S. Narumanchi, "Nanothermal interface materials: Technology review and recent results," *Journal of Electronic Packaging*, vol. 137, Oct. 2015. 040803.

[13] S. Wang, Y. Cheng, R. Wang, J. Sun, and L. Gao, "Highly thermal conductive copper nanowire composites with ultralow loading: Toward applications as thermal interface materials," *ACS Applied Materials & Interfaces*, vol. 6, pp. 6481–6486, May 2014.

[14] J. Xu, A. Munari, E. Dalton, A. Mathewson, and K. M. Razeeb, "Silver nanowire array-polymer composite as thermal interface material," *Journal of Applied Physics*, vol. 106, p. 124310, Dec. 2009.

[15] J. Zeng, Z. Cao, D. Yang, L. Sun, and L. Zhang, "Thermal conductivity enhancement of ag nanowires on an organic phase change material," *Journal of Thermal Analysis and Calorimetry*, vol. 101, no. 1, pp. 385 – 389, 2009.

[16] H. Huang, C. H. Liu, Y. Wu, and S. Fan, "Aligned carbon nanotube composite films for thermal management," *Advanced Materials*, vol. 17, pp. 1652–1656, July 2005.

[17] A. M. Marconnet, N. Yamamoto, M. A. Panzer, B. L. Wardle, and K. E. Goodson, "Thermal conduction in aligned carbon nanotube–polymer nanocomposites with high packing density," *ACS Nano*, vol. 5, pp. 4818–4825, June 2011.

[18] K. M. F. Shahil and A. A. Balandin, "Graphene–multilayer graphene nanocomposites as highly efficient thermal interface materials," *Nano Letters*, vol. 12, pp. 861–867, Feb. 2012.

[19] J. R. Potts, D. R. Dreyer, C. W. Bielawski, and R. S. Ruoff, "Graphene-based polymer nanocomposites," *Polymer*, vol. 52, pp. 5–25, Jan. 2011.

[20] M.-T. Hung, O. Choi, Y. S. Ju, and H. T. Hahn, "Heat conduction in graphite-nanoplatelet-reinforced polymer nanocomposites," *Applied Physics Letters*, vol. 89, p. 023117, July 2006.

[21] C. Zhi, Y. Bando, T. Terao, C. Tang, H. Kuwahara, and D. Golberg, "Towards thermoconductive, electrically insulating polymeric composites with boron nitride nanotubes as fillers," *Advanced Functional Materials*, vol. 19, pp. 1857–1862, June 2009.

[22] Z. Lin, A. Mcnamara, Y. Liu, K.-s. Moon, and C.-P. Wong, "Exfoliated hexagonal boron nitride-based polymer nanocomposite with enhanced thermal conductivity for electronic encapsulation," *Composites Science and Technology*, vol. 90, pp. 123–128, Jan. 2014.

[23] L. Sim, S. Ramanan, H. Ismail, K. Seetharamu, and T. Goh, "Thermal characterization of Al_2O_3 and ZnO reinforced silicone rubber as thermal pads for heat dissipation purposes," *Thermochimica Acta*, vol. 430, pp. 155–165, June 2005.

[24] Y. Yao, X. Zeng, K. Guo, R. Sun, and J.-b. Xu, "The effect of interfacial state on the thermal conductivity of functionalized Al_2O_3 filled glass fibers reinforced polymer composites," *Composites Part A: Applied Science and Manufacturing*, vol. 69, pp. 49–55, Feb. 2015.

[25] Y. Zhao, T. Semenic, and A. Bhunia, "Advanced packaging and thermal management for high power density gan devices," in *2013 IEEE Compound Semiconductor Integrated Circuit Symposium (CSICS)*, pp. 1–4, 2013.

[26] A. A. Balandin, S. Ghosh, W. Bao, I. Calizo, D. Teweldebrhan, F. Miao, and C. N. Lau, "Superior thermal conductivity of single-layer graphene," *Nano Letters*, vol. 8, pp. 902–907, Mar. 2008.

[27] S. Ghosh, I. Calizo, D. Teweldebrhan, E. P. Pokatilov, D. L. Nika, A. A. Balandin, W. Bao, F. Miao, and C. N. Lau, "Extremely high thermal conductivity of graphene: Prospects for thermal management applications in nanoelectronic circuits," *Applied Physics Letters*, vol. 92, p. 151911, Apr. 2008.

[28] J. H. Seol, I. Jo, A. L. Moore, L. Lindsay, Z. H. Aitken, M. T. Pettes, X. Li, Z. Yao, R. Huang, D. Broido, N. Mingo, R. S. Ruoff, and L. Shi, "Two-dimensional phonon transport in supported graphene," *Science*, vol. 328, no. 5975, pp. 213–216, 2010.

[29] W. Cai, A. L. Moore, Y. Zhu, X. Li, S. Chen, L. Shi, and R. S. Ruoff, "Thermal transport in suspended and supported monolayer graphene grown by chemical vapor deposition," *Nano Letters*, vol. 10, pp. 1645–1651, May 2010.

[30] F. Kargar, Z. Barani, R. Salgado, B. Debnath, J. S. Lewis, E. Aytan, R. K. Lake, and A. A. Balandin, "Thermal percolation threshold and thermal properties of composites with high loading of graphene and boron nitride fillers," *ACS Applied Materials & Interfaces*, vol. 10, pp. 37555–37565, Oct. 2018.

[31] S. Naghibi, F. Kargar, D. Wright, C. Y. T. Huang, A. Mohammadzadeh, Z. Barani, R. Salgado, and A. A. Balandin, "Noncuring graphene thermal

interface materials for advanced electronics," *Advanced Electronic Materials*, p. 1901303, 2020.

[32] J. S. Lewis, T. Perrier, A. Mohammadzadeh, F. Kargar, and A. A. Balandin, "Power cycling and reliability testing of epoxy-based graphene thermal interface materials," *C — Journal of Carbon Research*, vol. 6, no. 2, 2020.

[33] Q. Wang, W. Gao, and Z. Xie, "Highly thermally conductive room-temperature-vulcanized silicone rubber and silicone grease," *Journal of Applied Polymer Science*, vol. 89, no. 9, pp. 2397–2399, 2003.

[34] G.-W. Lee, M. Park, J. Kim, J. I. Lee, and H. G. Yoon, "Enhanced thermal conductivity of polymer composites filled with hybrid filler," *Composites Part A: Applied Science and Manufacturing*, vol. 37, pp. 727–734, May 2006.

[35] A. Yu, P. Ramesh, X. Sun, E. Bekyarova, M. E. Itkis, and R. C. Haddon, "Enhanced thermal conductivity in a hybrid graphite nanoplatelet - carbon nanotube filler for epoxy composites," *Advanced Materials*, vol. 20, pp. 4740–4744, Dec. 2008.

[36] S. Kemaloglu, G. Ozkoc, and A. Aytac, "Properties of thermally conductive micro and nano size boron nitride reinforced silicon rubber composites," *Thermochimica Acta*, vol. 499, pp. 40–47, Feb. 2010.

[37] T.-L. Li and S. L.-C. Hsu, "Enhanced thermal conductivity of polyimide films via a hybrid of micro- and nano-sized boron nitride," *The Journal of Physical Chemistry B*, vol. 114, pp. 6825–6829, May 2010.

[38] K. Yang and M. Gu, "Enhanced thermal conductivity of epoxy nanocomposites filled with hybrid filler system of triethylenetetramine-functionalized multi-walled carbon nanotube/silane-modified nano-sized silicon carbide," *Composites Part A: Applied Science and Manufacturing*, vol. 41, pp. 215–221, Feb. 2010.

[39] T. Zhou, X. Wang, X. Liu, and D. Xiong, "Improved thermal conductivity of epoxy composites using a hybrid multi-walled carbon nanotube/micro-SiC filler," *Carbon*, vol. 48, pp. 1171–1176, Apr. 2010.

[40] S. Y. Pak, H. M. Kim, S. Y. Kim, and J. R. Youn, "Synergistic improvement of thermal conductivity of thermoplastic composites with mixed boron nitride and multi-walled carbon nanotube fillers," *Carbon*, vol. 50, pp. 4830–4838, Nov. 2012.

[41] C.-C. Teng, C.-C. M. Ma, K.-C. Chiou, and T.-M. Lee, "Synergetic effect of thermal conductive properties of epoxy composites containing functionalized multi-walled carbon nanotubes and aluminum nitride," *Composites Part B: Engineering*, vol. 43, pp. 265–271, Mar. 2012.

[42] S. Choi and J. Kim, "Thermal conductivity of epoxy composites with a binary-particle system of aluminum oxide and aluminum nitride fillers," *Composites Part B: Engineering*, vol. 51, pp. 140–147, Aug. 2013.

[43] M.-H. Tsai, I.-H. Tseng, J.-C. Chiang, and J.-J. Li, "Flexible polyimide films hybrid with functionalized boron nitride and graphene oxide simultaneously to improve thermal conduction and dimensional stability," *ACS Applied Materials & Interfaces*, vol. 6, pp. 8639–8645, June 2014.

[44] L. Shao, L. Shi, X. Li, N. Song, and P. Ding, "Synergistic effect of BN and graphene nanosheets in 3D framework on the enhancement of thermal conductive properties of polymeric composites," *Composites Science and Technology*, vol. 135, pp. 83–91, Oct. 2016.

[45] Y.-K. Kim, J.-Y. Chung, J.-G. Lee, Y.-K. Baek, and P.-W. Shin, "Synergistic effect of spherical Al_2O_3 particles and BN nanoplates on the thermal transport properties of polymer composites," *Composites Part A: Applied Science and Manufacturing*, vol. 98, pp. 184–191, July 2017.

[46] C. Liu, M. Chen, D. Zhou, D. Wu, and W. Yu, "Effect of filler shape on the thermal conductivity of thermal functional composites," *Journal of Nanomaterials*, vol. 2017, 2017.

[47] S. Ramirez, K. Chan, R. Hernandez, E. Recinos, E. Hernandez, R. Salgado, A. Khitun, J. Garay, and A. Balandin, "Thermal and magnetic properties of nanostructured densified ferrimagnetic composites with graphene - graphite fillers," *Materials & Design*, vol. 118, pp. 75–80, Mar. 2017.

[48] Z.-G. Wang, F. Gong, W.-C. Yu, Y.-F. Huang, L. Zhu, J. Lei, J.-Z. Xu, and Z.-M. Li, "Synergetic enhancement of thermal conductivity by constructing hybrid conductive network in the segregated polymer composites," *Composites Science and Technology*, vol. 162, pp. 7–13, July 2018.

[49] K.-Y. Chun, Y. Oh, J. Rho, J.-H. Ahn, Y.-J. Kim, H. R. Choi, and S. Baik, "Highly conductive, printable and stretchable composite films of carbon nanotubes and silver," *Nature Nanotechnology*, vol. 5, pp. 853–857, Dec. 2010.

[50] D. Wang, T. Zhou, J.-W. Zha, J. Zhao, C.-Y. Shi, and Z.-M. Dang, "Functionalized graphene–$BaTiO_3$/ferroelectric polymer nanodielectric composites with high permittivity, low dielectric loss, and low percolation threshold," *Journal of Materials Chemistry A*, vol. 1, p. 6162, Apr. 2013.

[51] M. Shtein, R. Nadiv, M. Buzaglo, and O. Regev, "Graphene-based hybrid composites for efficient thermal management of electronic devices," *ACS Applied Materials & Interfaces*, vol. 7, pp. 23725–23730, Oct. 2015.

[52] J. S. Lewis, Z. Barani, A. S. Magana, F. Kargar, and A. A. Balandin, "Thermal and electrical conductivity control in hybrid composites with graphene and boron nitride fillers," *Materials Research Express*, vol. 6, p. 085325, May 2019.

[53] M. Shtein, R. Nadiv, M. Buzaglo, K. Kahil, and O. Regev, "Thermally conductive graphene-polymer composites: Size, percolation, and synergy effects," *Chemistry of Materials*, 2015.

[54] H. Chen, C. Zhao, S. Xu, and X. Yang, "Preparation and properties study of thermally conductive epoxy/modified boron nitride/graphene nanosheets composites," *IOP Conference Series: Materials Science and Engineering*, vol. 274, p. 012043, Dec. 2017.

[55] H. Gholivand and N. Donmezer, "Phonon mean free path in few layer graphene, hexagonal boron nitride, and composite bilayer h-BN/graphene," *IEEE Transactions on Nanotechnology*, vol. 16, pp. 752–758, Sept. 2017.

[56] A. A. Balandin, "Thermal properties of graphene and nanostructured carbon materials," *Nature Materials*, vol. 10, pp. 569–581, Aug. 2011.

[57] G. Wiedemann and R. Franz, "Ueber die wärme-leitungsfähigkeit der metalle," *Annalen der Physik*, vol. 165, no. 8, pp. 497–531, 1853.

[58] P. L. Bayley, "The electron theory of metallic conduction," Master's thesis, University of Arkansas, 1914.

[59] P. Klemens, "Thermal conductivity and lattice vibrational modes," in *Solid State Physics* (F. Seitz and D. Turnbull, eds.), vol. 7 of *Solid State Physics*, pp. 1 – 98, Academic Press, 1958.

[60] D. Gall, "Electron mean free path in elemental metals," *Journal of Applied Physics*, vol. 119, no. 8, p. 085101, 2016.

Chapter 2

Materials

2.1 Classic Filler Materials

The TIM field employs many different materials and shapes that span orders of magnitude of both intrinsic and realized thermal conductivities. As previously covered, the physical dimensions of the used material can also alter the filler's actualized thermal conductivity through boundary scattering and confinement-mediated changes in the lattice heat capacity resultant from altered phonon density of states [1].

Much research has been conducted into metallic fillers, particularly copper and silver, in a TIM [2–6]. These fillers are moderately to highly thermally conductive – up to ≈400 W/mK, unavoidably highly electrically conductive – above 1,000 S/cm, and it is easy to form different microscopic shapes with. However, working with ever-decreasing sizes of the material increases its surface area and oxidation rate, leading to challenges in the preparation of composites [7]. Figure 2.1a shows the material properties of potential and popular filler materials, while Figure 2.1b shows that which one could expect of resulting composites using those fillers in a random orientation. Table 1 shows many obtained thermal conductivities of

composites that researchers have achieved [8].[1]

Table 2.1: TIM Thermal Conductivity Table. RA, CPA, and IPA correspond to random alignment, cross-plane alignment, and in-plane alignment of fillers, respectively. Fillers that are described as scaffolded were attached to a larger, potentically sacrificed network prior to the introduction to a polymer.

Base Polymer	Filler	Cross-plane TC (W/mK)	Measurement Method	Refs.
	Misc. Fillers			
PDMS	None	0.2	ASTM D5470	[9]
Polyolefin	None	0.3	LFA	[10]
Epoxy	None	0.2-0.22	LFA	[11, 12]
Olefin Oil	None	0.145	THW	[13]
Mineral Oil	None	0.27-0.3	ASTM D5470	[14, 15]
Epoxy	None	0.17-0.22	LFA	[16–18]
Silver Epoxy	None	1.67	TPS	[19]
Paraffin	None	0.25	TPS	[20]
Aerogel	None	0.18	LFA	[21]
Lauric Acid	None	0.215	THW	[22]
Polyamide	None	0.196	LFA	[23]
1-tetradecanol	None	0.32	TPS	[3]
Commercial TIM	Undisclosed	0.52-5.8	ASTM D5470, LFA	[14, 24, 25]
Commercial TIM	added h-BN 2 *wt. %*/6 *wt. %*	0.56/.64	ASTM D5470	[25]
Epoxy	AlN 60/74 vol.%	3.8/8.2	ASTM D5470 similar	[26]
Epoxy	h-BN 43.6 vol.%	3.46	LFA	[27]
Epoxy	h-BN 2.9 vol.%/45 vol.%	0.32/5.5	TPS, LFA	[16]
Epoxy	h-BN 15 vol.% (CPA)	6.1	TPS	[28]
Epoxy	h-BN 44 vol.%	9.0	LFA	[29]
Epoxy	h-BN 34 vol.%	4.4	LFA	[30]
Epoxy	h-BN 30 *wt. %*	0.6	LFA	[31]
Epoxy	h-BN 40 vol.% (CPA)	5.5	LFA	[32]
Epoxy	h-BN 20 vol.%	1.2	LFA	[33]
Epoxy	h-BN 50 vol.% (Functionalized)	9.81	LFA	[34]
Epoxy	AlN 50 vol.%	1.21	TPS	[35]
Epoxy	Silica 50 *vol. %*	0.58	ASTM E1530	[36]
Epoxy	SiC 72 *wt. %* (Functionalized)	5.75	LFA	[37]
Polyimide	h-BN 7 *wt. %*	3	LFA	[38]
Polyimide	h-BN 60 *wt. %*	7.0	TPS	[39]

[1]This table is adapted from J. S. Lewis, T. Perrier, Z. Barani, F. Kargar, and A. A. Balandin, "Review of graphene-based thermal polymer nanocomposites: Current state of the art and future prospects," 2020. [Online]. Available: https://arxiv.org/abs/2008.10752.

Polyimide	h-BN 60 *wt. %*	5.4	TWA	[40]
Polyimide	h-BN 30 *wt. %*	0.72	LFA	[41]
PBT	h-BN 70 vol.% (Functionalized)	11	LFA	[42]
PMMA	h-BN 80 *wt. %* (Functionalized)	10.2	LFA	[42]
PCL	h-BN 20 *wt. %*	1.96	LFA	[43]
PVA	h-BN 30 *wt. %*	4.41	LFA	[44]
PVA	h-BN 10 *wt. %* (Functionalized)	5.4	LFA	[45]
1-tetradecanol	Ag nanowires 11.8 *vol. %*	1.46	TPS	[3]
Silicone Oil	ZnO nanoparticles 18.7 *vol. %*	0.44	TPS	[46]
Silicone Oil	Zno Columns 18.7 *vol. %*	0.55	TPS	[46]
Silicone Oil	ZnO Czech hedgehog structure 18.7 *vol. %*	0.83	TPS	[46]
Resin	SiC 25 *wt. %*	1.28	Unique Method	[47]
	Non-Graphene Carbon Fillers			
Epoxy	Small Graphite 4 *wt. %*/13 *wt. %*/20 *wt. %*	0.22/0.65/4.3	LFA	[12]
Epoxy	Large Graphite 4 *wt. %*/13 *wt. %*/20 *wt. %*	0.87/2.95/4.3	LFA	[12]
Epoxy	CF 20 *wt. %* (non-heated/heated)	0.35/3.75	LFA	[12]
Epoxy	Graphite 10 *wt. %*	0.5	LFA	[48]
Epoxy	MWCNT 20 *wt. %*	0.4	LFA	[49]
Epoxy	Graphite nanoplatelet (non/functionalized) 10 *wt. %*	0.65/1.75	LFA	[37]
Epoxy	Graphite 5.4 vol.% (thicknesses 60 nm/30 nm/4 nm)	1.1/1.35/1.43	ASTM C518	[11]
Epoxy	Graphite Nanoplatelet 14 *wt. %*	0.73	ASTM D5470	[50]
Silicone Oil	Graphite Nanoplatelet 14 *wt. %*	0.5	ASTM D5470	[50]
Hatcol 2372	Graphite Nanoplatelet 14 *wt. %*	0.48	ASTM D5470	[50]
Epoxy	SWCNT 1 wt. %	0.49	ASTM D5470 similar	[51]
Epoxy	Graphite 44.3 wt. %	1.7	TPS	[52]
Oil	MWCNT 1 vol.%	0.36	THW	[13]
CPE	SWCNT 50 *wt. %*	1.6	TDTR	[53]
Silver Epoxy	CB 5 vol.%	2	TPS	[19]
	Graphene Fillers			
Epoxy	GnP 20 *wt. %*	1.5	LFA	[49]
Epoxy	Graphene 10 vol.%	5.1	LFA	[24]

Epoxy	Graphene 11.4 vol.%/43.6 vol.%	1.9/8.0	LFA	[27]
Epoxy	Graphene 2.7 vol.%/44.6 vol.%	0.49/11.4	LFA	[16]
Epoxy	Graphene 55 *wt. %* (Thicknesses 3 nm/ 12 nm)	3.3/8	LFA	[54]
Epoxy	Graphene 1 *wt. %* (RA/CPA)	0.2/0.35	LFA	[55]
Epoxy	GnP 2 *wt. %* (Functionalized)	0.52	LFA	[56]
Epoxy	Graphene 10 *wt. %* (Functionalized)	1.53	LFA	[48]
Epoxy	rGO 2 *wt. %*	0.24	LFA	[17]
Epoxy	Graphene 1 *wt. %* (RA/CPA/IPA)	0.4/0.57/0.25	LFA	[18]
Epoxy	Graphene 0.92 vol.% (CPA)	2.13	LFA	[57]
Epoxy	Graphene 10 *wt. %*	0.67	LFA	[58]
Epoxy	Graphene 30 *wt. %*	4.9	LFA	[59]
Epoxy	Graphene 10 *vol. %*	3.35	LFA	[60]
Epoxy	GnP 8 *wt. %*	1.18	LFA	[61]
Epoxy	GnP 10 *wt. %*	6.5	LFA	[62]
Epoxy	Graphene alone/with PMMA 1 *wt. %*	0.6/1.4	ASTM D5470 similar	[63]
Epoxy	Graphene 5/10 vol.%	2.8/3.9	ASTM D5470 similar	[64]
Epoxy	GnP 25 *vol. %*	6.75	ASTM C518	[11]
Epoxy	Graphene 24 vol.%	12.4	DSC	[65]
Epoxy	Graphene 10.1 *wt. %*	4.0	TPS	[52]
Polyamide	rGO *wt. %*	0.416	LFA	[23]
Polyamide	rGO 5 *wt. %* (Functionalized)	0.41		[66]
Polyamide	rGO 8 *wt. %* (non/Functionalized)	3.34/5.1	TPS	[67]
Polyurethane	rGO 1.04 *wt. %*	0.8	LFA	[68]
Polyimide	Graphene 12 *wt. %*	0.41	LFA	[69]
Cellulose	rGO 30 *wt. %* (IPA)	0.07	LFA	[70]
Mineral Oil	Graphene 10 *wt. %*/20 *wt. %*/40 *wt. %*	3.1/4.8/6.7	ASTM D5470	[14]
Mineral Oil	Graphene 27% vol %	7.1	ASTM D5470	[15]
Silver Epoxy	Graphene 1 vol.%/5 vol.%	4.0/9.9	TPS	[19]
Paraffin	Graphene 0.5 *wt. %*/1 wt. %/20 *wt. %*	10/15/45	TPS	[20]
Commercial TIM	Added Graphene 2 *wt. %*/4 *wt. %*/6 *wt. %*	0.7/0.75/0.8	ASTM D5470	[25]
Commercial TIM	Added Graphene 2 vol.%	14	LFA	[24]
Polystyrene	Graphene 20 *wt. %*	0.48	LFA	[71]
Aerogel	rGO 20 vol.%	2.64	LFA	[21]
PDMS	Graphene 0.5 *wt. %* (Scaffolded)	0.4	ASTM D5470	[9]
Polyolefin	Graphene 10 *wt. %*	5.6	LFA	[10]

Eicosane	Graphene 10 *wt. %*	2.0	TPS	[72]
Lauric Acid	GnP 1 vol.%	0.49	THW	[22]
Methyl Vinyl Silicone	rGO 1.5 *wt. %*	2.7	LFA	[73]
PVDF	rGO 0.25 wt. %	2.35	LFA	[74]
	Hybrid Fillers			
Epoxy	Graphene 21.8 vol.%, h-BN 21.8 vol.%	6.5	LFA	[27]
Epoxy	GnP 40 *wt. %*, Cu-NP 35 *wt. %*	13.5	LFA	[7]
Epoxy	MWCNT grown on GnP 20 *wt. %*	2.4	LFA	[49]
Epoxy	AlN nanowires 30 vol.%, AlN spheres 30 vol.%	5.23	LFA	[75]
Epoxy	BN nanowires 12.8 vol.%, BN spheres 30 vol.%	3.6	LFA	[76]
Epoxy	Al_2O_3-attached GnP 12 *wt. %*	1.49	LFA	[77]
Epoxy	Ag-attached h-BN 25.1 vol.%	3.1	LFA	[78]
Epoxy	Graphene oxide 49.6 *wt. %*, MWCNT 0.4 *wt. %*	4.4	LFA	[79]
Epoxy	h-BN, SiC 40 vol.% total (CPA)	5.77	LFA	[80]
Epoxy	h-BN, rGO 13.2 *wt. %* total (CPA)	5.1	LFA	[81]
Epoxy	MWCNT 5 *wt. %*, SiC 55 *wt. %*	6.8	LFA	[82]
Epoxy	AlN 40.9 *wt. %*, Al_2O_3 17.5 *wt. %*	3.4	LFA	[83]
Epoxy	rGO 20 *wt. %*, Graphene 10 wt. % (Scaffolded)	6.7	LFA	[84]
Epoxy	AlN 25 vol.%, MWCNT 1 vol.%	1.21	TPS	[35]
Epoxy	Graphene oxide 6 *wt. %*, AlN 50 *wt. %*	2.77	TPS	[85]
Epoxy	MWCNT 4 *wt. %*, AlN 25 *wt. %*	1	TPS	[86]
Epoxy	MWCNT 15 *wt. %*, Cu 40 *wt. %*	0.6	TPS	[87]
Epoxy	Graphene 0.9 *wt. %*, MWCNT 0.1 *wt. %*	0.3	TPS	[88]
Epoxy	Silica-coated AlN 50 *vol. %*	1.96	ASTM E1530	[36]
Epoxy	Graphene 16 vol.%, h-BN 1 vol.%	4.72	DSC	[65]
Epoxy	Ag nanowires 4 vol.%, Al_2O_3 15 *wt. %*	1.08	TPS similar	[6]
Epoxy	Graphene 1.5 wt%, MgO 30 *wt. %*	0.51	ASTM D5470 similar	[89]

Epoxy	MgO-coated Graphene 7 *wt. %*	0.4	ASTM C518	[90]
Epoxy	Al_2O_3 30 *wt. %*, rGO 0.3 *wt. %*	0.33	ASTM E1461	[91]
Epoxy	Graphene oxide-encapsulated h-BN 40 *wt. %*	2.2	ASTM D5470	[92]
Polyimide	h-BN (μm scale) 21 wt. % h-BN (nm scale) 9 *wt. %*	1.2	TPS	[93]
Polyimide	BN-coated Cu Nanoparticles, Nanowires 10 *wt. %* total	4.3	TPS	[94]
Polyimide	BN 50 *wt. %*, Graphene 1 *wt. %*	2.11	ASTM D5470	[95]
Polyamide	Graphene 20 *wt. %*, h-BN 1.5 *wt. %*	1.76	LFA	[71]
Polyamide	Graphene oxide 6.8 *wt. %*, h-BN 1.6 *wt. %*	0.9	LFA	[96]
Polycarbonate	GnP 18 *wt. %*, MWCNT 2 *wt. %*	1.39	TPS	[97]
PDMS	Graphene (Scaffolded), CB 2 *wt. %*/8 *wt. %*	0.41//0.7	ASTM D5470	[9]
PPS	h-BN (μm scale) 40 *wt. %*, h-BN (nm scale) 20 *wt. %*	2.64	TPS	[98]
PPS	h-BN 50 *wt. %*, MWCNT 1 *wt. %*	1.74	TPS similar	[99]
PVA	Graphene, MWCNT each Ag-attached 20 vol.% total	12.3	LFA	[100]
Polystyrene	GnP 20 *wt. %*, h-BN 1.5 *wt. %*	0.66	LFA	[71]
PVDF	GnP 5 *wt. %*, Nickel 8 *wt. %*	0.66	LFA	[101]
Cyanate Ester	Graphene 5 *wt. %*, iron-nickel alloy 15 *wt. %*	4.1	TPS	[102]
Polylactic acid	Alumina 70 *wt. %*, graphene 1 *wt. %*	2.4	TPS	[103]

Similarly, considerable attention has been paid to ceramic filler materials [26, 46, 75, 104–108]. The span of electrical and thermal conductivities of this class of filler materials is wider than that of metals; the electrical conductivity span is many orders of magnitude greater than in metals. The large dynamic range of ceramic filler electrical conductivity is very much influenced by impurity doping, much the same as classic elemental semiconductors [109].

The carbon allotropes offer the highest thermal conductivities of materials that are feasibly usable as fillers. Though the electrical conductivity of sp^2-hybridized

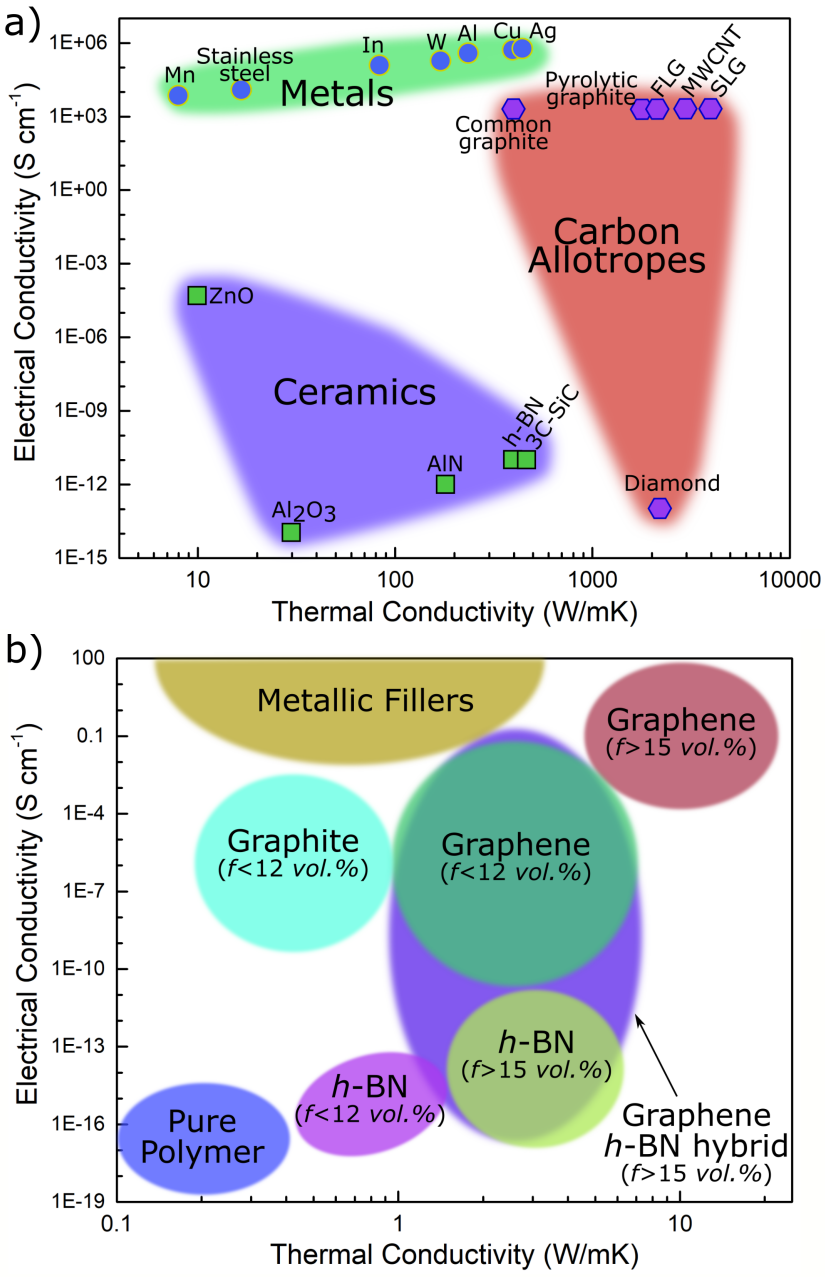

Figure 2.1: a) Electrical and Thermal Conductivity plot of popular and potential filler materials. b) The same plot with values that one could expect in composites composed of some popular filler materials. This figure is adapted with permission from J. S. Lewis, T. Perrier, Z. Barani, F. Kargar, and A. A. Balandin, "Review of graphene-based thermal polymer nanocomposites: Current state of the art and future prospects," 2020. [Online]. Available: https://arxiv.org/abs/ 2008.10752.

carbons can be nearly metallic, the lattice vibrational phonon thermal conductivity remains the dominant contributor due to the strong σ covalent bonds between them. The dominance of lattice thermal conduction in carbon materials can clearly seen in the sp^3-hybridized diamond that has strongly-insulating electrical conductivity but with a thermal conductivity of ≈2,000 W/mK.

2.2 Graphene

Graphene is a material that has seen tremendous study in the past fifteen years spurred on by the advent of mechanical exfoliation from graphite [110]. Graphene in its strict definition is a single atomic plane of carbon bound together with sp^2-hybridized σ covalent bonds in a hexagonal structure. Figure 2.2 shows SEM, Atomic Force Microscopy (AFM), and Scanning Tunneling Microscopy (STM) micrographs of different graphene specimens [111]. It's exciting properties include a comparable stiffness to diamond, having a very high carrier mobility, a high optical absorbance to thickness ratio predominantly governed by the out-of-plane π bonds, an extraordinary thermal conductivity, and being made up of exceedingly abundant carbon [112–116].

The material property of chief importance to the work at present is the thermal conductivity of graphene. The thermal conductivity of graphene is between 2,000 - 5,300 W/mK, with a large influence on defects and scattering from contact to other materials [115, 117–119]. Despite graphene's high electrical conductivity, its thermal transport mechanisms is quite the opposite to that of copper, with less than 1% of K_T coming from K_e, one estimate placing the contribution at 2 W/mK, corresponding to 0.1% at most of the contribution to K_T [120]. The vast majority of thermal conductivity in graphene is thus contributed to by phonons.

The graphene material used for in these works are commercially-sourced graphene

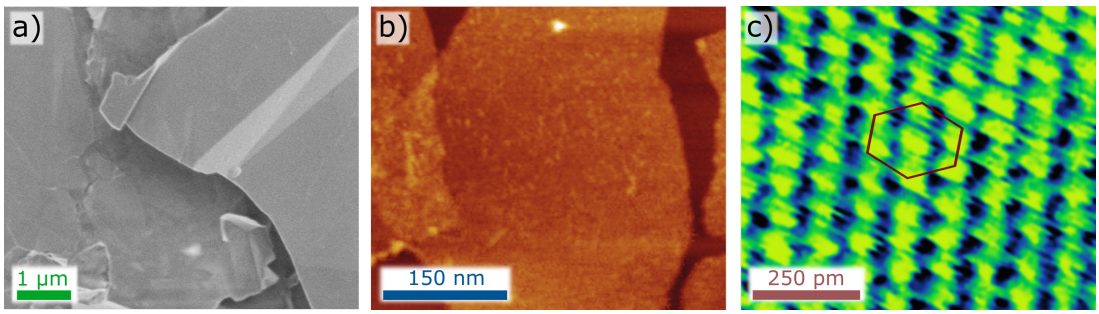

Figure 2.2: a) SEM of multi-layer graphene flakes. b) Atomic Force Microscopy micrograph of graphene flakes. c) Scanning Tunneling Microscopy micrograph of bilayer graphene. Note that each image is of different specimens. Panel b is adapted with permission from the publication J. I. Paredes, S. Villar-Rodil, P. Solis-Fernandez, A. Martinez-Alonso, and J. M. D. Tascon, "Atomic Force and Scanning Tunneling Microscopy Imaging of Graphene Nanosheets Derived from Graphite Oxide," *Langmuir*, vol. 25, pp. 5957–5968, May 2009. Copyright © American Chemical Society.

flakes derived from liquid-phase exfoliation that appears to the eye as a black, fluffy powder [121]. In the forthcoming discussion regarding the study of hybrid composites with graphene and *h*-BN, the used graphene (Graphene Supermarket) had lateral dimensions between 2 and 8 μm with a thickness up to 12 nm. In the following accelerated aging study, graphene (XG Sciences) of lateral dimensions up to 15 μm with comparable thicknesses was used. Due to the larger graphene flakes in the latter investigation providing longer pathways through composites, one would expect larger composite thermal conductivities at identical filler loading levels. It should be noted that due to the composite mixing procedures it is expected that some additional exfoliation of the graphene will occur, resulting in a thickness distribution spread approaching down to single-layer graphene [122]. It should be noted that each source of graphene had lateral dimensions considerably longer than the 775 nanometers of its phonon mean-free path at room temperature (RT) [117].

The graphene flakes were incorporated into the polymer matrix as received without any additional modification, such as surface functionalization. Researchers

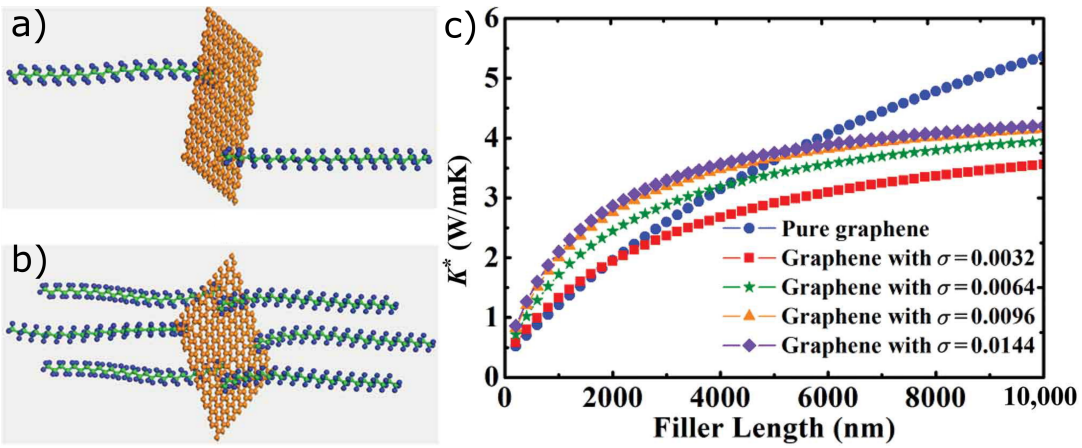

Figure 2.3: a) and b) Schematics of graphene with different areal densities of attached linear hydrocarbons. b) Thermal Conductivity, K^*, of composites with different areal densities, σ, of attached hydrocarbons. Reprinted with permission from the publication M. Wang, D. Galpaya, Z. B. Lai, Y. Xu, and C. Yan, "Surface functionalization on the thermal conductivity of graphene–polymer nanocomposites," *International Journal of Smart and Nano Materials*, vol. 5, no. 2, pp. 123–132, 2014. Published under the Creative Commons license by Taylor & Francis.

often functionalize the surface with an attached molecule or nanoparticle to prevent agglomeration or enhance the thermal coupling between flake and polymer matrix [123–127]. Figure 2.3a and 2.3b show schematics of graphene with attached linear hydrocarbons at low and high areal density. In Figure 2.3c, the composite thermal conductivity with varying areal densities is calculated via nonequilibrium molecular dynamics simulations versus graphene lateral dimensions. Interestingly, it is found that for smaller filler sizes – sizes at which heat must frequently move from one filler to the next – the functionalization helps composite thermal conductivity, while past $\approx$5 μm the non-functionalized graphene composite performs better. Given the lateral dimensions of the graphene materials used, it is expected that functionalization would at the very least not greatly improve composite thermal conductivity, perhaps even harm it, while requiring extra processing steps.

The thermal conductivity of multi-layer graphene with increasing layers re-

duces up to a thickness of ≈8 monolayers, at which point it stabilizes to that of high-quality graphite at ≈2,000 W/mK while still maintaining its flexibility [128–130]. On the other hand, it has been widely-reported that contact between single-layer graphene and a dissimilar substrate or other material results in a very strong inhibition of thermal conductivity [131–133]. Due to graphene contact with dissimilar materials causing a more aggressive reduction in thermal conductivity than increasing thickness, and thus contact with itself, researchers have found that using multiple layers of graphene can help insulate inner layers from other materials, suffering more modest reduction in thermal conductivity [134–137]. Due to this fact, the use of multi-layer graphene should not be assumed to be inferior to a composite that would be filled purely with single-layer graphene.

2.3 Hexagonal Boron Nitride

Hexagonal Boron Nitride (*h*-BN) is a single atomic plane material very much analogous to graphene with a honeycomb structure [138]. *h*-BN has long seen use as a dry lubricant – much like graphite – due to the fact that it is composed of soft sheets that can easily slide atop one another, as illustrated in figure 2.4. The material is a III-V compound with a large band gap of ≈5 eV [139]. *h*-BN has a high experimental thermal conductivity of between 230 and 480 W/mK and up to 1,000 W/mK when calculated from theory [140–146]. Unlike graphene's great thermal conductivity *and* electrical conductivity, the electrical conductivity of *h*-BN is quite low, ranging from between 10^{-11} and 10^{-8} S/cm [27, 147, 148]. The high electrical resistivity of *h*-BN makes it an attractive option to control composite electrical conductivity while still providing the highest possible thermal conductivity [65, 149].

The *h*-BN used in this dissertation was obtained from industry (US Research

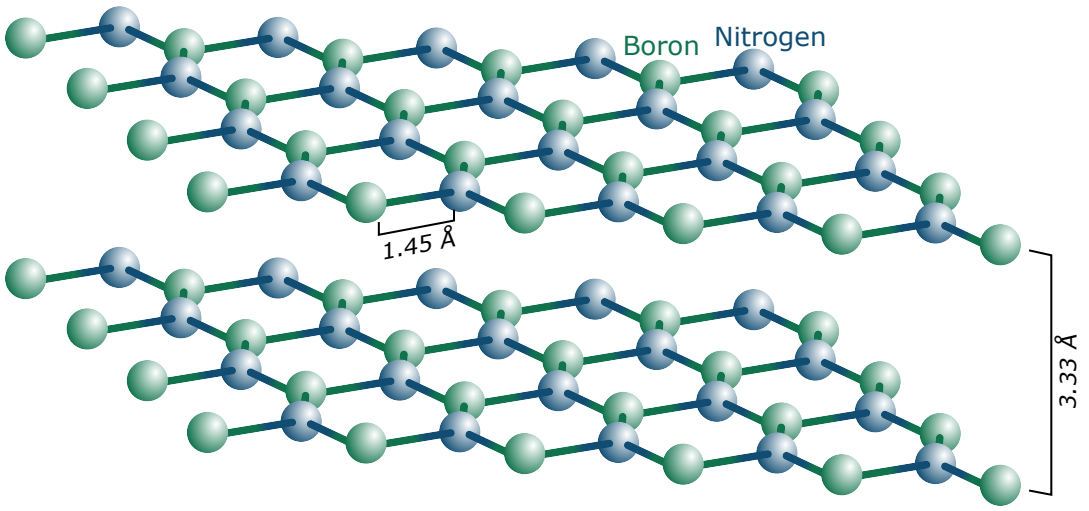

Figure 2.4: Schematic figure of two sheets of *h*-BN.

Nanomaterials, Inc.) and has similar dimensions to the graphene flakes used. Macroscopically, the *h*-BN flakes appears as a white powder. No additional modifications were made to the *h*-BN flakes.

2.4 Polymer Matrix

The polymer matrix used in this research is diglycidyl ether of bisphenol-A (DGEBA) resin (Allied High Tech Products, Inc.) with a Triethylenetetramine hardening agent. This is a thermosetting epoxy that sees extensive industrial use for numerous reasons, perhaps the greatest of which is its chemical resilience. Though thermosetting polymers are not exclusively used in electronics packaging, they do have preferential usage due to their thermal stability. Where a thermoplastic can melt if an electronic device's operating temperature is high enough, the corresponding phase change of thermoplastics – known as the glass transition temperature – results in far more modest property alterations compared to the direct conversion to a liquid. The glass transition temperature was found to occur at ≈90 °C by differential scanning calorimetry (DSC), while similar studies reveal a

glass transition at a close temperature of ≈100 °C [150, 151]. Figure 2.5 shows the results of DSC experiments on the cured polymer with an sharp, continuous increase of specific heat, characteristic of the glass transition, past 80 °C. Beyond this temperature the mechanical rigidity and thermal transport properties will diminish as it behaves more as a rubber [64, 152].

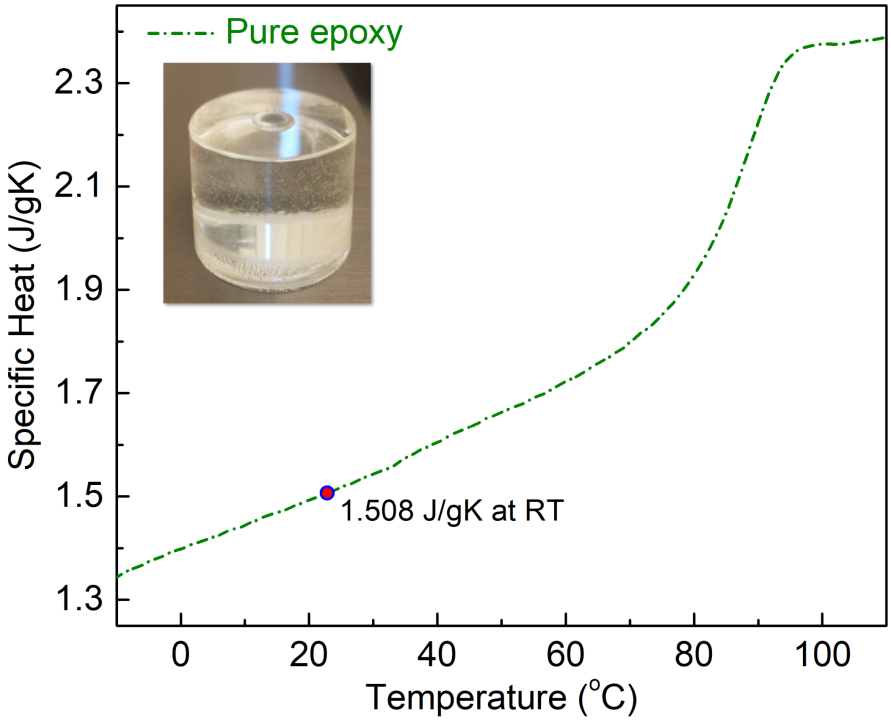

Figure 2.5: DSC experiment results showing a sharp increase in specific heat at elevated temperatures. Inset image is of pure DGEBA epoxy. Reprinted with permission from the publication J. S. Lewis, Z. Barani, A. S. Magana, F. Kargar, and A. A. Balandin, "Thermal and electrical conductivity control in hybrid composites with graphene and boron nitride fillers" *Materials Research Express*, vol. 6, no. 8, p. 085325, May 2019. Copyright © Institute of Physics.

This polymer matrix is considered a great analog for all polymers used in practical applications as TIMs and as a result is extremely popular in this field of research. All prepared DGEBA epoxies were cured at RT with a stoichiometric ratio of 100:12, DGEBA resin to hardener. Composites were filled with graphene and *h*-BN that were assumed to be inert, thus the stoichiometric ratio of resin and

hardener were not altered with the inclusion of filler.

2.5 Composite Preparation

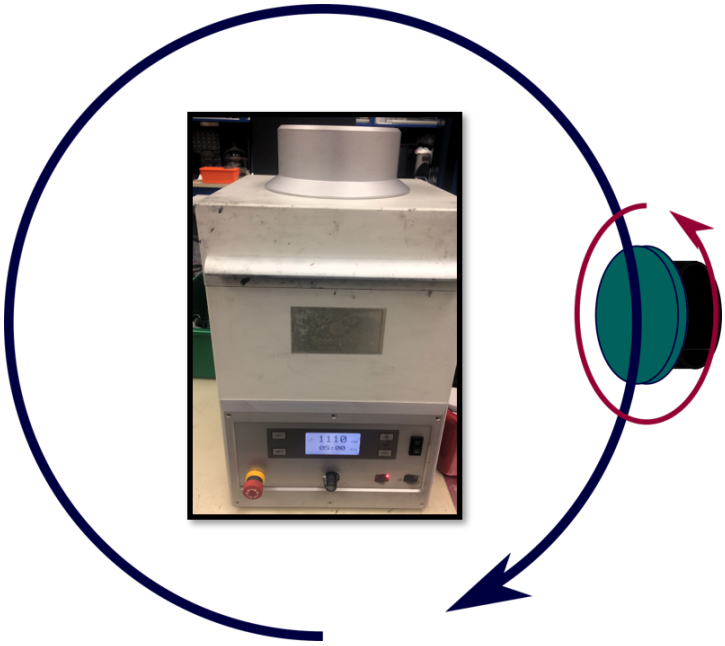

Figure 2.6: Schematic showing the revolution and rotation motion of a cup that mixes its contents. Central image shows the machine used in this work.

The preparation procedure generally began with a roughly targeted value of DGEBA resin that immediately underwent a quick – $\approx$ 2 minutes – rough vacuum treatment. Given the amount of DGEBA resin, the requisite weights of filler materials necessary; be it graphene, *h*-BN, or both and the hardening agent were calculated, weighed, and dispersed into the mold that contained the resin. In hybrid-filled composites, the graphene and *h*-BN fillers were separately mixed together prior to inclusion into the resin. The mold with resin and fillers were then mixed in a commercial 2-axis planetary mixer (FlackTek Inc., *SpeedMixer*™), like shown in Figure 2.6. Composites with a high loading above $\approx$ 25 *vol. %* required manually breaking agglomerations with tools to ensure quality mixing.

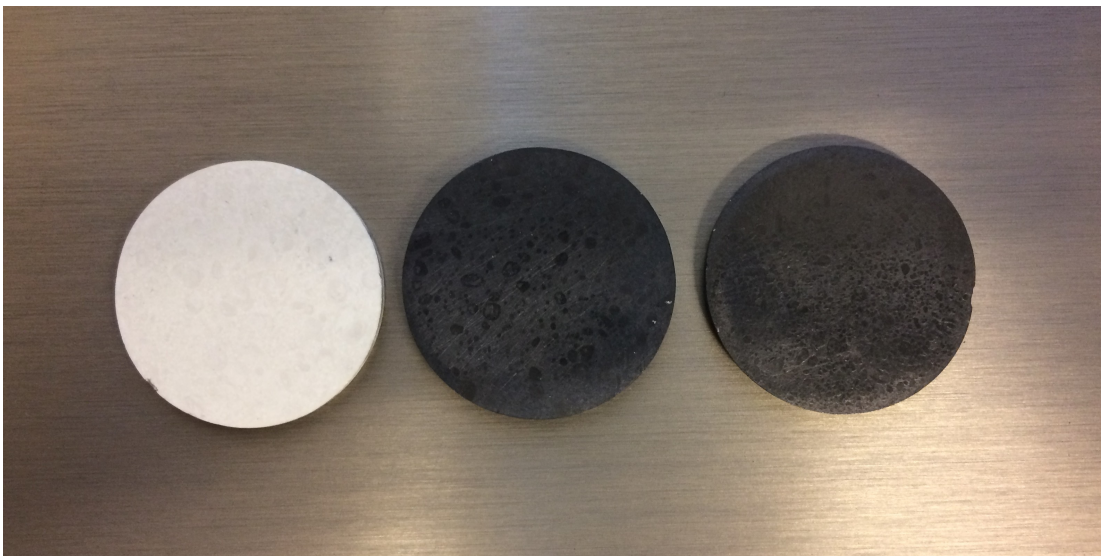

Figure 2.7: Three samples of representative geometries. Hybrid composite samples pictured from left to right: 00 *vol. %* of graphene and 43.6 *vol. %* of *h*-BN, 21.8 *vol. %* graphene and 21.8 *vol. %* of *h*-BN, and 43.6 *vol. %* of graphene and 00 *vol. %* of *h*-BN. The pictured composite samples are at end-of-process and thus have some blemishes that wouldn't normally be as striking.

Then the hardener was added and mixed as previously. The composites were cured at RT over night under just enough pressure applied by a mechanical piston making direct contact to the material to overcome the agglomeration surface tension and achieve a uniform, singular composite. The pressure used for this varied based on the filler loading level, but was always below 20 bars. No application of pressure was necessary in composites of very low filler concentration, $\leq$ 10 *vol. %*.

Once the samples were cured they were then broken out of the mold and are polished to the desired geometry of a one inch diameter cylinder at approximately 2 mm in thickness. This geometry is chosen specifically for compatibility with our thermal analysis techniques. Figure 2.7 shows three representative, post-process samples. Scratches atop the surface are an artifact of the polishing process.

Bibliography

[1] A. A. Balandin, "Thermal properties of graphene and nanostructured carbon materials," *Nature Materials*, vol. 10, pp. 569–581, Aug. 2011.

[2] G. A. Gelves, U. Sundararaj, and J. A. Haber, "Electrostatically dissipative polystyrene nanocomposites containing copper nanowires," *Macromolecular Rapid Communications*, vol. 26, no. 21, pp. 1677–1681, 2005.

[3] J. Zeng, Z. Cao, D. Yang, L. Sun, and L. Zhang, "Thermal conductivity enhancement of ag nanowires on an organic phase change material," *Journal of Thermal Analysis and Calorimetry*, vol. 101, no. 1, pp. 385 – 389, 2009.

[4] S. I. White, R. M. Mutiso, P. M. Vora, D. Jahnke, S. Hsu, J. M. Kikkawa, J. Li, J. E. Fischer, and K. I. Winey, "Electrical percolation behavior in silver nanowire–polystyrene composites: Simulation and experiment," *Advanced Functional Materials*, vol. 20, no. 16, pp. 2709–2716, 2010.

[5] W. Yu, J. Zhao, M. Wang, Y. Hu, L. Chen, and H. Xie, "Thermal conductivity enhancement in thermal grease containing different CuO structures," *Nanoscale research letters*, vol. 10, no. 1, pp. 1–8, 2015.

[6] C. Chen, H. Wang, Y. Xue, Z. Xue, H. Liu, X. Xie, and Y.-W. Mai, "Structure, rheological, thermal conductive and electrical insulating properties of high-performance hybrid epoxy/nanosilica/AgNWs nanocomposites," *Composites Science and Technology*, vol. 128, pp. 207 – 214, 2016.

[7] Z. Barani, A. Mohammadzadeh, A. Geremew, C.-Y. Huang, D. Coleman, L. Mangolini, F. Kargar, and A. A. Balandin, "Thermal properties of the binary-filler hybrid composites with graphene and copper nanoparticles," *Advanced Functional Materials*, vol. 30, no. 8, p. 1904008, 2020.

[8] J. S. Lewis, T. Perrier, Z. Barani, F. Kargar, and A. A. Balandin, "Review of graphene-based thermal polymer nanocomposites: Current state of the art and future prospects," 2020. [Online]. Available: https://arxiv.org/abs/2008.10752.

[9] Y.-H. Zhao, Y.-F. Zhang, Z.-K. Wu, and S.-L. Bai, "Synergic enhancement of thermal properties of polymer composites by graphene foam and carbon black," *Composites Part B: Engineering*, vol. 84, pp. 52 – 58, 2016.

[10] T. Cui, Q. Li, Y. Xuan, and P. Zhang, "Preparation and thermal properties of the graphene–polyolefin adhesive composites: Application in thermal interface materials," *Microelectronics Reliability*, vol. 55, no. 12, Part A, pp. 2569 – 2574, 2015.

[11] A. Yu, P. Ramesh, M. E. Itkis, E. Bekyarova, and R. C. Haddon, "Graphite nanoplatelet-epoxy composite thermal interface materials," *Journal of Physical Chemistry C*, vol. 111, pp. 7565–7569, May 2007.

[12] B. Debelak and K. Lafdi, "Use of exfoliated graphite filler to enhance polymer physical properties," *Carbon*, vol. 45, pp. 1727–1734, Aug. 2007.

[13] S. U. S. Choi, Z. G. Zhang, W. Yu, F. E. Lockwood, and E. A. Grulke, "Anomalous thermal conductivity enhancement in nanotube suspensions," *Applied Physics Letters*, vol. 79, no. 14, pp. 2252–2254, 2001.

[14] B. K. Mahadevan, S. Naghibi, F. Kargar, and A. A. Balandin, "Non-curing thermal interface materials with graphene fillers for thermal management of concentrated photovoltaic solar cells," *C — Journal of Carbon Research*, vol. 6, p. 2, Dec. 2019.

[15] S. Naghibi, F. Kargar, D. Wright, C. Y. T. Huang, A. Mohammadzadeh, Z. Barani, R. Salgado, and A. A. Balandin, "Noncuring graphene thermal interface materials for advanced electronics," *Advanced Electronic Materials*, p. 1901303, 2020.

[16] F. Kargar, Z. Barani, R. Salgado, B. Debnath, J. S. Lewis, E. Aytan, R. K. Lake, and A. A. Balandin, "Thermal percolation threshold and thermal properties of composites with high loading of graphene and boron nitride fillers," *ACS Applied Materials & Interfaces*, vol. 10, pp. 37555–37565, Oct. 2018.

[17] G. B. Olowojoba, S. Eslava, E. S. Gutierrez, A. J. Kinloch, C. Mattevi, V. G. Rocha, and A. C. Taylor, "In situ thermally reduced graphene oxide/epoxy composites: thermal and mechanical properties," *Applied Nanoscience (Switzerland)*, vol. 6, pp. 1015–1022, Oct. 2016.

[18] H. Yan, Y. Tang, W. Long, and Y. Li, "Enhanced thermal conductivity in polymer composites with aligned graphene nanosheets," *Journal of Materials Science*, vol. 49, pp. 5256–5264, May 2014.

[19] V. Goyal and A. A. Balandin, "Thermal properties of the hybrid graphene-metal nano-micro-composites: Applications in thermal interface materials," *Applied Physics Letters*, vol. 100, no. 7, p. 073113, 2012.

[20] P. Goli, S. Legedza, A. Dhar, R. Salgado, J. Renteria, and A. A. Balandin, "Graphene-enhanced hybrid phase change materials for thermal management of Li-ion batteries," *Journal of Power Sources*, vol. 248, pp. 37 – 43, 2014.

[21] Y. Zhong, M. Zhou, F. Huang, T. Lin, and D. Wan, "Effect of graphene aerogel on thermal behavior of phase change materials for thermal management," *Solar Energy Materials and Solar Cells*, vol. 113, pp. 195 – 200, 2013.

[22] S. Harish, D. Orejon, Y. Takata, and M. Kohno, "Thermal conductivity enhancement of lauric acid phase change nanocomposite with graphene nanoplatelets," *Applied Thermal Engineering*, vol. 80, pp. 205 – 211, 2015.

[23] P. Ding, S. Su, N. Song, S. Tang, Y. Liu, and L. Shi, "Highly thermal conductive composites with polyamide-6 covalently-grafted graphene by an in situ polymerization and thermal reduction process," *Carbon*, vol. 66, pp. 576 – 584, 2014.

[24] K. M. F. Shahil and A. A. Balandin, "Graphene–multilayer graphene nanocomposites as highly efficient thermal interface materials," *Nano Letters*, vol. 12, pp. 861–867, Feb. 2012.

[25] F. Kargar, R. Salgado, S. Legedza, J. Renteria, and A. A. Balandin, "A comparative study of the thermal interface materials with graphene and boron nitride fillers," in *Carbon Nanotubes, Graphene, and Associated Devices VII* (M. Razeghi, Y. H. Lee, and M. Ghazinejad, eds.), vol. 9168, pp. 70 – 74, International Society for Optics and Photonics, SPIE, 2014.

[26] M. Ohashi, S. Kawakami, Y. Yokogawa, and G.-C. Lai, "Spherical aluminum nitride fillers for heat-conducting plastic packages," *Journal of the American Ceramic Society*, vol. 88, no. 9, pp. 2615–2618, 2005.

[27] J. S. Lewis, Z. Barani, A. S. Magana, F. Kargar, and A. A. Balandin, "Thermal and electrical conductivity control in hybrid composites with graphene and boron nitride fillers," *Materials Research Express*, vol. 6, p. 085325, May 2019.

[28] J. Han, G. Du, W. Gao, and H. Bai, "An anisotropically high thermal conductive boron nitride/epoxy composite based on nacre-mimetic 3D network," *Advanced Functional Materials*, vol. 29, no. 13, p. 1900412, 2019.

[29] C. Yu, J. Zhang, Z. Li, W. Tian, L. Wang, J. Luo, Q. Li, X. Fan, and Y. Yao, "Enhanced through-plane thermal conductivity of boron nitride/epoxy composites," *Composites Part A: Applied Science and Manufacturing*, vol. 98, pp. 25 – 31, 2017.

[30] J. Hu, Y. Huang, Y. Yao, G. Pan, J. Sun, X. Zeng, R. Sun, J.-B. Xu, B. Song, and C.-P. Wong, "Polymer composite with improved thermal conductivity by constructing a hierarchically ordered three-dimensional interconnected network of BN," *ACS Applied Materials & Interfaces*, vol. 9, no. 15, pp. 13544–13553, 2017.

[31] Z. Lin, A. Mcnamara, Y. Liu, K.-s. Moon, and C.-P. Wong, "Exfoliated hexagonal boron nitride-based polymer nanocomposite with enhanced thermal conductivity for electronic encapsulation," *Composites Science and Technology*, vol. 90, pp. 123–128, Jan. 2014.

[32] K. Kim and J. Kim, "Vertical filler alignment of boron nitride/epoxy composite for thermal conductivity enhancement via external magnetic field," *International Journal of Thermal Sciences*, vol. 100, pp. 29 – 36, 2016.

[33] C. Yuan, B. Xie, M. Huang, R. Wu, and X. Luo, "Thermal conductivity enhancement of platelets aligned composites with volume fraction from 10% to 20%," *International Journal of Heat and Mass Transfer*, vol. 94, pp. 20 – 28, 2016.

[34] J. Yu, H. Mo, and P. Jiang, "Polymer/boron nitride nanosheet composite with high thermal conductivity and sufficient dielectric strength," *Polymers for Advanced Technologies*, vol. 26, no. 5, pp. 514–520, 2015.

[35] C.-C. Teng, C.-C. M. Ma, K.-C. Chiou, and T.-M. Lee, "Synergetic effect of thermal conductive properties of epoxy composites containing functionalized multi-walled carbon nanotubes and aluminum nitride," *Composites Part B: Engineering*, vol. 43, pp. 265–271, Mar. 2012.

[36] C. P. Wong and R. S. Bollampally, "Thermal conductivity, elastic modulus, and coefficient of thermal expansion of polymer composites filled with ceramic particles for electronic packaging," *Journal of Applied Polymer Science*, vol. 74, no. 14, pp. 3396–3403, 1999.

[37] T. Zhou, X. Wang, P. Cheng, T. Wang, D. Ziong, and X. Wang, "Improving the thermal conductivity of epoxy resin by the addition of a mixture of graphite nanoplatelets and silicon carbide microparticles," *eXPRESS Polymer Letters*, vol. 7, no. 7, pp. 585–594, 2013.

[38] Z.-G. Wang, F. Gong, W.-C. Yu, Y.-F. Huang, L. Zhu, J. Lei, J.-Z. Xu, and Z.-M. Li, "Synergetic enhancement of thermal conductivity by constructing hybrid conductive network in the segregated polymer composites," *Composites Science and Technology*, vol. 162, pp. 7–13, July 2018.

[39] K. Sato, H. Horibe, T. Shirai, Y. Hotta, H. Nakano, H. Nagai, K. Mitsuishi, and K. Watari, "Thermally conductive composite films of hexagonal boron nitride and polyimide with affinity-enhanced interfaces," *J. Mater. Chem.*, vol. 20, pp. 2749–2752, 2010.

[40] M. Tanimoto, T. Yamagata, K. Miyata, and S. Ando, "Anisotropic thermal diffusivity of hexagonal boron nitride-filled polyimide films: Effects of filler particle size, aggregation, orientation, and polymer chain rigidity," *ACS Applied Materials & Interfaces*, vol. 5, no. 10, pp. 4374–4382, 2013.

[41] H. Song, B. Kim, Y. Kim, Y.-S. Bae, J. Kim, and Y. Yoo, "Synergistic effects of various ceramic fillers on thermally conductive polyimide composite films and their model predictions," *Polymers*, vol. 11, p. 484, Mar. 2019.

[42] T. Morishita and H. Okamoto, "Facile exfoliation and noncovalent superacid functionalization of boron nitride nanosheets and their use for highly thermally conductive and electrically insulating polymer nanocomposites," *ACS Applied Materials & Interfaces*, vol. 8, no. 40, pp. 27064–27073, 2016.

[43] J. Lee, H. Jung, S. Yu, S. Man Cho, V. K. Tiwari, D. Babu Velusamy, and C. Park, "Boron nitride nanosheets (BNNSs) chemically modified by "grafting-from" polymerization of poly(caprolactone) for thermally conductive polymer composites," *Chemistry – An Asian Journal*, vol. 11, no. 13, pp. 1921–1928, 2016.

[44] B.-H. Xie, X. Huang, and G.-J. Zhang, "High thermal conductive polyvinyl alcohol composites with hexagonal boron nitride microplatelets as fillers," *Composites Science and Technology*, vol. 85, pp. 98 – 103, 2013.

[45] H. Shen, J. Guo, H. Wang, N. Zhao, and J. Xu, "Bioinspired modification of h-BN for high thermal conductive composite films with aligned structure," *ACS Applied Materials & Interfaces*, vol. 7, no. 10, pp. 5701–5708, 2015.

[46] H. Du, Y. Qi, W. Yu, J. Yin, and H. Xie, "T-shape ZnO whisker: A more effective thermal conductive filler than spherical particles for the thermal grease," *International Journal of Heat and Mass Transfer*, vol. 112, pp. 1052 – 1056, 2017.

[47] W. X. Wang, X. Lu, J. Liu, M. O. Olorunyomi, T. Aronsson, and D. Shangguan, "New nano-thermal interface materials (nano-TIMs) with SiC nanoparticles used for heat removal in electronics packaging applications," in *2006 International Conference on Electronic Materials and Packaging*, pp. 1–5, 2006.

[48] S. H. Song, K. H. Park, B. H. Kim, Y. W. Choi, G. H. Jun, D. J. Lee, B.-S. Kong, K.-W. Paik, and S. Jeon, "Enhanced thermal conductivity of epoxy–graphene composites by using non-oxidized graphene flakes with noncovalent functionalization," *Advanced Materials*, vol. 25, no. 5, pp. 732–737, 2013.

[49] L. Yu, J. S. Park, Y.-S. Lim, C. S. Lee, K. Shin, H. J. Moon, C.-M. Yang, Y. S. Lee, and J. H. Han, "Carbon hybrid fillers composed of carbon nanotubes directly grown on graphene nanoplatelets for effective thermal conductivity in epoxy composites," *Nanotechnology*, vol. 24, p. 155604, Mar. 2013.

[50] X. Tian, M. E. Itkis, E. B. Bekyarova, and R. C. Haddon, "Anisotropic thermal and electrical properties of thin thermal interface layers of graphite nanoplatelet-based composites," *Scientific Reports*, vol. 3, p. 1710, Apr. 2013.

[51] M. J. Biercuk, M. C. Llaguno, M. Radosavljevic, J. K. Hyun, A. T. Johnson, and J. E. Fischer, "Carbon nanotube composites for thermal management," *Applied Physics Letters*, vol. 80, no. 15, pp. 2767–2769, 2002.

[52] Y.-X. Fu, Z.-X. He, D.-C. Mo, and S.-S. Lu, "Thermal conductivity enhancement of epoxy adhesive using graphene sheets as additives," *International Journal of Thermal Sciences*, vol. 86, pp. 276 – 283, 2014.

[53] C.-K. Mai, J. Liu, C. M. Evans, R. A. Segalman, M. L. Chabinyc, D. G. Cahill, and G. C. Bazan, "Anisotropic thermal transport in thermoelectric composites of conjugated polyelectrolytes/single-walled carbon nanotubes," *Macromolecules*, vol. 49, no. 13, pp. 4957–4963, 2016.

[54] F. Kargar, Z. Barani, M. Balinskiy, A. S. Magana, J. S. Lewis, and A. A. Balandin, "Dual-functional graphene composites for electromagnetic shielding and thermal management," *Advanced Electronic Materials*, vol. 5, no. 1, p. 1800558, 2019.

[55] J. Renteria, S. Legedza, R. Salgado, M. Balandin, S. Ramirez, M. Saadah, F. Kargar, and A. Balandin, "Magnetically-functionalized self-aligning graphene fillers for high-efficiency thermal management applications," *Materials & Design*, vol. 88, pp. 214 – 221, 2015.

[56] S. Chatterjee, J. Wang, W. Kuo, N. Tai, C. Salzmann, W. Li, R. Hollertz, F. Nüesch, and B. Chu, "Mechanical reinforcement and thermal conductivity in expanded graphene nanoplatelets reinforced epoxy composites," *Chemical Physics Letters*, vol. 531, pp. 6 – 10, 2012.

[57] G. Lian, C. C. Tuan, L. Li, S. Jiao, Q. Wang, K. S. Moon, D. Cui, and C. P. Wong, "Vertically aligned and interconnected graphene networks for high thermal conductivity of epoxy composites with ultralow loading," *Chemistry of Materials*, vol. 28, pp. 6096–6104, Sept. 2016.

[58] S. G. Prolongo, R. Moriche, A. Jiménez-Suárez, M. Sánchez, and A. Ureña, "Epoxy adhesives modified with graphene for thermal interface materials," *The Journal of Adhesion*, vol. 90, no. 10, pp. 835–847, 2014.

[59] B. Tang, G. Hu, H. Gao, and L. Hai, "Application of graphene as filler to improve thermal transport property of epoxy resin for thermal interface materials," *International Journal of Heat and Mass Transfer*, vol. 85, pp. 420 – 429, 2015.

[60] A. A. Dmitriev, A. S. Dmitriev, P. Makarov, and I. Mikhailova, "New nanocomposite surfaces and thermal interface materials based on mesoscopic microspheres, polymers and graphene flakes," *AIP Conference Proceedings*, vol. 1957, no. 1, p. 020003, 2018.

[61] Y. Wang, J. Yu, W. Dai, Y. Song, D. Wang, L. Zeng, and N. Jiang, "Enhanced thermal and electrical properties of epoxy composites reinforced with graphene nanoplatelets," *Polymer Composites*, vol. 36, no. 3, pp. 556–565, 2015.

[62] R. Moriche, S. Prolongo, M. Sánchez, A. Jiménez-Suárez, F. Chamizo, and A. Ureña, "Thermal conductivity and lap shear strength of GNP/epoxy nanocomposites adhesives," *International Journal of Adhesion and Adhesives*, vol. 68, pp. 407 – 410, 2016.

[63] O. Eksik, S. F. Bartolucci, T. Gupta, H. Fard, T. Borca-Tasciuc, and N. Koratkar, "A novel approach to enhance the thermal conductivity of epoxy nanocomposites using graphene core–shell additives," *Carbon*, vol. 101, pp. 239 – 244, 2016.

[64] W. Park, Y. Guo, X. Li, J. Hu, L. Liu, X. Ruan, and Y. P. Chen, "High-performance thermal interface material based on few-layer graphene composite," *Journal of Physical Chemistry C*, vol. 119, pp. 26753–26759, Nov. 2015.

[65] M. Shtein, R. Nadiv, M. Buzaglo, and O. Regev, "Graphene-based hybrid composites for efficient thermal management of electronic devices," *ACS Applied Materials & Interfaces*, vol. 7, pp. 23725–23730, Oct. 2015.

[66] N. Song, J. Yang, P. Ding, S. Tang, and L. Shi, "Effect of polymer modifier chain length on thermal conductive property of polyamide 6/graphene nanocomposites," *Composites Part A: Applied Science and Manufacturing*, vol. 73, pp. 232 – 241, 2015.

[67] E.-C. Cho, J.-H. Huang, C.-P. Li, C.-W. Chang-Jian, K.-C. Lee, Y.-S. Hsiao, and J.-H. Huang, "Graphene-based thermoplastic composites and their application for LED thermal management," *Carbon*, vol. 102, pp. 66 – 73, 2016.

[68] A. Li, C. Zhang, and Y.-F. Zhang, "RGO/TPU composite with a segregated structure as thermal interface material," *Composites Part A: Applied Science and Manufacturing*, vol. 101, pp. 108 – 114, 2017.

[69] J. Gong, Z. Liu, J. Yu, D. Dai, W. Dai, S. Du, C. Li, N. Jiang, Z. Zhan, and C.-T. Lin, "Graphene woven fabric-reinforced polyimide films with enhanced and anisotropic thermal conductivity," *Composites Part A: Applied Science and Manufacturing*, vol. 87, pp. 290 – 296, 2016.

[70] N. Song, D. Jiao, P. Ding, S. Cui, S. Tang, and L. Shi, "Anisotropic thermally conductive flexible films based on nanofibrillated cellulose and aligned graphene nanosheets," *J. Mater. Chem. C*, vol. 4, pp. 305–314, 2016.

[71] X. Cui, P. Ding, N. Zhuang, L. Shi, N. Song, and S. Tang, "Thermal conductive and mechanical properties of polymeric composites based on solution-exfoliated boron nitride and graphene nanosheets: A morphology-promoted synergistic effect," *ACS Applied Materials & Interfaces*, vol. 7, pp. 19068–19075, Sept. 2015.

[72] X. Fang, L. W. Fan, Q. Ding, X. Wang, X. L. Yao, J. F. Hou, Z. T. Yu, G. H. Cheng, Y. C. Hu, and K. F. Cen, "Increased thermal conductivity of eicosane-based composite phase change materials in the presence of graphene nanoplatelets," *Energy and Fuels*, vol. 27, pp. 4041–4047, July 2013.

[73] H. Zhang, Y. Lin, D. Zhang, W. Wang, Y. Xing, J. Lin, H. Hong, and C. Li, "Graphene nanosheet/silicone composite with enhanced thermal conductivity and its application in heat dissipation of high-power light-emitting diodes," *Current Applied Physics*, vol. 16, no. 12, pp. 1695 – 1702, 2016.

[74] P. Kumar, M. K. Yadav, N. Panwar, A. Kumar, and R. Singhal, "Temperature dependent thermal conductivity of free-standing reduced graphene oxide/poly (vinylidene fluoride-co-hexafluoropropylene) composite thin film," *Materials Research Express*, vol. 6, p. 115604, Sept. 2019.

[75] T. M. L. Dang, C.-Y. Kim, Y. Zhang, J.-F. Yang, T. Masaki, and D.-H. Yoon, "Enhanced thermal conductivity of polymer composites via hybrid fillers of anisotropic aluminum nitride whiskers and isotropic spheres," *Composites Part B: Engineering*, vol. 114, pp. 237 – 246, 2017.

[76] K. Kim, M. Kim, and J. Kim, "Thermal and mechanical properties of epoxy composites with a binary particle filler system consisting of aggregated and whisker type boron nitride particles," *Composites Science and Technology*, vol. 103, pp. 72 – 77, 2014.

[77] R. Sun, H. Yao, H.-B. Zhang, Y. Li, Y.-W. Mai, and Z.-Z. Yu, "Decoration of defect-free graphene nanoplatelets with alumina for thermally conductive and electrically insulating epoxy composites," *Composites Science and Technology*, vol. 137, pp. 16 – 23, 2016.

[78] F. Wang, X. Zeng, Y. Yao, R. Sun, J. Xu, and C.-P. Wong, "Silver nanoparticle-deposited boron nitride nanosheets as fillers for polymeric composites with high thermal conductivity," *Scientific Reports*, vol. 6, p. 19394, Jan. 2016.

[79] H. Im and J. Kim, "Thermal conductivity of a graphene oxide–carbon nanotube hybrid/epoxy composite," *Carbon*, vol. 50, no. 15, pp. 5429 – 5440, 2012.

[80] K. Kim, H. Ju, and J. Kim, "Vertical particle alignment of boron nitride and silicon carbide binary filler system for thermal conductivity enhancement," *Composites Science and Technology*, vol. 123, pp. 99 – 105, 2016.

[81] Y. Yao, J. Sun, X. Zeng, R. Sun, J.-B. Xu, and C.-P. Wong, "Construction of 3D skeleton for polymer composites achieving a high thermal conductivity," *Small*, vol. 14, no. 13, p. 1704044, 2018.

[82] T. Zhou, X. Wang, X. Liu, and D. Xiong, "Improved thermal conductivity of epoxy composites using a hybrid multi-walled carbon nanotube/micro-SiC filler," *Carbon*, vol. 48, pp. 1171–1176, Apr. 2010.

[83] S. Choi and J. Kim, "Thermal conductivity of epoxy composites with a binary-particle system of aluminum oxide and aluminum nitride fillers," *Composites Part B: Engineering*, vol. 51, pp. 140–147, Aug. 2013.

[84] B. Tang, X. Li, W. Huang, H. Yu, and X. Ling, "Graphene-assisted thermal interface materials with a satisfied interface contact level between the matrix and fillers," *Nanoscale research letters*, vol. 13, no. 1, p. 276, 2018.

[85] W. Yuan, Q. Xiao, L. Li, and T. Xu, "Thermal conductivity of epoxy adhesive enhanced by hybrid graphene oxide/AlN particles," *Applied Thermal Engineering*, vol. 106, pp. 1067 – 1074, 2016.

[86] A. Ma, W. Chen, and Y. Hou, "Enhanced thermal conductivity of epoxy composites with MWCNTs/AlN hybrid filler," *Polymer-Plastics Technology and Engineering*, vol. 51, no. 15, pp. 1578–1582, 2012.

[87] P. Zhang, Q. Li, and Y. Xuan, "Thermal contact resistance of epoxy composites incorporated with nano-copper particles and the multi-walled carbon nanotubes," *Composites Part A: Applied Science and Manufacturing*, vol. 57, pp. 1 – 7, 2014.

[88] S.-Y. Yang, W.-N. Lin, Y.-L. Huang, H.-W. Tien, J.-Y. Wang, C.-C. M. Ma, S.-M. Li, and Y.-S. Wang, "Synergetic effects of graphene platelets and carbon nanotubes on the mechanical and thermal properties of epoxy composites," *Carbon*, vol. 49, no. 3, pp. 793 – 803, 2011.

[89] C. Liu, C. Chen, H. Wang, M. Chen, D. Zhou, Z. Xu, and W. Yu, "Synergistic effect of irregular shaped particles and graphene on the thermal conductivity of epoxy composites," *Polymer Composites*, vol. 40, no. S2, pp. E1294–E1300, 2019.

[90] F.-p. Du, W. Yang, F. Zhang, C.-Y. Tang, S.-p. Liu, L. Yin, and W.-C. Law, "Enhancing the heat transfer efficiency in graphene–epoxy nanocomposites using a magnesium oxide–graphene hybrid structure," *ACS Applied Materials & Interfaces*, vol. 7, no. 26, pp. 14397–14403, 2015.

[91] C. Zeng, S. Lu, L. Song, X. Xiao, J. Gao, L. Pan, Z. He, and J. Yu, "Enhanced thermal properties in a hybrid graphene–alumina filler for epoxy composites," *RSC Adv.*, vol. 5, pp. 35773–35782, 2015.

[92] T. Huang, X. Zeng, Y. Yao, R. Sun, F. Meng, J. Xu, and C. Wong, "Boron nitride@graphene oxide hybrids for epoxy composites with enhanced thermal conductivity," *RSC Adv.*, vol. 6, pp. 35847–35854, 2016.

[93] T.-L. Li and S. L.-C. Hsu, "Enhanced thermal conductivity of polyimide films via a hybrid of micro- and nano-sized boron nitride," *The Journal of Physical Chemistry B*, vol. 114, pp. 6825–6829, May 2010.

[94] Y. Zhou, S. Yu, H. Niu, and F. Liu, "Synergistic improvement in thermal conductivity of polyimide nanocomposite films using boron nitride coated copper nanoparticles and nanowires," *Polymers*, vol. 10, p. 1412, Dec. 2018.

[95] M.-H. Tsai, I.-H. Tseng, J.-C. Chiang, and J.-J. Li, "Flexible polyimide films hybrid with functionalized boron nitride and graphene oxide simultaneously to improve thermal conduction and dimensional stability," *ACS Applied Materials & Interfaces*, vol. 6, pp. 8639–8645, June 2014.

[96] L. Shao, L. Shi, X. Li, N. Song, and P. Ding, "Synergistic effect of BN and graphene nanosheets in 3D framework on the enhancement of thermal conductive properties of polymeric composites," *Composites Science and Technology*, vol. 135, pp. 83–91, Oct. 2016.

[97] J. Yu, H. K. Choi, H. S. Kim, and S. Y. Kim, "Synergistic effect of hybrid graphene nanoplatelet and multi-walled carbon nanotube fillers on the thermal conductivity of polymer composites and theoretical modeling of the synergistic effect," *Composites Part A: Applied Science and Manufacturing*, vol. 88, pp. 79 – 85, 2016.

[98] J. Gu, Y. Guo, X. Yang, C. Liang, W. Geng, L. Tang, N. Li, and Q. Zhang, "Synergistic improvement of thermal conductivities of polyphenylene sulfide composites filled with boron nitride hybrid fillers," *Composites Part A: Applied Science and Manufacturing*, vol. 95, pp. 267 – 273, 2017.

[99] S. Y. Pak, H. M. Kim, S. Y. Kim, and J. R. Youn, "Synergistic improvement of thermal conductivity of thermoplastic composites with mixed boron nitride and multi-walled carbon nanotube fillers," *Carbon*, vol. 50, pp. 4830–4838, Nov. 2012.

[100] Y. Zhou, X. Zhuang, F. Wu, and F. Liu, "High-performance thermal management nanocomposites: Silver functionalized graphene nanosheets and multiwalled carbon nanotube," *Crystals*, vol. 8, p. 398, Oct. 2018.

[101] B. Zhao, S. Wang, C. Zhao, R. Li, S. M. Hamidinejad, Y. Kazemi, and C. B. Park, "Synergism between carbon materials and Ni chains in flexible poly(vinylidene fluoride) composite films with high heat dissipation to improve electromagnetic shielding properties," *Carbon*, vol. 127, pp. 469 – 478, 2018.

[102] F. Ren, D. Song, Z. Li, L. Jia, Y. Zhao, D. Yan, and P. Ren, "Synergistic effect of graphene nanosheets and carbonyl iron–nickel alloy hybrid filler on electromagnetic interference shielding and thermal conductivity of cyanate ester composites," *J. Mater. Chem. C*, vol. 6, pp. 1476–1486, 2018.

[103] J. Jiang, S. Yang, L. Li, and S. Bai, "High thermal conductivity polylactic acid composite for 3D printing: Synergistic effect of graphene and alumina," *Polymers for Advanced Technologies*, vol. 31, no. 6, pp. 1291–1299, 2020.

[104] L. Sim, S. Ramanan, H. Ismail, K. Seetharamu, and T. Goh, "Thermal characterization of Al_2O_3 and ZnO reinforced silicone rubber as thermal pads for heat dissipation purposes," *Thermochimica Acta*, vol. 430, pp. 155–165, June 2005.

[105] W. Zhou, "Thermal and dielectric properties of the AlN particles reinforced linear low-density polyethylene composites," *Thermochimica Acta*, vol. 512, no. 1, pp. 183 – 188, 2011.

[106] W. Yu, H. Xie, Y. Li, and L. Chen, "Experimental investigation on thermal conductivity and viscosity of aluminum nitride nanofluid," *Particuology*, vol. 9, no. 2, pp. 187 – 191, 2011.

[107] Z. Gao and L. Zhao, "Effect of nano-fillers on the thermal conductivity of epoxy composites with micro-Al_2O_3 particles," *Materials & Design (1980-2015)*, vol. 66, pp. 176–182, Feb. 2015.

[108] J. Theerthagiri, S. Salla, R. A. Senthil, P. Nithyadharseni, A. Madankumar, P. Arunachalam, T. Maiyalagan, and H.-S. Kim, "A review on ZnO nanostructured materials: energy, environmental and biological applications," *Nanotechnology*, vol. 30, p. 392001, July 2019.

[109] J. Han, P. Mantas, and A. Senos, "Effect of Al and Mn doping on the electrical conductivity of ZnO," *Journal of the European Ceramic Society*, vol. 21, no. 10, pp. 1883 – 1886, 2001.

[110] K. S. Novoselov, A. K. Geim, S. V. Morozov, D. Jiang, Y. Zhang, S. V. Dubonos, I. V. Grigorieva, and A. A. Firsov, "Electric field effect in atomically thin carbon films," *Science (New York, N.Y.)*, vol. 306, pp. 666–9, Oct. 2004.

[111] J. I. Paredes, S. Villar-Rodil, P. Solis-Fernandez, A. Martinez-Alonso, and J. M. D. Tascon, "Atomic force and scanning tunneling microscopy imaging of graphene nanosheets derived from graphite oxide," *Langmuir*, vol. 25, pp. 5957–5968, May 2009.

[112] C. Lee, X. Wei, J. W. Kysar, and J. Hone, "Measurement of the elastic properties and intrinsic strength of monolayer graphene," *Science (New York, N.Y.)*, vol. 321, pp. 385–8, July 2008.

[113] K. I. Bolotin, K. J. Sikes, Z. Jiang, M. Klima, G. Fudenberg, J. Hone, P. Kim, and H. L. Stormer, "Ultrahigh electron mobility in suspended graphene," *Solid State Communications*, vol. 146, pp. 351–355, June 2008.

[114] J. S. Bunch, A. M. van der Zande, S. S. Verbridge, I. W. Frank, D. M. Tanenbaum, J. M. Parpia, H. G. Craighead, and P. L. McEuen, "Electromechanical resonators from graphene sheets," *Science (New York, N.Y.)*, vol. 315, pp. 490–3, Jan. 2007.

[115] A. A. Balandin, S. Ghosh, W. Bao, I. Calizo, D. Teweldebrhan, F. Miao, and C. N. Lau, "Superior thermal conductivity of single-layer graphene," *Nano Letters*, vol. 8, pp. 902–907, Mar. 2008.

[116] G. Speranza, "The role of functionalization in the applications of carbon materials: An overview," *C — Journal of Carbon Research*, vol. 5, p. 84, Dec. 2019.

[117] S. Ghosh, I. Calizo, D. Teweldebrhan, E. P. Pokatilov, D. L. Nika, A. A. Balandin, W. Bao, F. Miao, and C. N. Lau, "Extremely high thermal conductivity of graphene: Prospects for thermal management applications in nanoelectronic circuits," *Applied Physics Letters*, vol. 92, p. 151911, Apr. 2008.

[118] J. H. Seol, I. Jo, A. L. Moore, L. Lindsay, Z. H. Aitken, M. T. Pettes, X. Li, Z. Yao, R. Huang, D. Broido, N. Mingo, R. S. Ruoff, and L. Shi, "Two-dimensional phonon transport in supported graphene," *Science*, vol. 328, no. 5975, pp. 213–216, 2010.

[119] W. Cai, A. L. Moore, Y. Zhu, X. Li, S. Chen, L. Shi, and R. S. Ruoff, "Thermal transport in suspended and supported monolayer graphene grown by chemical vapor deposition," *Nano Letters*, vol. 10, pp. 1645–1651, May 2010.

[120] H. Wang, K. Kurata, T. Fukunaga, H. Ago, H. Takamatsu, X. Zhang, T. Ikuta, K. Takahashi, T. Nishiyama, and Y. Takata, "Simultaneous measurement of electrical and thermal conductivities of suspended monolayer graphene," *Journal of Applied Physics*, vol. 119, no. 24, p. 244306, 2016.

[121] Y. Xu, H. Cao, Y. Xue, B. Li, and W. Cai, "Liquid-phase exfoliation of graphene: An overview on exfoliation media, techniques, and challenges," *Nanomaterials*, vol. 8, p. 942, Nov. 2018.

[122] K. R. Paton, E. Varrla, C. Backes, R. J. Smith, U. Khan, A. O'Neill, C. Boland, M. Lotya, O. M. Istrate, P. King, T. Higgins, S. Barwich, P. May, P. Puczkarski, I. Ahmed, M. Moebius, H. Pettersson, E. Long, J. Coelho, S. E. O'Brien, E. K. McGuire, B. M. Sanchez, G. S. Duesberg, N. McEvoy, T. J. Pennycook, C. Downing, A. Crossley, V. Nicolosi, and J. N. Coleman, "Scalable production of large quantities of defect-free few-layer graphene by shear exfoliation in liquids," *Nature Materials*, vol. 13, pp. 624–630, Apr. 2014.

[123] M. Wang, D. Galpaya, Z. B. Lai, Y. Xu, and C. Yan, "Surface functionalization on the thermal conductivity of graphene–polymer nanocomposites," *International Journal of Smart and Nano Materials*, vol. 5, no. 2, pp. 123–132, 2014.

[124] Y. Wang, H. F. Zhan, Y. Xiang, C. Yang, C. M. Wang, and Y. Y. Zhang, "Effect of covalent functionalization on thermal transport across graphene-polymer interfaces," *Journal of Physical Chemistry C*, vol. 119, pp. 12731–12738, June 2015.

[125] Y. Wang, C. Yang, Y.-W. Mai, and Y. Zhang, "Effect of non-covalent functionalisation on thermal and mechanical properties of graphene-polymer nanocomposites," *Carbon*, vol. 102, pp. 311 – 318, 2016.

[126] X. Liu, G. Zhang, and Y. W. Zhang, "Thermal conduction across graphene cross-linkers," *Journal of Physical Chemistry C*, vol. 118, pp. 12541–12547, June 2014.

[127] Z. Zabihi and H. Araghi, "Effect of functional groups on thermal conductivity of graphene/paraffin nanocomposite," *Physics Letters A*, vol. 380, no. 45, pp. 3828 – 3831, 2016.

[128] D. L. Nika, E. P. Pokatilov, A. S. Askerov, and A. A. Balandin, "Phonon thermal conduction in graphene: Role of umklapp and edge roughness scattering," *Phys. Rev. B*, vol. 79, p. 155413, Apr. 2009.

[129] D. L. Nika, S. Ghosh, E. P. Pokatilov, and A. A. Balandin, "Lattice thermal conductivity of graphene flakes: Comparison with bulk graphite," *Applied Physics Letters*, vol. 94, no. 20, p. 203103, 2009.

[130] D. L. Nika, A. S. Askerov, and A. A. Balandin, "Anomalous size dependence of the thermal conductivity of graphene ribbons," *Nano letters*, vol. 12, no. 6, pp. 3238–3244, 2012.

[131] M. T. Pettes, I. Jo, Z. Yao, and L. Shi, "Influence of polymeric residue on the thermal conductivity of suspended bilayer graphene," *Nano letters*, vol. 11, no. 3, pp. 1195–1200, 2011.

[132] M. M. Sadeghi, I. Jo, and L. Shi, "Phonon-interface scattering in multilayer graphene on an amorphous support," *Proceedings of the National Academy of Sciences*, vol. 110, no. 41, pp. 16321–16326, 2013.

[133] G. C. Correa, C. J. Foss, and Z. Aksamija, "Interface thermal conductance of van der Waals monolayers on amorphous substrates," *Nanotechnology*, vol. 28, p. 135402, Mar. 2017.

[134] W. Jang, Z. Chen, W. Bao, C. N. Lau, and C. Dames, "Thickness-dependent thermal conductivity of encased graphene and ultrathin graphite," *Nano Letters*, vol. 10, pp. 3909–3913, Oct. 2010.

[135] J. Renteria, D. Nika, and A. Balandin, "Graphene thermal properties: Applications in thermal management and energy storage," *Applied Sciences*, vol. 4, p. 525–547, Nov. 2014.

[136] Y. Sun, B. Tang, W. Huang, S. Wang, Z. Wang, X. Wang, Y. Zhu, and C. Tao, "Preparation of graphene modified epoxy resin with high thermal conductivity by optimizing the morphology of filler," *Applied Thermal Engineering*, vol. 103, pp. 892 – 900, 2016.

[137] X. Shen, Z. Wang, Y. Wu, X. Liu, Y. B. He, and J. K. Kim, "Multilayer graphene enables higher efficiency in improving thermal conductivities of graphene/epoxy composites," *Nano Letters*, vol. 16, pp. 3585–3593, June 2016.

[138] L. Song, L. Ci, H. Lu, P. B. Sorokin, C. Jin, J. Ni, A. G. Kvashnin, D. G. Kvashnin, J. Lou, B. I. Yakobson, and P. M. Ajayan, "Large scale growth and characterization of atomic hexagonal boron nitride layers," *Nano Letters*, vol. 10, pp. 3209–3215, Aug. 2010.

[139] D. Golberg, Y. Bando, Y. Huang, T. Terao, M. Mitome, C. Tang, and C. Zhi, "Boron nitride nanotubes and nanosheets," *ACS Nano*, vol. 4, pp. 2979–2993, June 2010.

[140] E. K. Sichel, R. E. Miller, M. S. Abrahams, and C. J. Buiocchi, "Heat capacity and thermal conductivity of hexagonal pyrolytic boron nitride," *Physical Review B*, vol. 13, pp. 4607–4611, May 1976.

[141] C. Sevik, A. Kinaci, J. B. Haskins, and T. Çağin, "Characterization of thermal transport in low-dimensional boron nitride nanostructures," *Phys. Rev. B*, vol. 84, p. 085409, Aug. 2011.

[142] L. Lindsay and D. A. Broido, "Theory of thermal transport in multilayer hexagonal boron nitride and nanotubes," *Phys. Rev. B*, vol. 85, p. 035436, Jan. 2012.

[143] C. Sevik, A. Kinaci, J. B. Haskins, and T. Çağin, "Influence of disorder on thermal transport properties of boron nitride nanostructures," *Phys. Rev. B*, vol. 86, p. 075403, Aug. 2012.

[144] I. Jo, M. T. Pettes, J. Kim, K. Watanabe, T. Taniguchi, Z. Yao, and L. Shi, "Thermal conductivity and phonon transport in suspended few-layer hexagonal boron nitride," *Nano Letters*, vol. 13, pp. 550–554, Feb. 2013.

[145] H. Zhou, J. Zhu, Z. Liu, Z. Yan, X. Fan, J. Lin, G. Wang, Q. Yan, T. Yu, P. M. Ajayan, and J. M. Tour, "High thermal conductivity of suspended few-layer hexagonal boron nitride sheets," *Nano Research*, vol. 7, pp. 1232–1240, Aug. 2014.

[146] C. Wang, J. Guo, L. Dong, A. Aiyiti, X. Xu, and B. Li, "Superior thermal conductivity in suspended bilayer hexagonal boron nitride," *Scientific Reports*, vol. 6, pp. 1–6, May 2016.

[147] K. Nose, H. Oba, and T. Yoshida, "Electric conductivity of boron nitride thin films enhanced by in situ doping of zinc," *Applied Physics Letters*, vol. 89, no. 11, p. 112124, 2006.

[148] M. R. Uddin, S. Majety, J. Li, J. Y. Lin, and H. X. Jiang, "Layer-structured hexagonal (BN)C semiconductor alloys with tunable optical and electrical properties," *Journal of Applied Physics*, vol. 115, no. 9, p. 093509, 2014.

[149] M. Shtein, R. Nadiv, M. Buzaglo, K. Kahil, and O. Regev, "Thermally conductive graphene-polymer composites: Size, percolation, and synergy effects," *Chemistry of Materials*, 2015.

[150] D. J. Plazek and I. C. Choy, "The physical properties of bisphenol-a-based epoxy resins during and after curing. II. Creep behavior above and below the glass transition temperature," *Journal of Polymer Science Part B: Polymer Physics*, vol. 27, no. 2, pp. 307–324, 1989.

[151] L. Matějka, P. Chabanne, L. Tighzert, and J. P. Pascault, "Cationic polymerization of diglycidyl ether of bisphenol A," *Journal of Polymer Science Part A: Polymer Chemistry*, vol. 32, no. 8, pp. 1447–1458, 1994.

[152] W. dos Santos, J. de Sousa, and R. Gregorio, "Thermal conductivity behaviour of polymers around glass transition and crystalline melting temperatures," *Polymer Testing*, vol. 32, no. 5, pp. 987 – 994, 2013.

Chapter 3

Methods

3.1 Laser Flash Analysis

The Laser Flash Analysis (LFA) system is a transient thermal properties analysis technique that directly measures the thermal diffusivity of a material with a known thickness [1, 2]. It is a mature technique that has extensive adoption in the TIM research field. The thermal conductivity of a sample can be determined from the classic relationship $K = \rho C_p \alpha$, where ρ is the volumetric mass density, C_p is the specific heat, and α is the thermal diffusivity that can be directly measured in LFA. Thus, the thermal conductivity can be determined with the addition of two other experimental techniques, such as density via Archimedes' Principle and Differential Scanning Calorimetry, or by trivial rule of mixtures calculations.

Thermal diffusivity is the thermal parameter directly measured by the LFA technique. This parameter is more challenging to intuitively understand compared to the more popular thermal conductivity metric. Thermal diffusivity, α, is a proportionality constant from the heat diffusion equation:

$$\frac{\partial T}{\partial t} = \alpha \nabla^2 T \tag{3.1}$$

where T is a temperature distribution function and t is time. α, a property of the material of interest, sets the relation between how far a given temperature gradient diffuses with advancing time. It is purely a response rate of the material and alone provides no information about the amount of energy transmitted like thermal conductivity.

The LFA technique works by shining a light source – in this case a Xenon flash lamp – on the flat bottom surface of a sample of interest. Due to this, it is crucial that the sample absorbs the incoming light at a very minute depth or be coated in a material that does. As the light is absorbed on this surface it heats up, creating a temperature gradient between it and the top surface. This produces a heat wave traveling towards the cooler surface, as per the 2$^{\text{nd}}$ Law of Thermodynamics. At the moment the heat wave reaches the opposing, top surface, it's temperature rises. As a typical black body radiates per Planck's Law, as the temperature increases, the amount of total radiated energy increases as does its spectrum blue-shift. The LFA machine uses a low-bandgap, liquid nitrogen-cooled detector whose terminal voltage difference increases with greater intensity of radiation of sufficient energy. Figure 3.1 shows the equipment used in this study.

The theory of the LFA begins from Carslaw and Jaeger; the temperature over time for an insulated solid of thickness L and initial temperature $T(x,0)$ is [1,3]:

$$T(x,t) = \frac{1}{L}\int_0^L T(x,0)dx + \frac{2}{L}\sum_{n=1}^{\infty} \exp\left(-\frac{n^2\pi^2\alpha t}{L^2}\right) \times \cos\left(\frac{n\pi x}{L}\right)\int_0^L T(x,0)\cos\left(\frac{n\pi x}{L}\right)dx \quad (3.2)$$

where α is the thermal diffusivity of the sample typically in units of cm^2/sec. Flashing a lamp whose energy (H) is then homogeneously and instantaneously absorbed at the surface located at x=0 within a depth of g gives the following

Figure 3.1: LFA 467 HyperFlash equipment by NETZSCH GmbH used in this study.

temperatures at that moment:

$$T(x,0) = \frac{H}{\rho C g} \qquad \text{for } 0 < \mathrm{x} < \mathrm{g} \tag{3.3}$$

$$T(x,0) = 0 \qquad \text{for } \mathrm{g} < \mathrm{x} < \mathrm{L} \tag{3.4}$$

where ρ is the volumetric mass density in g/cm^3 and C is the specific heat capacity in cal/g°C. Using these initial conditions, Equation 3.1 can be rewritten as follows:

$$T(x,t) = \frac{H}{\rho C L}\left[1 + 2\sum_{n=1}^{\infty}\cos\left(\frac{n\pi x}{L}\frac{\sin(n\pi g/L)}{n\pi g/L}\right) \times \exp\left(\frac{-n^2\pi^2\alpha t}{L^2}\right)\right] \tag{3.5}$$

Because g is a very small value for opaque samples and coatings, the small-angle approximation may be made on Equation 3.5, resulting in the following expression for the temperature at the rear surface of the sample.

$$T(L,t) = \frac{H}{\rho C L}\left[1 + 2\sum_{n=1}^{\infty}(-1)^n \exp\left(\frac{-n^2\pi^2\alpha t}{L^2}\right)\right] \tag{3.6}$$

Combining parameters into the new functions below:

$$V(L,t) = \frac{T(L,t)}{T_M} \tag{3.7}$$

$$\omega = \frac{\pi^2\alpha t}{L^2} \tag{3.8}$$

alters equation 3.6 to:

$$V = 1 + 2\sum_{n=1}^{\infty}\big(-1\big)^n \exp\Big(-n^2\omega\Big) \tag{3.9}$$

Since the function of V is a ratio of the temperature at the back surface over time to the maximum temperature reached, its value can never exceed unity. When V reaches half of its maximum – 0.5 – ω has a value of 1.38 at that point. Plugging this value in Equation 3.8 and rearranging yields the thermal diffusivity:

$$\alpha = \frac{1.38L^2}{\pi^2 t_{\frac{1}{2}}} \tag{3.10}$$

When attaining the specific heat capacity or thermal conductivity via this tech-

nique, the total amount of heat supplied to the sample must be known. The specific heat capacity is shown below:

$$C = \frac{H}{\rho L T_M} \tag{3.11}$$

and, finally, the thermal conductivity is:

$$K = \frac{\alpha H}{L T_M} = \alpha \rho C \tag{3.12}$$

3.2 Transient Plane Source

The Transient Plane Source (Hot Disk® TPS 3500) method determines thermal properties of samples by passing a current through a sensor, shown in Figure 3.2a, typically sandwiched between two identical samples of interest, schematically depicted in Figure 3.2b, then recording the temperature-dependent resistance of the sensor over time [4]. The recorded resistance over time will be affected by the thermal properties of the sample that surrounds the sensor. Specific experimental parameters such as the time of recording and total output power must be carefully selected based on the sample size and expected thermal properties for both experimental accuracy and instrument safety. For instance, should too great of an electrical current be passed through the coil the sample under analysis may not be able to cool the sensor fast enough, resulting in the sensor burning itself out.

The resistance of the sensor at any time is given by the following expression [4]:

$$R(t) = R_0 \Big[1 + \gamma \overline{\Delta T(\tau)} \Big] \tag{3.13}$$

where R_0 is the resistance of the element at equilibrium, γ is the temperature coefficient that relates the temperature to resistance, and $\overline{\Delta T(\tau)}$ is the mean of

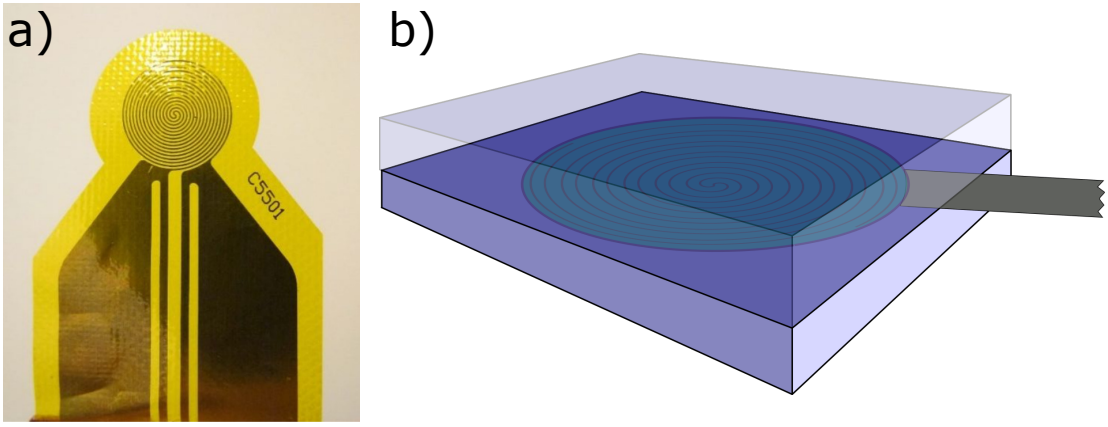

Figure 3.2: a) Picture of a Transient Plane Source sensor with yellow Kapton encasing. b) Schematic of this sensor between material of interest for analysis. Note that this schematic exaggerates the size of the sensor to the sample dimensions.

the time-dependent temperature increase. The parameter τ is defined as:

$$\tau = \sqrt{\frac{t\alpha}{a^2}} \tag{3.14}$$

where α is the thermal diffusivity and a is the radius of the sensor [4]. Rearranging Equation 3.13 results in:

$$\overline{\Delta T(\tau)} = \Delta T_{ave}(\tau) + \Delta T_i = \frac{R(t)/R_0 - 1}{\gamma} \tag{3.15}$$

where ΔT_i is the temperature difference between the sensor and adjacent sample surfaces and is primarily determined by quality of thermal contact between the two. Figure 3.3 represents ΔT_i with a typical measurement's temperature curve in which the temperature of the sample always lags behind the temperature of the sensor.

The average temperature change is directly obtained from Carslaw and Jaegar [3]:

$$\overline{\Delta T(\tau)} = \frac{P_0 D_s(\tau)}{\pi^{3/2} a K} \tag{3.16}$$

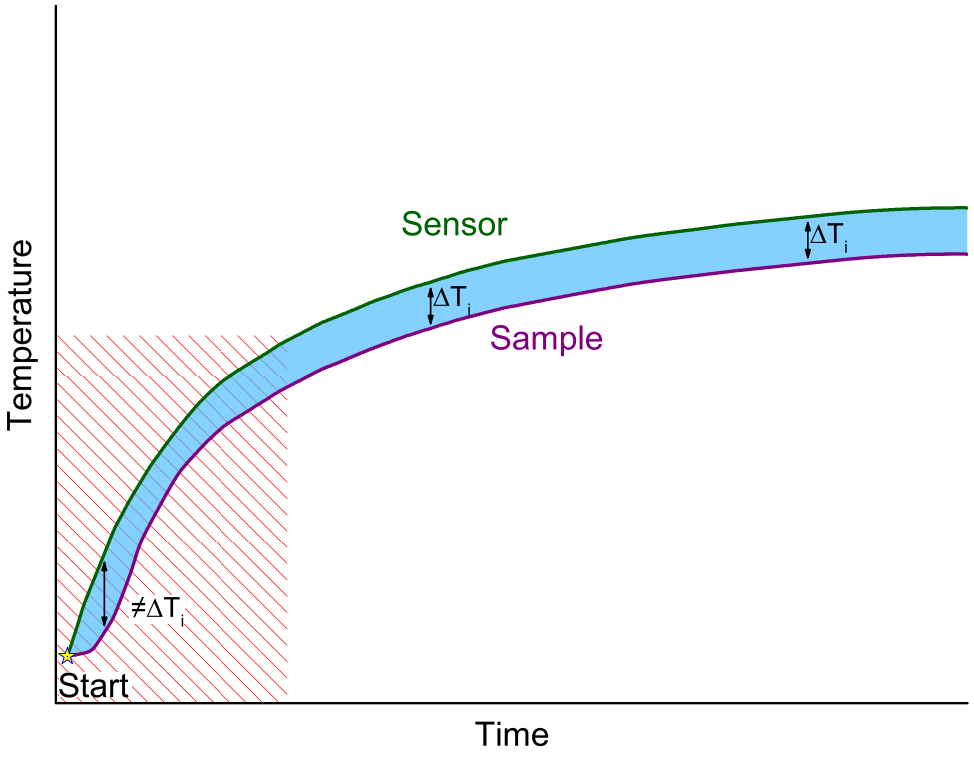

Figure 3.3: Plot of the temperature behaviors of the sensor (green) and the sample surface (purple) over time with the difference shaded blue. Note that soon after the beginning of an experiment there is a larger, unrepresentative temperature difference between the two that stabilizes as the experiment progresses in time.

where P_0 is the total dissipated power, K is the thermal conductivity, and $D_s(\tau)$ is a time-dependent function constructed for the circular sensor geometry with m number of rings, expressed below:

$$D_s(\tau) = \frac{1}{\Big[m\big(m+1\big)\Big]^2} \int_0^\tau \sigma^{-2} \left[\sum_{l=1}^{m} l \sum_{k=1}^{m} k \exp\left(-\frac{l^2+k^2}{4m^2\sigma^2} \right) \left(\frac{lk}{2m^2\sigma^2} \right) I_0 \right] d\sigma \tag{3.17}$$

where I_0 is a modified Bessel function. Plotting the experimental temperature increase versus $D_s(\tau)$ results in a line whose slope m is of course [5]:

$$m = \frac{P_0}{\pi^{3/2} a K} \tag{3.18}$$

With all other parameters in Equation 3.18 known, the thermal conductivity is then determined.

3.3 Archimedes' Principle Density

Density must be measured accurately in order to calculate the thermal conductivity with the LFA method. This method determines the density of a sample by comparison of its measured weight in and out of water, i.e. with and without a considerable volume-dependent buoyancy force contributing to readings. The equipment made by Mettler Toledo Inc. is shown in Figure 3.4.

The density of a sample is determined with measurements of weight in and out of water and calculated with the following equation

$$\rho = \frac{W_a}{W_a - W_l}\Big(\rho_l - \rho_a\Big) + \rho_a \tag{3.19}$$

where W_a is the sample's measured weight in gas, atmospheric pressure air in these instances; W_l is the measured weight in liquid, de-ionized water in these instances; ρ_l is the volumetric mass density of the liquid; and ρ_a is the same density metric of the gas used.

3.4 Specific Heat Capacity Calculations

The specific heat capacities of composites were determined via calculation from the Maxwell-Garnett effective medium approximation, often called the Kopp-Neumann rule when applied to composite specific heat capacities [6, 7].

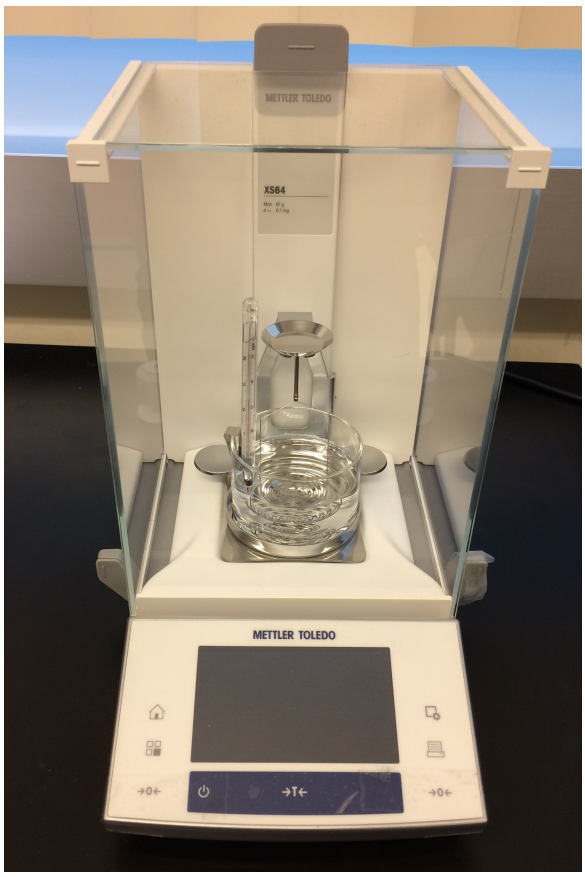

Figure 3.4: Density measuring scale based on the comparison of sample weight while in and out of water. Reprinted with permission from the publication J. S. Lewis, Z. Barani, A. S. Magana, F. Kargar, and A. A. Balandin, "Thermal and electrical conductivity control in hybrid composites with graphene and boron nitride fillers" *Materials Research Express*, vol. 6, no. 8, p. 085325, May 2019. Copyright © Institute of Physics.

$$C_T = \sum_{i=1}^{N} C_i f_i \tag{3.20}$$

where the total composite specific heat, C_T, is a sum of the products of each constituent component's specific heat and the volume fraction that they comprise. The sum of f_i alone is unity for all complete composites.

Specific heats for the materials discussed in the previous chapter used in these calculations came both from literature and DSC experiments. The specific heat of graphite from RT, at which point it is 0.72 J/gK, to 125 °C was used in place of

graphene because deviation between the two only occurs below 100 K, a temperature range far below typical interest in these composite materials [8–11]. *h*-BN has a specific heat of 0.807 J/gK at RT [12]. For cured DGEBA epoxy, the specific heat capacity up to 125 °C was experimentally measured with DSC. Using these values, final composite specific heats were calculated.

Bibliography

[1] W. J. Parker, R. J. Jenkins, C. P. Butler, and G. L. Abbott, "Flash method of determining thermal diffusivity, heat capacity, and thermal conductivity," *Journal of Applied Physics*, vol. 32, no. 9, pp. 1679–1684, 1961.

[2] P. S. Gaal, M. A. Thermitus, and D. E. Stroe, "Thermal conductivity measurements using the flash method," *Journal of Thermal Analysis and Calorimetry*, vol. 78, no. 1, pp. 185–189, 2004.

[3] H. S. Carslaw and J. C. Jaeger, *Conduction of heat in solids*. Clarendon Press, 1959.

[4] S. E. Gustafsson, "Transient plane source techniques for thermal conductivity and thermal diffusivity measurements of solid materials," *Review of Scientific Instruments*, vol. 62, no. 3, pp. 797–804, 1991.

[5] Hot Disk®, "Hot Disk thermal constants analyzer instruction manual," 2014.

[6] J. C. M. Garnett and J. Larmor, "VII. Colours in metal glasses, in metallic films, and in metallic solutions," *Philosophical Transactions of the Royal Society of London. Series A, Containing Papers of a Mathematical or Physical Character*, vol. 205, no. 387-401, pp. 237–288, 1906.

[7] J. E. Hurst and B. K. Harrison, "Estimation of liquid and solid heat capacities using a modified kopp's rule," *Chemical Engineering Communications*, vol. 112, no. 1, pp. 21–30, 1992.

[8] A. Butland and R. Maddison, "The specific heat of graphite: An evaluation of measurements," *Journal of Nuclear Materials*, vol. 49, no. 1, pp. 45 – 56, 1973.

[9] J. Hone, "Phonons and thermal properties of carbon nanotubes," in *Carbon Nanotubes: Synthesis, Structure, Properties, and Applications* (M. S. Dresselhaus, G. Dresselhaus, and P. Avouris, eds.), pp. 273–286, Berlin, Heidelberg: Springer Berlin Heidelberg, 2001.

[10] D. L. Nika, A. I. Cocemasov, and A. A. Balandin, "Specific heat of twisted bilayer graphene: Engineering phonons by atomic plane rotations," *Applied Physics Letters*, vol. 105, p. 031904, July 2014.

[11] A. I. Cocemasov, D. L. Nika, and A. A. Balandin, "Engineering of the thermodynamic properties of bilayer graphene by atomic plane rotations: the role of the out-of-plane phonons," *Nanoscale*, vol. 7, pp. 12851–12859, Aug. 2015.

[12] A. S. Dworkin, D. J. Sasmor, and E. R. Van Artsdalen, "The thermodynamics of boron nitride; low-temperature heat capacity and entropy; heats

of combustion and formation," *The Journal of Chemical Physics*, vol. 22, pp. 837–842, May 1954.

Chapter 4

Graphene and *h*-BN hybrid composites

4.1 Motivation

There is considerable interest in polymer composites with as high of possible thermal conductivity with controlled electrical conductivity [1–5]. This is primarily due to the fact that curing, encapsulating TIMs make direct contact with active circuit elements in semiconductor products. Similarly, non-curing TIMs are fit between junctions in which thermal expansion and contractions tend to "pump" TIM out of the junction over usage, which can lead to spilling onto active circuit elements. The focus of this work is attaining tunable improvement of thermal and electrical conductivity [6]. The majority of high thermal conductivity materials – sp^2 carbons and metals – inevitably produce electrically conductive composites with their inclusion. The separate control of these two parameters is achieved with selective hybridization between graphene and *h*-BN filler materials. The samples prepared have been made at several constant filler loading fractions: 11.4 *vol. %*, 18.1 *vol. %*, 25.5 *vol. %*, and 43.6 *vol. %*. Within each of these total filler loading

fractions the constituency of graphene and *h*-BN is varied to determine the contributions of each individual filler to the overall composite electrical and thermal conductivity. Importantly, the morphology of the graphene and *h*-BN used were intentionally similar. This decision has important implications on widely-reported hybrid-filled synergistic thermal conductivity enhancement – when the use of two fillers results in higher thermal conductivity than either single filler at identical total load level – because this research provides contrapositive empirical evidence to either verify or subvert the importance of morphology on the mechanism of synergy [7–21].

4.2 Raman Spectra

Raman experiments were conducted to confirm the presence of the expected materials in the composites and are presented in Figure 4.1. Characteristic D, G, D', and 2D peaks all irrefutably prove the inclusion of graphene in the composite. Due to the use of 633 nanometer laser excitation and the graphene D peak's dependence on excitation energy, it appears in this study at approximately 1335 cm^{-1} [22]. The existence of the *h*-BN E_{2g} vibrational mode verifies its presence in the composites [23]. Due to the high loading level of the composite studied, very little interaction between laser and DGEBA polymer occurred, resulting in little noticeable polymer peaks. However, at $\approx$1175 cm^{-1} some minute peaks are present, which is consistent with literature on this polymer type [24, 25].

4.3 SEM Analysis

Of principal importance for the improvement of thermal conductivity in a filled composite is the contact, or at least close proximity, of neighboring filler particles.

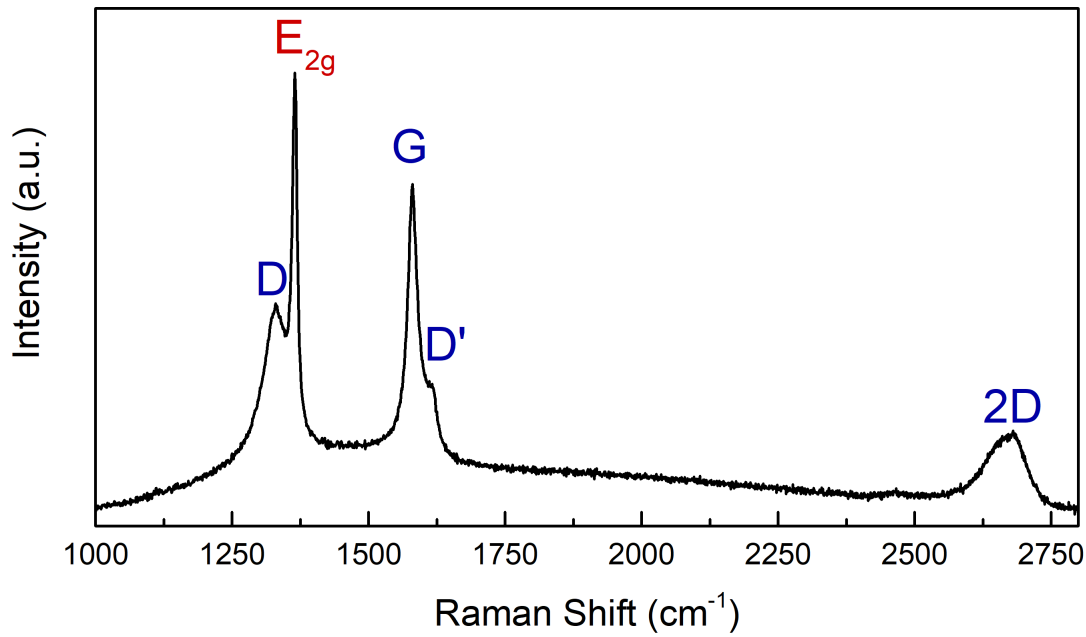

Figure 4.1: Raman spectra obtained from a composite composed of 21.8 *vol. %* graphene and 21.8 *vol. %* *h*-BN. Blue-lettered peak assignments correspond to graphene vibrations and the red-lettered peak assignment represents *h*-BN vibrations. Reprinted with permission from the publication J. S. Lewis, Z. Barani, A. S. Magana, F. Kargar, and A. A. Balandin, "Thermal and electrical conductivity control in hybrid composites with graphene and boron nitride fillers" *Materials Research Express*, vol. 6, no. 8, p. 085325, May 2019. Copyright © Institute of Physics.

The ultimate goal in general TIM research is to replace the path that heat would need to take in the highly insulating polymer matrix to primarily through the highly conducting filler material. To get an understanding of how well the flakes were dispersed in the prepared composite and how close they ended up in proximity to one another, Scanning Electron Microscopy was used to visualize graphene and *h*-BN dispersions. Figure 4.2 shows a custom software pseudo-colorized image of fractured surface of a hybrid-filled sample at 12.7 *vol. %* each of graphene and *h*-BN [26]. The flakes that appear more blue or green through the majority of its breadth is graphene. The flakes that have more rigid edges and appear more pink throughout their surface due to electrical charging are *h*-BN. The two flake types

Figure 4.2: Pseudo-colorized SEM of a 20 *wt. %* graphene and 20 *wt. %* *h*-BN sample with a 1 micron scale bar. Reprinted with permission from the publication J. S. Lewis, Z. Barani, A. S. Magana, F. Kargar, and A. A. Balandin, "Thermal and electrical conductivity control in hybrid composites with graphene and boron nitride fillers" *Materials Research Express*, vol. 6, no. 8, p. 085325, May 2019. Copyright © Institute of Physics.

being in close proximity to one another shows how they can both contribute to thermal conductivity but due to *h*-BN's poor electrical conductivity, still serve to suppress the composite's overall electrical conductivity. It appears, qualitatively speaking in this image, that the *h*-BN flakes may even be serving to separate adjacent graphene flakes, creating a potential mechanism for enhanced electrical conductivity modulation.

4.4 Sample Density

The densities of all lower filler concentration samples, presented in Figure 4.3 were found to be quite uniform within an individual total filler concentration. In the case of the very highly-filled samples, there is greater variance in the measured density with a reducing trend for increasing constituent fraction of graphene due to there being greater voids inside of the high graphene constituency composites and bubble accumulation on the surface. As a result, the trend is an artificial byproduct of experimental error in those samples. The density of the composites increases with the increasing total *vol. %* because the density of the powders is greater than that of the epoxy matrix. The densities of each filler is comparable to one another, explaining the composite's true density displaying a lack of a dependence on altering constituent fractions at each total fraction data set.

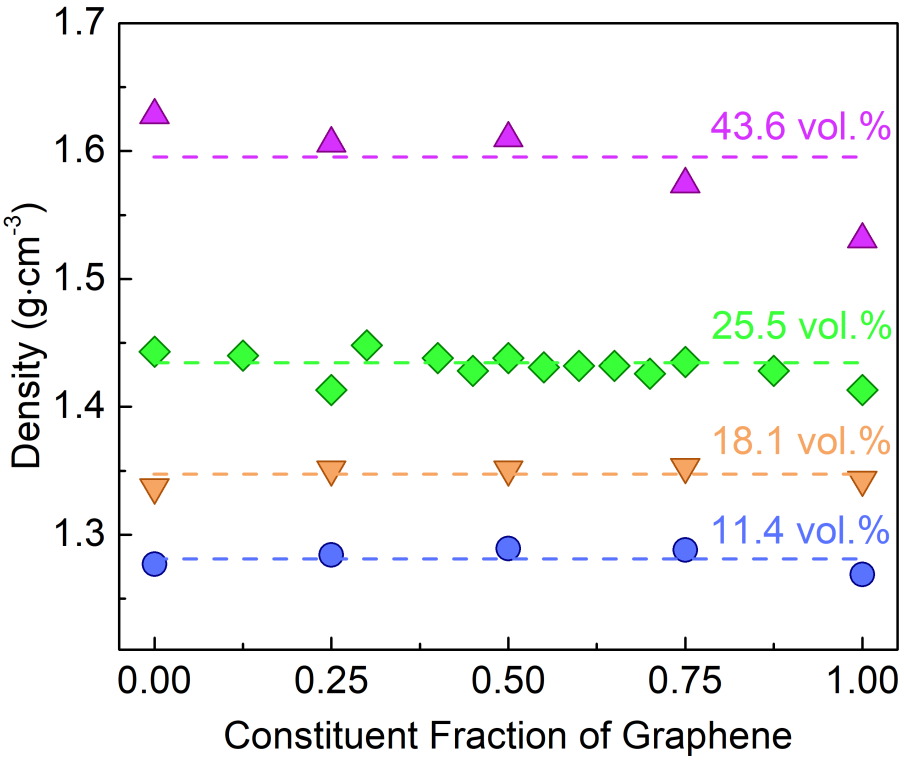

Figure 4.3: Measured densities of samples at each total *vol. %* shown in different colors. An x-axis value of 0.00 corresponds to a sample that has 0% constituent fraction of graphene and 100% constituent fraction of *h*-BN. The average value for each individual total *vol. %* level is shown as a dashed line. Reprinted with permission from the publication J. S. Lewis, Z. Barani, A. S. Magana, F. Kargar, and A. A. Balandin, "Thermal and electrical conductivity control in hybrid composites with graphene and boron nitride fillers" *Materials Research Express*, vol. 6, no. 8, p. 085325, May 2019. Copyright © Institute of Physics.

In the case of 43.6 *vol. %* total filler samples, the decrease in density at increasing graphene constituency will be accounted for through error estimation in the determination of thermal conductivity.

4.5 Specific Heat Capacity

As discussed in section 3.4, the composite specific heat capacities were calculated from the Kopp-Neumann Rule, which will then be used in the calculation of thermal conductivity. The specific heat capacities for the pure epoxy determined by Differential Scanning Calorimetry, *h*-BN, and graphene is 1.5 J/gK, .807 J/gK, and 0.72 J/gK, respectively [27, 28]. Figure 4.4 shows the calculated specific heat capacities of the composites. Given that each filler material has a substantially lower specific heat capacity than the DGEBA epoxy and graphene's is slightly below *h*-BN's, increasing the total filler level greatly reduces and increasing constituent fraction of graphene slighly reduces composite specific heat capacity.

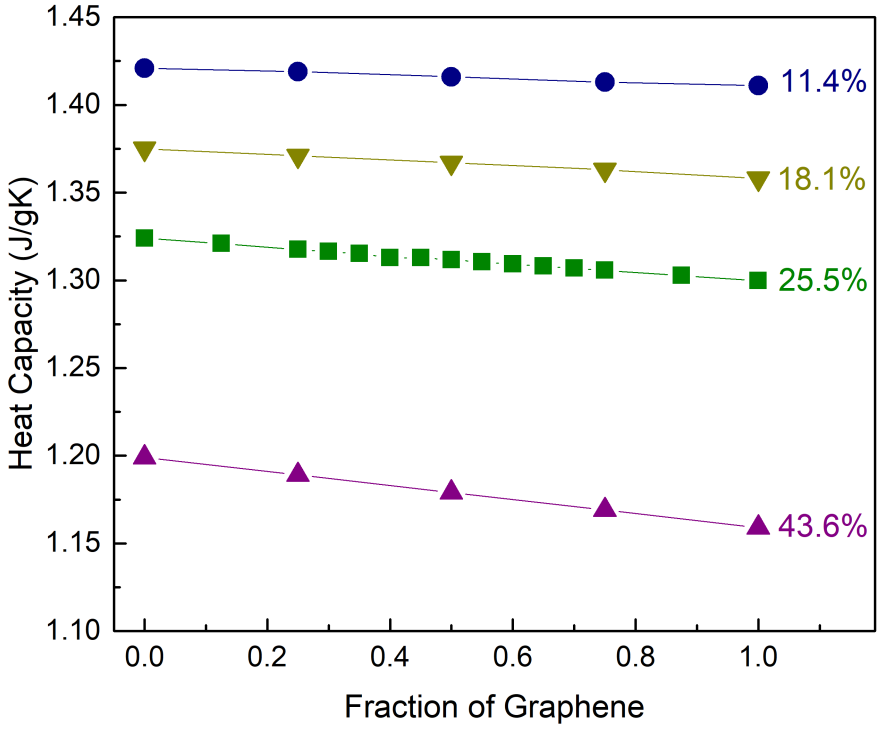

Figure 4.4: Calculated heat capacities of TIM composites through the Effective Medium Approximation.

4.6 Thermal Diffusivity

Figure 4.5 shows the thermal diffusivity results from LFA experiments for the prepared composites. As expected, the thermal diffusivity increases with more total filler content as well as for samples with greater graphene constituency. Importantly, there is a nearly perfectly linear trend in samples of 43.6 *vol. %*. The 25.5 *vol. %* samples, on the other hand, have much greater data scatter; this is due to the fact that these samples are close to the thermal percolation. Subsequent composites analyzed at this filler loading level will result in a wide spread because better and worse percolative networks will be achieved as a result of the random mixing process.

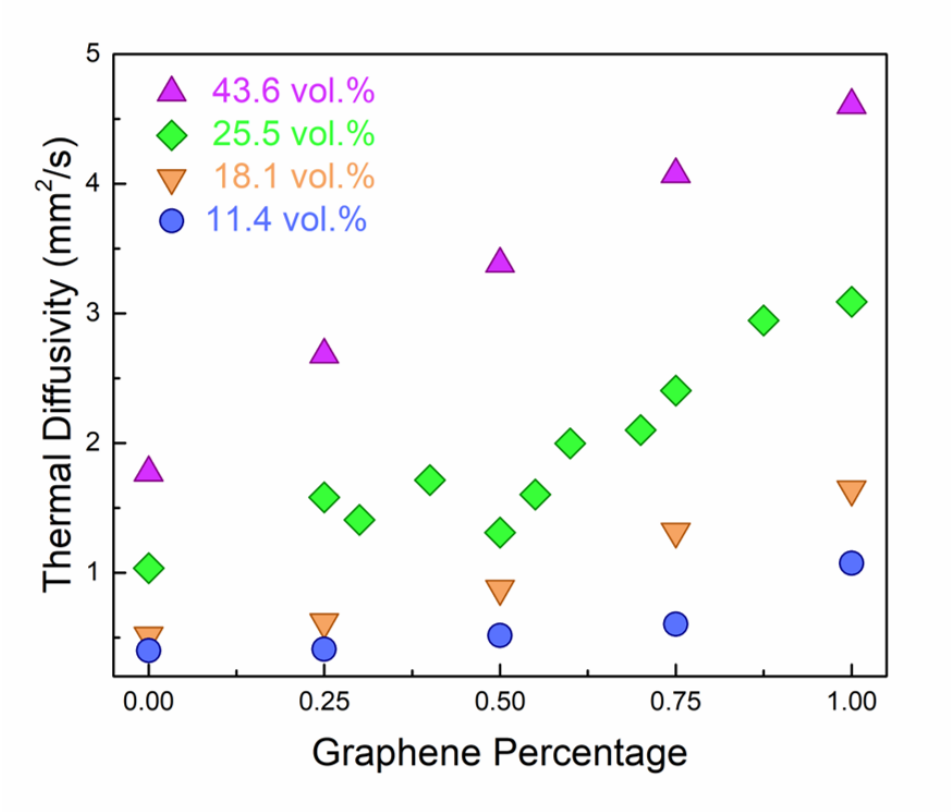

Figure 4.5: Thermal diffusivities of prepared composites directly measured by LFA. Reprinted with permission from the publication J. S. Lewis, Z. Barani, A. S. Magana, F. Kargar, and A. A. Balandin, "Thermal and electrical conductivity control in hybrid composites with graphene and boron nitride fillers" *Materials Research Express*, vol. 6, no. 8, p. 085325, May 2019. Copyright © Institute of Physics.

4.7 Thermal Conductivity

The most popular metric for thermal transport in materials is thermal conductivity. The thermal conductivities of the prepared composites is product of data found in Figures 4.3, 4.4, and 4.5. Figure 4.6 shows the thermal conductivity data for the prepared epoxy composites.

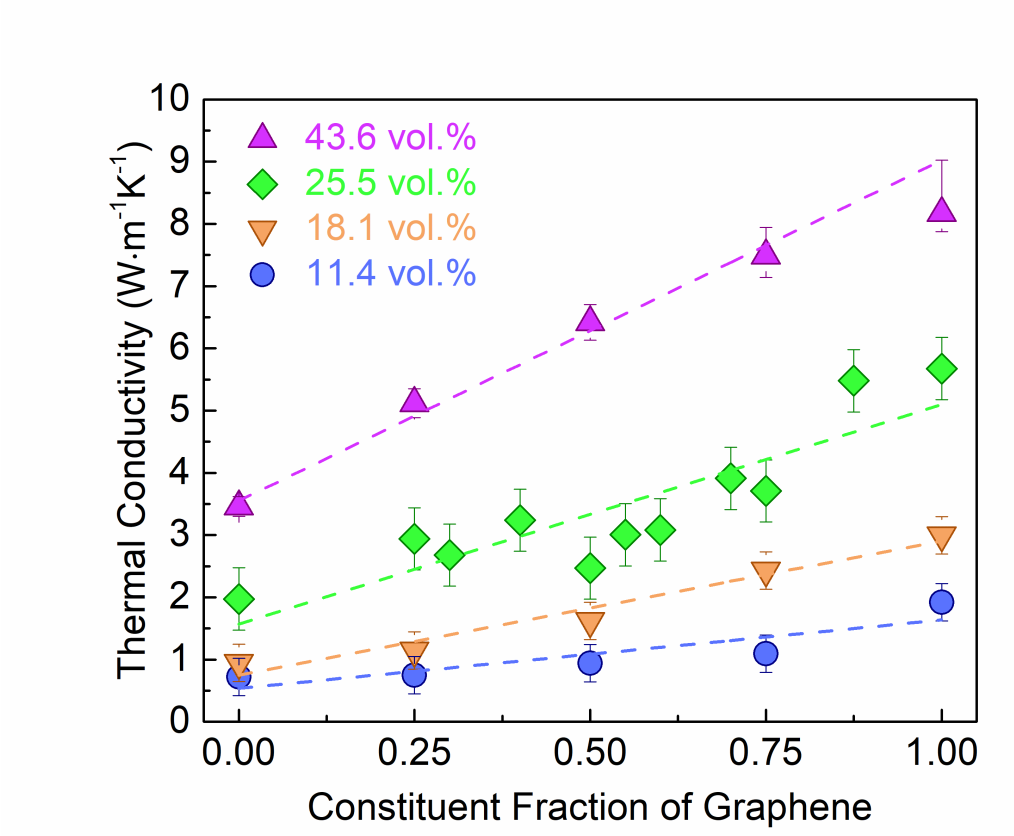

Figure 4.6: Thermal conductivities of samples at different total load fractions with varying constituency of graphene and *h*-BN. Reprinted with permission from the publication J. S. Lewis, Z. Barani, A. S. Magana, F. Kargar, and A. A. Balandin, "Thermal and electrical conductivity control in hybrid composites with graphene and boron nitride fillers" *Materials Research Express*, vol. 6, no. 8, p. 085325, May 2019. Copyright © Institute of Physics.

In all instances higher filler loading levels had superior thermal conductivity and, accounting for random data scatter, the total filler increasing the graphene constituent fraction resulted in greater thermal conductivity performance. At a total filler level of 43.6 *vol. %*, altering the filler loading from *h*-BN to graphene changed the thermal conductivity from 3.46 to 8.2 W/mK. In the 43.6 *vol. %* purely graphene-filled sample there is a clear failure to follow the monotonic trend with altering constituent fraction. This is purely a result of the experimental error in the measurement of the sample's density. As a result the error bar is adjusted

to accommodate the assuredly low estimate for the composite's thermal conductivity. Despite works prior into binary filler composites often showing a synergistic enhancement, no indication of such behavior was seen; the superior intrinsic thermal conductivity of graphene over *h*-BN was always the dominant factor in the composites. Because the two fillers used had comparable morphologies, the lack of a discernible synergistic enhancement verifies that filler morphology must play a role in synergistic behaviors. This demonstrates a very clear strategy for the control of thermal conductivity by altering both the total and constituency fraction of composites.

4.8 Electrical Conductivity

Electrical conductivity measurements were conducted with a simple, yet popular two-probe technique after painting opposing surfaces with silver paint and then measuring the resistance through the sample [29,30]. Knowing the geometry of the sample allows for the direct determination of electrical conductivity. This method is superior in measurement of cross-plane electrical conductivity to the 4-probe and Van der Pauw methods with these flattened cylinder sample shapes.

The inclusion of most carbon materials into the composites increases the electrical conductivity, as has been widely reported [29–35]. However, only in very high concentrations of *h*-BN do composites exhibit measurable electrical conductivity, consistent with what could be expected with known electrical conductivity ranges of *h*-BN [36, 37]. In prior works that used both graphene and *h*-BN as binary fillers, the small size of the *h*-BN filler relative to the graphene allowed it to fit between graphene flakes and electrically isolate them [38, 39]. This led to a dramatic decrease in electrical conductivity with a very remote concentration of *h*-BN filler. The present results, shown in figure 4.7, verify that it is indeed a

geometric effect that has such a large control on the overall electrical conductivity of these composites. Furthermore, an effective means to finely control composite electrical conductivity with graphene and *h*-BN is clearly presented. The range of electrical conductivity exhibited is at least eleven orders of magnitude. Any target electrical conductivity between 10^{-12} and 0.1 S/cm have been confirmed to be plausible in these hybrid composites, specifically dependent on the total and constituent fraction of the two materials.

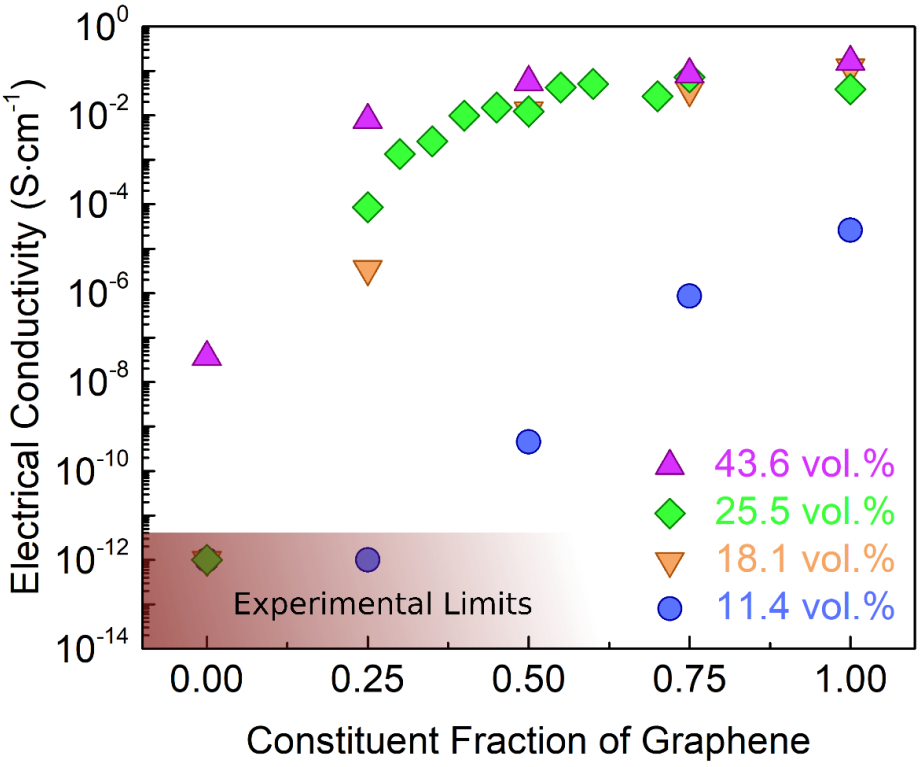

Figure 4.7: Electrical conductivities of samples at different total load fractions with varying constituency of graphene and *h*-BN. The red-shaded region shows the experimental limitations, points in which are given the lowest possible reading, not their true values. Reprinted with permission from the publication J. S. Lewis, Z. Barani, A. S. Magana, F. Kargar, and A. A. Balandin, "Thermal and electrical conductivity control in hybrid composites with graphene and boron nitride fillers" *Materials Research Express*, vol. 6, no. 8, p. 085325, May 2019. Copyright © Institute of Physics.

4.9 Discussion

An impressive composite thermal conductivity of 8.2 W/mK was achieved in this study. This value established an upper-bound of thermal conductivity in the minimally processed graphene and *h*-BN composites. Additional processing steps can increase the total thermal conductivity of the composites further. Sacrificing some composite thermal conductivity performance offers detailed control of the composite electrical conductivity, affected by both lowering the total filler level and the constituent fraction from graphene to *h*-BN. The linear relationship of composite thermal conductivity on constituent fraction alteration allows for easy prediction of expected thermal conductivity for any different combination of hybrid filler constituent fractions. Given the behaviors of thermal and electrical conductivity, it is likely true that the widest range of electrical conductivity control with the greatest possible thermal conductivity enhancement would occur in composites of ≈ 30 *vol. %* with a constituent ratio of ≈12% graphene.

Bibliography

[1] W. Cui, F. Du, J. Zhao, W. Zhang, Y. Yang, X. Xie, and Y.-W. Mai, "Improving thermal conductivity while retaining high electrical resistivity of epoxy composites by incorporating silica-coated multi-walled carbon nanotubes," *Carbon*, vol. 49, no. 2, pp. 495 – 500, 2011.

[2] C. Chen, H. Wang, Y. Xue, Z. Xue, H. Liu, X. Xie, and Y.-W. Mai, "Structure, rheological, thermal conductive and electrical insulating properties of high-performance hybrid epoxy/nanosilica/AgNWs nanocomposites," *Composites Science and Technology*, vol. 128, pp. 207 – 214, 2016.

[3] R. Sun, H. Yao, H.-B. Zhang, Y. Li, Y.-W. Mai, and Z.-Z. Yu, "Decoration of defect-free graphene nanoplatelets with alumina for thermally conductive and electrically insulating epoxy composites," *Composites Science and Technology*, vol. 137, pp. 16 – 23, 2016.

[4] S. Song, J. Wang, C. Liu, J. Wang, and Y. Zhang, "A facile route to fabricate thermally conductive and electrically insulating polymer composites with 3d interconnected graphene at an ultralow filler loading," *Nanoscale*, vol. 11, pp. 15234–15244, 2019.

[5] J. S. Lewis, T. Perrier, Z. Barani, F. Kargar, and A. A. Balandin, "Review of graphene-based thermal polymer nanocomposites: Current state of the art and future prospects," 2020. [Online]. Available: https://arxiv.org/abs/2008.10752.

[6] J. S. Lewis, Z. Barani, A. S. Magana, F. Kargar, and A. A. Balandin, "Thermal and electrical conductivity control in hybrid composites with graphene and boron nitride fillers," *Materials Research Express*, vol. 6, p. 085325, May 2019.

[7] A. Yu, P. Ramesh, X. Sun, E. Bekyarova, M. E. Itkis, and R. C. Haddon, "Enhanced thermal conductivity in a hybrid graphite nanoplatelet - carbon nanotube filler for epoxy composites," *Advanced Materials*, vol. 20, pp. 4740–4744, Dec. 2008.

[8] S. Kemaloglu, G. Ozkoc, and A. Aytac, "Properties of thermally conductive micro and nano size boron nitride reinforced silicon rubber composites," *Thermochimica Acta*, vol. 499, pp. 40–47, Feb. 2010.

[9] T.-L. Li and S. L.-C. Hsu, "Enhanced thermal conductivity of polyimide films via a hybrid of micro- and nano-sized boron nitride," *The Journal of Physical Chemistry B*, vol. 114, pp. 6825–6829, May 2010.

[10] K. Yang and M. Gu, "Enhanced thermal conductivity of epoxy nanocomposites filled with hybrid filler system of triethylenetetramine-functionalized

multi-walled carbon nanotube/silane-modified nano-sized silicon carbide," *Composites Part A: Applied Science and Manufacturing*, vol. 41, pp. 215–221, Feb. 2010.

[11] T. Zhou, X. Wang, X. Liu, and D. Xiong, "Improved thermal conductivity of epoxy composites using a hybrid multi-walled carbon nanotube/micro-SiC filler," *Carbon*, vol. 48, pp. 1171–1176, Apr. 2010.

[12] S. Y. Pak, H. M. Kim, S. Y. Kim, and J. R. Youn, "Synergistic improvement of thermal conductivity of thermoplastic composites with mixed boron nitride and multi-walled carbon nanotube fillers," *Carbon*, vol. 50, pp. 4830–4838, Nov. 2012.

[13] C.-C. Teng, C.-C. M. Ma, K.-C. Chiou, and T.-M. Lee, "Synergetic effect of thermal conductive properties of epoxy composites containing functionalized multi-walled carbon nanotubes and aluminum nitride," *Composites Part B: Engineering*, vol. 43, pp. 265–271, Mar. 2012.

[14] W. Yu, H. Xie, L. Yin, J. Zhao, L. Xia, and L. Chen, "Exceptionally high thermal conductivity of thermal grease: Synergistic effects of graphene and alumina," *International Journal of Thermal Sciences*, vol. 91, pp. 76 – 82, 2015.

[15] X. Cui, P. Ding, N. Zhuang, L. Shi, N. Song, and S. Tang, "Thermal conductive and mechanical properties of polymeric composites based on solution-exfoliated boron nitride and graphene nanosheets: A morphology-promoted synergistic effect," *ACS Applied Materials & Interfaces*, vol. 7, pp. 19068–19075, Sept. 2015.

[16] L. Shao, L. Shi, X. Li, N. Song, and P. Ding, "Synergistic effect of BN and graphene nanosheets in 3D framework on the enhancement of thermal conductive properties of polymeric composites," *Composites Science and Technology*, vol. 135, pp. 83–91, Oct. 2016.

[17] C. Liu, M. Chen, D. Zhou, D. Wu, and W. Yu, "Effect of filler shape on the thermal conductivity of thermal functional composites," *Journal of Nanomaterials*, vol. 2017, 2017.

[18] Z.-G. Wang, F. Gong, W.-C. Yu, Y.-F. Huang, L. Zhu, J. Lei, J.-Z. Xu, and Z.-M. Li, "Synergetic enhancement of thermal conductivity by constructing hybrid conductive network in the segregated polymer composites," *Composites Science and Technology*, vol. 162, pp. 7 – 13, 2018.

[19] L. Zhang, W. Zhu, Y. Huang, and S. Qi, "Synergetic effects of silver nanowires and graphene oxide on thermal conductivity of epoxy composites," *Nanomaterials*, vol. 9, p. 1264, Sept. 2019.

[20] H. Song, B. Kim, Y. Kim, Y.-S. Bae, J. Kim, and Y. Yoo, "Synergistic effects of various ceramic fillers on thermally conductive polyimide composite films and their model predictions," *Polymers*, vol. 11, p. 484, Mar. 2019.

[21] J. Jiang, S. Yang, L. Li, and S. Bai, "High thermal conductivity polylactic acid composite for 3D printing: Synergistic effect of graphene and alumina," *Polymers for Advanced Technologies*, vol. 31, no. 6, pp. 1291–1299, 2020.

[22] A. C. Ferrari, "Raman spectroscopy of graphene and graphite: Disorder, electron–phonon coupling, doping and nonadiabatic effects," *Solid State Communications*, vol. 143, pp. 47–57, July 2007.

[23] Q. Cai, D. Scullion, A. Falin, K. Watanabe, T. Taniguchi, Y. Chen, E. J. G. Santos, and L. H. Li, "Raman signature and phonon dispersion of atomically thin boron nitride," *Nanoscale*, vol. 9, pp. 3059–3067, Mar. 2017.

[24] K. E. Chike, M. L. Myrick, R. E. Lyon, and S. M. Angel, "Raman and near-infrared studies of an epoxy resin," *Appl. Spectrosc.*, vol. 47, pp. 1631–1635, Oct. 1993.

[25] R. Ullah and Y. Zheng, "Raman spectroscopy of 'Bisphenol A'," *Journal of Molecular Structure*, vol. 1108, pp. 649 – 653, 2016.

[26] J. D. Hunter, "Matplotlib: A 2D graphics environment," *Computing in Science and Engineering*, 2007.

[27] A. S. Dworkin, D. J. Sasmor, and E. R. Van Artsdalen, "The thermodynamics of boron nitride; low-temperature heat capacity and entropy; heats of combustion and formation," *The Journal of Chemical Physics*, vol. 22, pp. 837–842, May 1954.

[28] A. Butland and R. Maddison, "The specific heat of graphite: An evaluation of measurements," *Journal of Nuclear Materials*, vol. 49, no. 1, pp. 45 – 56, 1973.

[29] J. Sandler, M. Shaffer, T. Prasse, W. Bauhofer, K. Schulte, and A. Windle, "Development of a dispersion process for carbon nanotubes in an epoxy matrix and the resulting electrical properties," *Polymer*, vol. 40, pp. 5967–5971, Oct. 1999.

[30] Q. Wang, J. Dai, W. Li, Z. Wei, and J. Jiang, "The effects of CNT alignment on electrical conductivity and mechanical properties of SWNT/epoxy nanocomposites," *Composites Science and Technology*, vol. 68, pp. 1644–1648, June 2008.

[31] J. Sandler, J. Kirk, I. Kinloch, M. Shaffer, and A. Windle, "Ultra-low electrical percolation threshold in carbon-nanotube-epoxy composites," *Polymer*, vol. 44, no. 19, pp. 5893 – 5899, 2003. In Honour of Ian Ward's 75th Birthday.

[32] W. Bauhofer and J. Z. Kovacs, "A review and analysis of electrical percolation in carbon nanotube polymer composites," *Composites Science and Technology*, vol. 69, no. 10, pp. 1486 – 1498, 2009.

[33] B. Kim, S. Pfeifer, S. Park, and P. R. Bandaru, "The experimental determination of the onset of electrical and thermal conductivity percolation thresholds in carbon nanotube-polymer composites," *MRS Proceedings*, vol. 1312, pp. mrsf10–1312–ii07–06, 2011.

[34] Y. Wang, J. Yu, W. Dai, Y. Song, D. Wang, L. Zeng, and N. Jiang, "Enhanced thermal and electrical properties of epoxy composites reinforced with graphene nanoplatelets," *Polymer Composites*, vol. 36, no. 3, pp. 556–565, 2015.

[35] P. Kumar, S. Yu, F. Shahzad, S. M. Hong, Y.-H. Kim, and C. M. Koo, "Ultrahigh electrically and thermally conductive self-aligned graphene/polymer composites using large-area reduced graphene oxides," *Carbon*, vol. 101, pp. 120 – 128, 2016.

[36] K. Nose, H. Oba, and T. Yoshida, "Electric conductivity of boron nitride thin films enhanced by in situ doping of zinc," *Applied Physics Letters*, vol. 89, no. 11, p. 112124, 2006.

[37] M. R. Uddin, S. Majety, J. Li, J. Y. Lin, and H. X. Jiang, "Layer-structured hexagonal (BN)C semiconductor alloys with tunable optical and electrical properties," *Journal of Applied Physics*, vol. 115, no. 9, p. 093509, 2014.

[38] M. Shtein, R. Nadiv, M. Buzaglo, K. Kahil, and O. Regev, "Thermally conductive graphene-polymer composites: Size, percolation, and synergy effects," *Chemistry of Materials*, 2015.

[39] M. Shtein, R. Nadiv, M. Buzaglo, and O. Regev, "Graphene-based hybrid composites for efficient thermal management of electronic devices," *ACS Applied Materials & Interfaces*, vol. 7, pp. 23725–23730, Oct. 2015.

Chapter 5

Accelerated Aging TIM Reliability

5.1 Motivation

The overall TIM research field is very active, with many publications a year in different filler materials and polymer matrices [1].[1] However, the vast majority of these works never consider the performance of these materials over a realistic lifespan. Along with the associated costs, one of the primary reasons polymeric TIMs receive such preferential usage in industry is due to its lifespan performance versus, for instance, metallic and pad TIMs. It is perceived by the current authors to be a short-coming of TIM research that lifespan performance of novel TIMs is so seldom considered, especially in graphene-based TIMs, likely borne from the time commitment such a study would entail. TIMs are by their very nature applied in very difficult environments and need to maintain performance for as long

[1]This chapter, prior to section 5.4, is excerpted from J. S. Lewis, T. Perrier, Z. Barani, F. Kargar, and A. A. Balandin, "Review of graphene-based thermal polymer nanocomposites: Current state of the art and future prospects," 2020. [Online]. Available: https://arxiv.org/abs/2008.10752.

as possible, very often for the entire lifespan of the device. As the devices are turned on and off, operated in humid environments, and exposed to environmental contaminants their intrinsic material characteristics can alter as well as the morphology of the mating surface in which they are applied. Each of these alterations can lead to catastrophic failure from cracking or being pumped out of the junction as a result of the thermal expansions, contractions, and warping over the course of high and low power device state fluctuations. Perhaps the largest factor affecting the lifespan performance of TIMs in-junction is the coefficient of thermal expansion mismatches between TIM and junction. The problems that can arise can take the form of cracks, voids, or intrinsic denaturing of the TIM [2].

Though the fraction of published works that report lifespan performance to total works published in polymeric TIMs is quite low, researchers have considered this often overlooked aspect [2–5]. The literature on this matter, unfortunately, is quite inconsistent likely due to the lack of a universal standard technique for reliability and the likelihood that any developed standard technique would be unable to provide predictive performance for every individual device application. There are three classes of accelerated aging techniques that most of the experiments conducted into TIM reliability can be categorized within: Elevated temperature storage, temperature cycling, and power cycling [3].

Elevated temperature storage procedures hold a TIM typically in a junction sandwich at a uniform elevated temperature for an extended period of time. Very importantly, they may or may not employ a high humidity environment to simulate important moisture interactions. The performance of TIMs in this test varies greatly depending on the TIM and junction materials, showing both enhanced and hindered performance over the course of treatment [6–13]. Likewise, a TIM can either experience enhancement from humidity resultant from increased wetting

or experience harm the adhesion ability of the polymer matrix [7, 14].The lack of consistency in this type of procedure has numerous causes from differences in the procedure, different materials, chemical degradation, and physical form changes.

More representative of realistic TIM conditions is the temperature cycling procedure. In this technique the TIM often inside of an overall junction are cyclically placed in uniform high and low temperature environments. This procedure more closely approximates real-world TIM conditions because of the fact that TIMs operate at a wide range of temperatures. This procedure allows for multiple thermal expansions and contractions to occur, which is an important parameter in TIM pump out and cracking. The results in literature for this procedure are inconsistent as well, with most non-curing TIMs performing better [10, 13, 15]. It was observed previously that most of these instances of improvement were attributed to a reduction of the BLT and increased wetting, each mechanism not a contributing factor to cured TIMs [3].

Likely the most representative accelerated aging method is power cycling. In this technique a TIM often with its accompanying junction are cyclically heated from a localized source, resulting in a temperature gradient. This method captures thermal expansion and contraction mechanisms experienced in TIM applications the closest. Non-curing TIMs typically exhibit a reduction in performance between 20% and 60%, showing the superiority of this technique in reproducing real world behavior [3]. Because the sample is being heated from one side, it is of greater importance that one consider the rate of heating. If the heat were too high in the localized spot that the heater is located then it would increase the effective thermal expansion mismatch in either just the TIM or the entire TIM and junction sandwich.

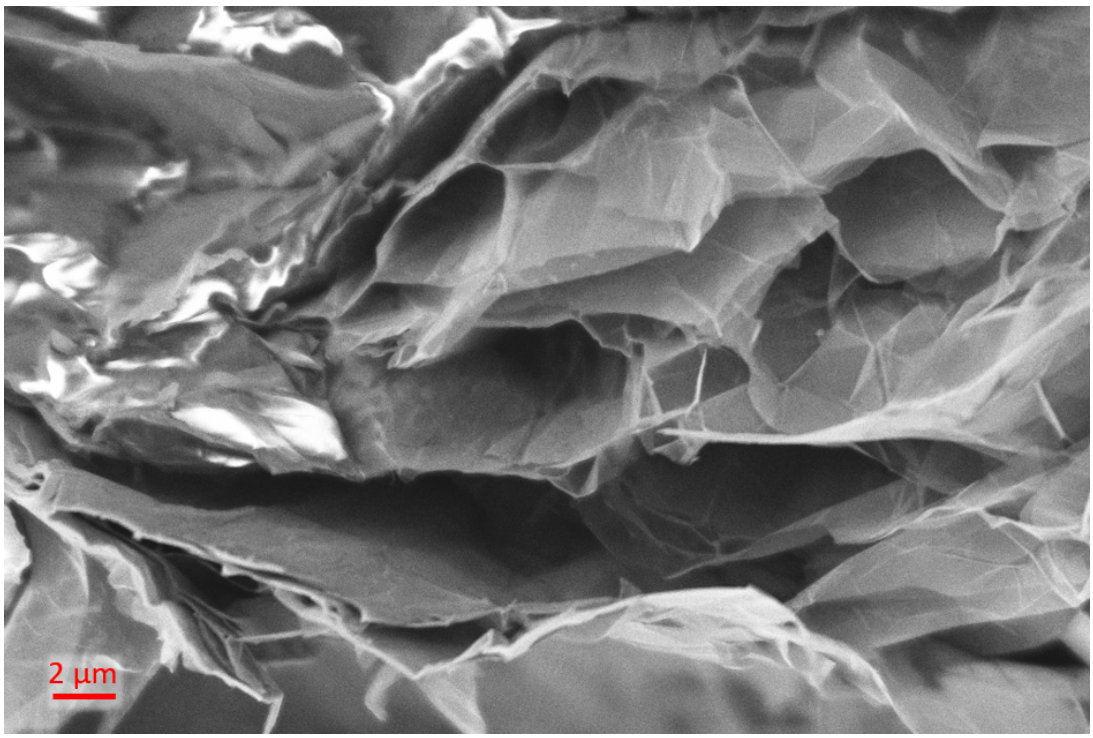

Figure 5.1: SEM of a fractured surface of 5.4 *vol. %* graphene TIM. Due to the relatively low graphene content, regions of substantial charging can be seen due to the large amount of DGEBA present in the composite. Reprinted from the publication Jacob S. Lewis, Timothy Perrier, Amirmahdi Mohammadzadeh, Fariborz Kargar, and Alexander A. Balandin. Power cycling and reliability testing of epoxy-based graphene thermal interface materials. *C — Journal of Carbon Research*, 6(2), 2020. Published under the Creative Commons license by MDPI.

5.2 Accelerated Aging Treatment Procedure

This author worked on a power-cycled reliability study on graphene-filled epoxy TIMs, without an adjoining junction [16]. A SEM micrograph of a fractured surface of a 5.4 *vol. %* is shown in Figure 5.1. The decision to not examine the TIM inside a junction sandwich stemmed from a desire to analyze the intrinsic thermal conductivity lifespan performance and to simplify the procedure for reproducibility. A custom Nichrome wire heating loop between Kapton was fabricated to be used as the localized heating element. As part of a control system, a Type-J thermocouple was fixed to the back of the sample as a feedback to inform how much

electrical power to supply the heating coil. In the Python programming language, a calibration algorithm determined the amount of power that was needed to supply to the coil to achieve the desired temperature range without any assumptions of material properties. It then ran unattended with intermittent re-calibration events. The requisite power was determined by initially "over-powering" the element, that is to say to supply a power well beyond what was expected to be necessary, to quickly heat the sample to the region of interest, then lowering the power closer to an expected power that would achieve an operating temperature of 120 °C. The sample was then held at that temperature for eight minutes to determine the equilibrium temperature at that power. The difference between the measured thermocouple temperature and that desired informed the heating coil power steps to take, with larger differences justifying larger power steps in subsequent calibration iterations. The end result of this procedure was a power supply power level that would achieve the desired temperature. Figure 5.2 shows a schematic of the power cycle treatment procedure. A small electronics fan was additionally programmatically controlled to speed the cooling phase of the power cycle. Figure 5.2c shows the plot of temperature over time provided natively by the developed software. Each data point corresponds to a single temperature measurement after thermal equilibrium, immediately after which the sample is cooled or heated. The outlier points at ≈ 140 °C are an artifact of the calibration procedure. The sample is re-calibrated in case there are any unforeseen noteworthy changes in the sample's thermal properties and safety concerns.

5.3 Results

At specified power cycle counts, samples were removed from the power cycling apparatus and were experimented with LFA to directly measure their thermal dif-

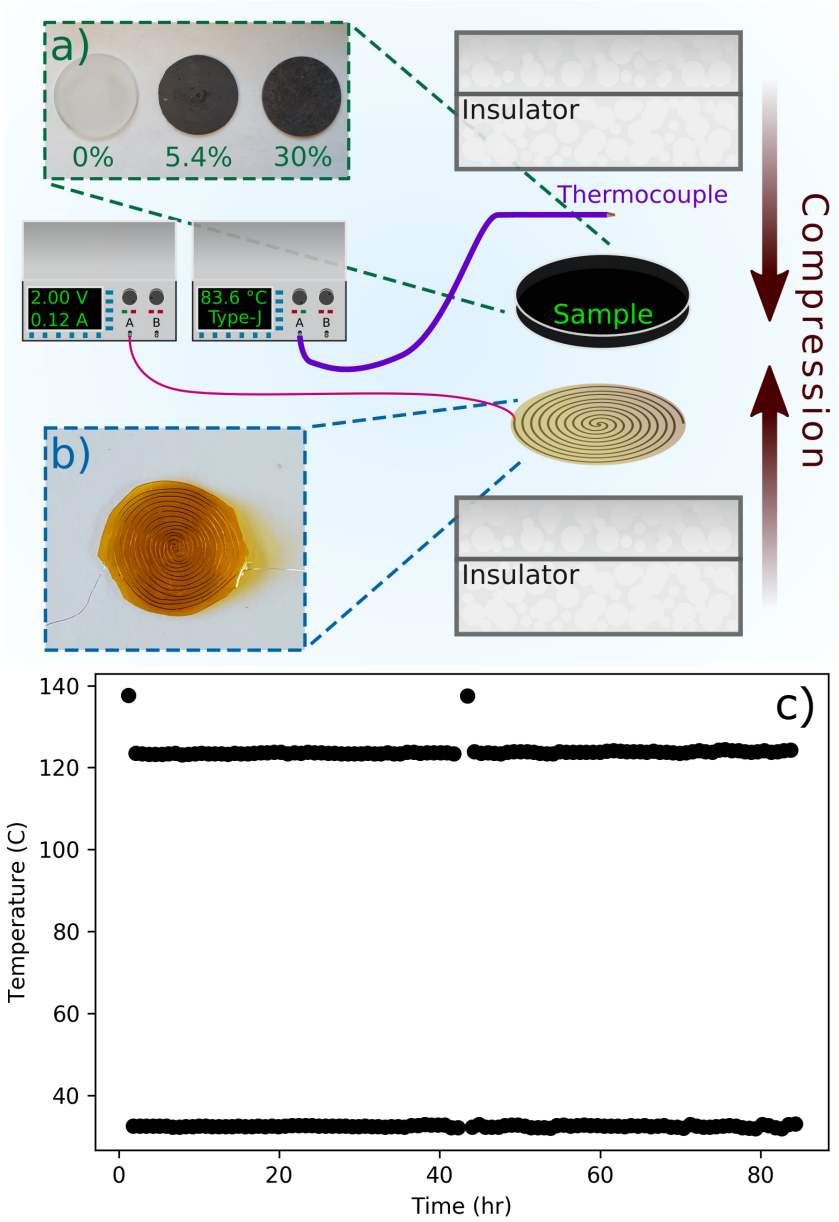

Figure 5.2: Top: schematic of the power cycling procedure. The insulators, thermocouple, sample, and heating coil were all fixed in position with light compression. a) shows an image of the samples pre-treatment and b) shows an image of an example heating coil. c) Automatically-generated plot of temperature at end of cycle step. The two levels correspond to individual measurements made at the end of the high and low temperature phases. Reprinted from the publication J. S. Lewis, T. Perrier, A. Mohammadzadeh, F. Kargar, and A. A. Balandin, "Power cycling and reliability testing of epoxy-based graphene thermal interface materials," *C — Journal of Carbon Research*, vol. 6, no. 2, 2020. Published under the Creative Commons license by MDPI.

fusivity. The Figures 5.3a, 5.3b, shows the thermal diffusivities and conductivities for pure epoxy, while 5.3c and 5.3d shows that of 5.4 *vol. %*, and 5.3e and 5.3f shows that of 30 *vol. %* samples. For all samples and at all power cycle counts, the thermal diffusivity reduced with increasing temperature. The initial RT diffusivities were 0.17, 1.25, and 4.6 mm^2/s, in order of increasing load level. After each sample's cycling treatments, their RT thermal diffusivities reached 0.17, 1.57, and 5.40 mm^2/s, in the same order, corresponding to a cycled percent enhancement of 0%, 25.6%, and 17.4%. Interestingly, a clear increase in thermal diffusivity can be seen in loaded samples over the course of cycling. Though the pure epoxy sample does show modest improvement over the course of its cycling, it can only be seen at elevated temperatures, whereas the loaded samples show a more marked improvement at lower temperatures.

Using the classic definition of thermal conductivity, $K = \alpha\rho C_p$, LFA experiments for α, Archimedes' Principle experiments for ρ, and the Kopp-Neumann rule for C_p, the TCs of the composites were determined. After power cycling, the 30 *vol. %* sample achieved a thermal conductivity of 9.3 W/mK at RT, placing the sample among the highest reported for graphene-enhanced TIMs at this loading level [17, 18]. The pure epoxy sample did experience thermal conductivity enhancement only past 100 °C, with a modest enhancement of 7.7% at that temperature, from 0.39 to ≈0.42 W/mK. However, the 5.4 *vol. %* and 30 *vol. %* samples each improved substantially over the course of cycling, constituting an improvement of 24.9% and 17.3%, respectively. The tendency for the thermal conductivity of each composite to increase with temperature is primarily dictated by the composites' specific heat capacity behavior as temperature is varied.

In each sample and at all cycle counts, the thermal conductivity at 125 °C is lower than at 100 °C. This is attributed to the fact that the glass transition tem-

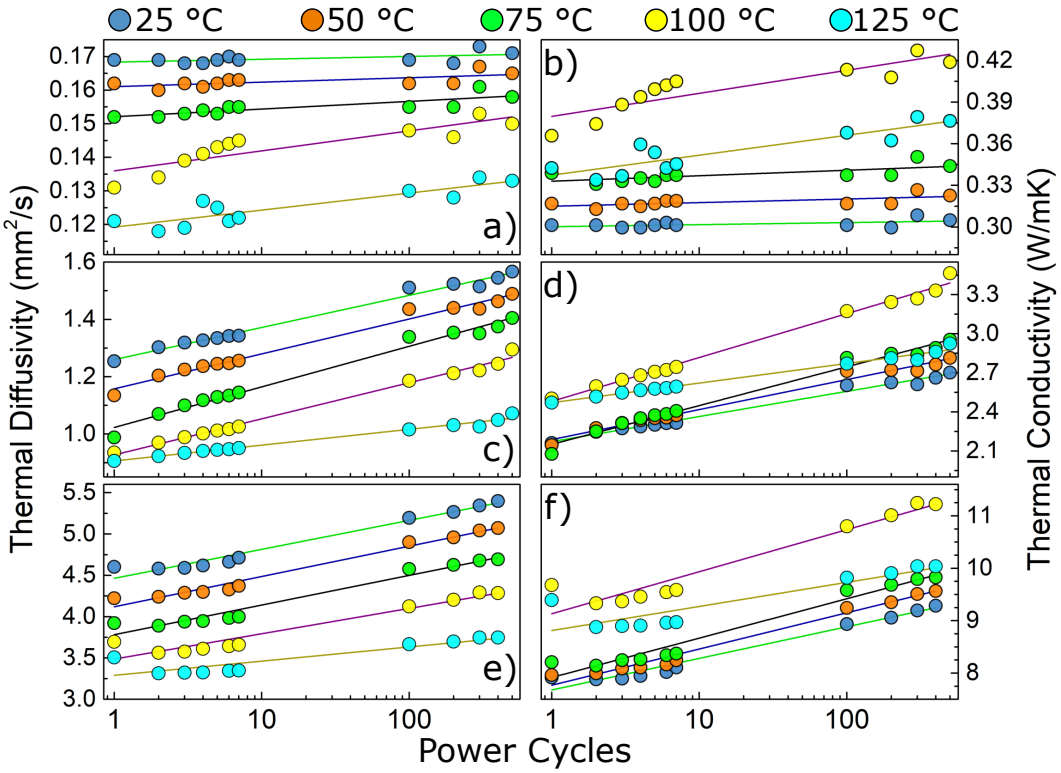

Figure 5.3: Panels on the left show thermal diffusivity and panels on the right show TC. a) Pure epoxy samples b) 5.4 *vol. %* samples c) 30 *vol. %* samples. Reprinted from the publication J. S. Lewis, T. Perrier, A. Mohammadzadeh, F. Kargar, and A. A. Balandin, "Power cycling and reliability testing of epoxy-based graphene thermal interface materials," *C — Journal of Carbon Research*, vol. 6, no. 2, 2020. Published under the Creative Commons license by MDPI.

perature of this material is at around 100 °C and thermal properties are known to degrade in polymers beyond this temperature [19–21]. It has been reported previously that polymer glass transitions can be elevated with volumetric substitution of inert materials, such as graphene [22, 23]. The appearance of a reduction in performance at 125 °C indicates that any elevation of glass transition point must be less than 25 °C in total. An increase of 30 °C was seen previously in a PMMA polymer matrix with the inclusion of functionalized graphene. This suggests that graphene does not greatly inhibit the epoxy's cross-linking.

No sample's performance decreased over the entire course of power cycling

treatments. At low temperature, the pure epoxy sample's thermal conductivity performance remained largely unchanged. Interestingly, the samples loaded with graphene, 5.4 *vol. %* and 30 *vol. %*, showed a consistent increase in performance over the course of treatment. Due to the elimination of junction alterations as a factor to influence the TIM performance, the obtained results effectively present the intrinsic lifespan behavior of graphene TIMs in what should be a more reproducible experiment due to its simplification. Should this study have been conducted in a junction it is very possible that the performance over the course of treatment would have decreased, as happened previously in a lifespan study of silver-filled epoxies [24].

Khuu *et al.* conducted accelerated lifespan research into a pure epoxy TIM that showed modest thermal resistance reductions of 8%, suggested to be caused by increasing the level of epoxy cross-linking [11]. Our study on pure epoxy is mostly in agreement with the previous results with only modest increases in thermal conductivity – which would provide for a reduction in observed thermal resistance – and negligible difference at temperatures below 100 °C. When graphene is added to the epoxy, however, a clear increase in thermal conductivity at all temperatures is observed over the course of power cycling, amounting to a percent enhancement of 24.9% in 5.4 *vol. %* and 17.3% in 30 *vol. %*. Clearly from these results, graphene must play an essential role in the intrinsic TIM performance over the course of accelerated aging.

It was reasoned that the increased cross-linking mechanism for enhanced performance proposed earlier could explain the large increase in graphene-epoxy TIMs but only modest increase in pure epoxy TIMs. If the epoxy matrix is increasing its level of cross-linking then it is swelling and simultaneously getting more and more rigid, leading to tighter mechanical coupling between graphene and epoxy

matrix [19]. This would lead to a lower Kapitza resistance between the two materials. As polymers are elevated in temperature the cross-linking rate can increase and once that reaction has taken place, it is irreversible with respect to temperature. This can explain why the over the course of power cycling the performance improves and why the improvement occurs even when tested at RT.

5.4 Simulated VLSI Device TIM Experiments

Using slight tweaks to the accelerated aging instrument designed for the accelerated aging studies, a separate functionality was derived that could determine the equilibrium temperature of the heating element of Figure 5.2b when attached to a heat sink with different TIMs. Better performing TIMs will result in lower operating temperature of the heating coil, that acts as a more finely controllable stand-in for a VLSI chip, for increasing rates of heat dissipation. The increased thermal coupling that a superior TIM would provide between the coil and heat sink would result in higher temperatures of the heat sink, leading to a faster rate of heat dissipation into the environment, finally resulting in a lower coil temperature. Figure 5.4 shows the stock Intel Corporation heat sink used in the study, with the attached fan removed. This heat sink was chosen due to its ubiquity, appropriate size, and thermal resistance.

The samples were fabricated by placing the to-be-cured TIM onto the coil, the insertion of shims between heat sink and coil with a thickness of $\approx$0.45 mm, then clamping the the stack together overnight until cured. Prior to experiment, the electrical leads to the coil were connected to the programmable power supply and the thermocouple was placed on the back of the heating coil with a thermally insulating bulk polytetrafluoroethylene material on the bottom. To ensure contact of all elements, the stack was lightly clamped together. It should be noted that

Figure 5.4: Picture of an Intel Corporation heat sink used in these experiments. Multiple identical models were purchased, cooling fans removed, visibly inspected for defects, particularly at the mating surface, then attached to a coil with a TIM.

though there was a few millimeters of rubber material to thermally insulate the C-clamp from the heat sink, during the experiment the clamp was observed to be at a slightly elevated temperature. As a result, the clamp must be considered somewhat a part of the heat sink assembly.

The controlling software issued a command to the power supply to pass a current through the heating coil, Joule heating it in much the same manner as before. The thermocouple was continuously read and logged. The temperature was considered stable when the most recent temperature recording was within 2%, 1%, and 0.4% above or below the reading 30, 20, and 5 previously, respectively. When this condition was met, the temperature was noted and the power supply current was increased again. Figure 5.5a shows raw temperature readings over time with visible derivative discontinuities resulting from a determined stable temperature and the subsequent ramping of power supply current. In the inset figure, a mag-

nified region is presented with a 2nd degree polynomial fit extrapolated forward in time showing that the algorithm's definition of a stable temperature negligibly underestimated the true equilibrium temperature but saved substantial time during the course of the experiment. The controlling software was designed to increment to higher powers indefinitely, realistically confined by the capacity of the equipment, and was shut off when a reading of 140 °C was recorded for both safety and due to the fact that is beyond the temperature range of interest.

Figure 5.3b shows the determined stable temperatures for pure epoxy, 5 *vol. %*, and 10 *vol. %*. Substantial improvement in the operating temperature was observed for epoxy TIM that was loaded with graphene. At a heat dissipation of 13 Watts, the operating temperature of the heating coil with pure epoxy used as TIM to the heat sink was 118 °C while the clear trend established from data collected with the 10 *wt. %* graphene-loaded sample show the coil would operate at $\approx$ 95 °C. It is important to note that at the baseline measurement with the coil off, and thus the data points at 0 Watts, the 10 *wt. %* graphene TIM coil temperature is higher, which shows a higher RT during this experiment. Having a higher relative RT would serve to vertically translate this data set up relative to the others, hiding some of the performance improvement. The slight reduction of slope at higher rates of heat dissipation is an artifact of the controlling software determining equilibrium through relative comparison to prior temperature measurements. The very minor deviation from a linear behavior verifies that the equilibrium-finding algorithm is fair, though not perfect, for the temperature ranges considered. Further work into this project will in addition employ an absolute comparison to previous recordings to address this.

An operating temperature of 100 °C at 14 Watts is not acceptable for the VLSI industry that produce graphics processing products that can dissipate over

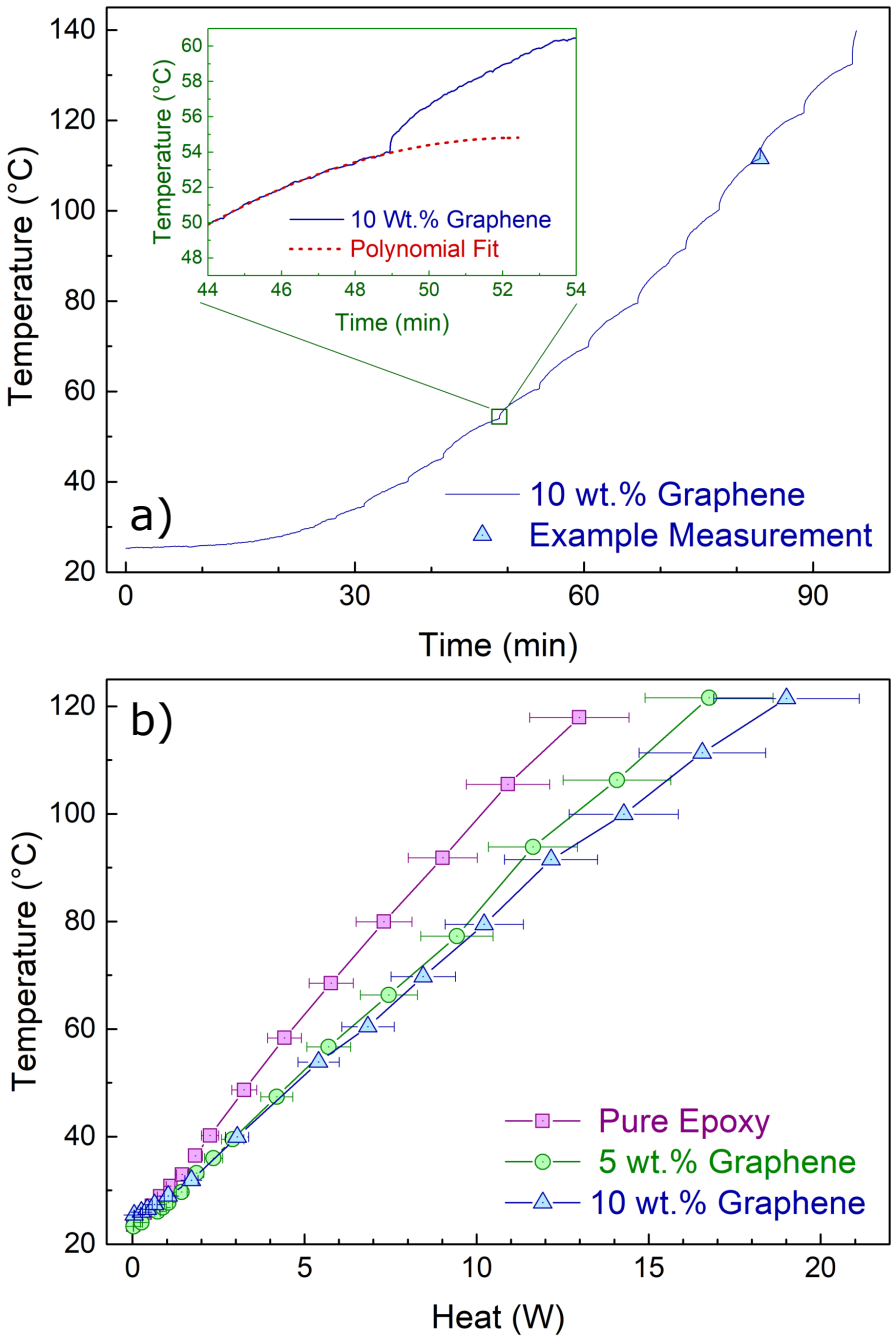

Figure 5.5: a) Temperature measured from a thermocouple in contact with the heating coil. Drastic jumps in temeprature are a result of a switch to higher coil power. Inset figure shows a magnified region in which a 2nd degree polynomial is fit and extrapolated forward in time. b) Stable temperature readings at different rates of heat dissipation. Lower temperature readings for an individual amount of heat corresponds to a superior TIM.

200 Watts. In a more direct comparison, the heat sink used is designed for central processing unit devices that dissipate around 50 Watts. The two major differences between these experiments and the real world usage of these heat sinks are that the active cooling fans were intentionally removed to reduce experimental complexity and the BLT of the TIM was kept far thicker than in the real world so that any uncertainty in thickness will comprise a very small percentage of the total value, thus preserving consistency of results.

5.5 Discussion

The designed instrument for accelerated aging and operating temperature analysis is both powerful and versatile. Using it, the unexpected enhancement in graphene and DGEBA composite intrinsic thermal conductivity was demonstrated in up to 500 power cycling treatments. These results are valuable to industry due to the numerous, punishing cycles that TIMs undergo in their lifespan. With little controlling software tweaking, a comparison of operating temperatures at different device heating was conducted. This provides very clear translation between the thermal conductivity of these materials and the operating temperatures of devices in which they are intended to serve.

Bibliography

[1] J. S. Lewis, T. Perrier, Z. Barani, F. Kargar, and A. A. Balandin, "Review of graphene-based thermal polymer nanocomposites: Current state of the art and future prospects," 2020. [Online]. Available: https://arxiv.org/abs/2008.10752.

[2] A. Gupta, Yongmei Liu, N. Zamora, and T. Paddock, "Thermal imaging for detecting thermal interface issues in assembly and reliability stressing," in *Thermal and Thermomechanical Proceedings 10th Intersociety Conference on Phenomena in Electronics Systems, 2006. ITHERM 2006.*, pp. 4 pp.–945, 2006.

[3] J. Due and A. J. Robinson, "Reliability of thermal interface materials: A review," *Applied Thermal Engineering*, vol. 50, no. 1, pp. 455 – 463, 2013.

[4] A. Li, C. Zhang, and Y.-F. Zhang, "RGO/TPU composite with a segregated structure as thermal interface material," *Composites Part A: Applied Science and Manufacturing*, vol. 101, pp. 108 – 114, 2017.

[5] M. Li, J. Liu, S. Pan, J. Zhang, Y. Liu, J. Liu, and H. Lu, "Highly oriented graphite aerogel fabricated by confined liquid-phase expansion for anisotropically thermally conductive epoxy composites," *ACS Applied Materials & Interfaces*, vol. 12, pp. 27476–27484, May 2020.

[6] X. Luo, Y. Xu, and D. D. L. Chung, "Thermal stability of thermal interface pastes, evaluated by thermal contact conductance measurement," *Journal of Electronic Packaging*, vol. 123, pp. 309–311, June 2000.

[7] S. L. B. Dal, "Degradation mechanisms of siloxane-based thermal interface materials under reliability stress conditions," in *2004 IEEE International Reliability Physics Symposium. Proceedings*, pp. 537–542, 2004.

[8] C. Ramaswamy, S. Shinde, F. Pompeo, W. Sablinski, and S. Bradley, "Phase change materials as a viable thermal interface material for high-power electronic applications," in *The Ninth Intersociety Conference on Thermal and Thermomechanical Phenomena In Electronic Systems (IEEE Cat. No.04CH37543)*, vol. 2, pp. 687–691, 2004.

[9] L. Bharatham, Wong Shaw Fong, J. Torresola, and Chen Chee Koang, "Qualification of phase change thermal interface material for wave solder heat sink on FCBGA package," in *2005 7th Electronic Packaging Technology Conference*, vol. 2, pp. 6 pp.–, 2005.

[10] A. Gowda, D. Esler, S. N. Paisner, S. Tonapi, K. Nagarkar, and K. Srihari, "Reliability testing of silicone-based thermal greases [IC cooling applications]," in *Semiconductor Thermal Measurement and Management IEEE Twenty First Annual IEEE Symposium, 2005.*, pp. 64–71, 2005.

[11] V. Khuu, M. Osterman, A. Bar-Cohen, and M. Pecht, "Effects of temperature cycling and elevated temperature/humidity on the thermal performance of thermal interface materials," *IEEE Transactions on Device and Materials Reliability*, vol. 9, no. 3, pp. 379–391, 2009.

[12] C. Chen, C. Ni, H. Pan, C. Chang, and D. Liu, "Practical evaluation for long-term stability of thermal interface material," *Experimental Techniques*, vol. 33, no. 1, pp. 28–32, 2009.

[13] S. N. Paisner, M. Touzelbaev, G. Refai-Ahmed, and Y. Yang, "New developments for a no-pump-out high-performance thermal grease," in *2010 12th IEEE Intersociety Conference on Thermal and Thermomechanical Phenomena in Electronic Systems*, pp. 1–4, 2010.

[14] N. Goel, T. K. Anoop, A. Bhattacharya, J. A. Cervantes, R. K. Mongia, S. V. Machiroutu, H. Lin, Y. Huang, K. Fan, B. Denq, C. Liu, C. Lin, C. Tien, and J. Pan, "Technical review of characterization methods for thermal interface materials (TIM)," in *2008 11th Intersociety Conference on Thermal and Thermomechanical Phenomena in Electronic Systems*, pp. 248–258, 2008.

[15] A. Gowda, A. Zhong, D. Esler, J. David, T. Sandeep, K. Srihari, and F. Schattenmann, "Design of a high reliability and low thermal resistance interface material for microelectronics," in *Proceedings of the 5th Electronics Packaging Technology Conference (EPTC 2003)*, pp. 557–562, 2003.

[16] J. S. Lewis, T. Perrier, A. Mohammadzadeh, F. Kargar, and A. A. Balandin, "Power cycling and reliability testing of epoxy-based graphene thermal interface materials," *C — Journal of Carbon Research*, vol. 6, no. 2, 2020.

[17] F. Kargar, Z. Barani, R. Salgado, B. Debnath, J. S. Lewis, E. Aytan, R. K. Lake, and A. A. Balandin, "Thermal percolation threshold and thermal properties of composites with high loading of graphene and boron nitride fillers," *ACS Applied Materials & Interfaces*, vol. 10, pp. 37555–37565, Oct. 2018.

[18] F. Kargar, Z. Barani, M. Balinskiy, A. S. Magana, J. S. Lewis, and A. A. Balandin, "Dual-functional graphene composites for electromagnetic shielding and thermal management," *Advanced Electronic Materials*, vol. 5, no. 1, p. 1800558, 2019.

[19] R. P. Kreahling and D. E. Kline, "Thermal conductivity, specific heat, and dynamic mechanical behavior of diglycidyl ether of bisphenol a cured with m-phenylenediamine," *Journal of Applied Polymer Science*, vol. 13, no. 11, pp. 2411–2425, 1969.

[20] W. Park, Y. Guo, X. Li, J. Hu, L. Liu, X. Ruan, and Y. P. Chen, "High-performance thermal interface material based on few-layer graphene composite," *Journal of Physical Chemistry C*, vol. 119, pp. 26753–26759, Nov. 2015.

[21] W. dos Santos, J. de Sousa, and R. Gregorio, "Thermal conductivity behaviour of polymers around glass transition and crystalline melting temperatures," *Polymer Testing*, vol. 32, no. 5, pp. 987 – 994, 2013.

[22] A. Yasmin and I. M. Daniel, "Mechanical and thermal properties of graphite platelet/epoxy composites," *Polymer*, vol. 45, no. 24, pp. 8211 – 8219, 2004.

[23] T. Ramanathan, A. A. Abdala, S. Stankovich, D. A. Dikin, M. Herrera-Alonso, R. D. Piner, D. H. Adamson, H. C. Schniepp, X. Chen, R. S. Ruoff, S. T. Nguyen, I. A. Aksay, R. K. Prud'Homme, and L. C. Brinson, "Functionalized graphene sheets for polymer nanocomposites," *Nature Nanotechnology*, vol. 3, no. 6, pp. 327–331, 2008.

[24] A. Bjorneklett, T. Tuhus, L. Halbo, and H. Kristiansen, "Thermal resistance, thermomechanical stress and thermal cycling endurance of silicon chips bonded with adhesives," in *[1993 Proceedings] Ninth Annual IEEE Semiconductor Thermal Measurement and Management Symposium*, pp. 136–143, 1993.

Chapter 6

Conclusions

The technological progress of numerous fields including semiconductor, aerospace, and sustainable energy industries experience problems associated with the growing inadequacy of standard thermal dissipation solutions. In these fields, generated heat is typically dissipated through a heat sink or simply spread to a wide area, which may be dissipated to the environment through convection and radiation. In the case of heat sink thermal dissipation strategies, surface imperfections at the physical junction require the use of an interstitial material to take the place of the thermally resistant stagnant air. The materials that fit this role the best, primarily determined by its malleability and low cost, are polymers with mixtures of microscopic high thermal conductivity filers inside. Because the solid materials in use at each end of the physical junction have a thermal conductivity ranging between 10 and 400 W/mK, there is a strong motivation to increase the thermal conductivity of polymer-based thermal interface materials from relatively low thermal conductivity of the pristine polymers, which is typically around 0.25 W/mK.

As a result of the exceptionally high intrinsic thermal conductivity of single- and few-layer graphene, advantageous geometry, and flexibility, substantial inter-

est exists in the material as fillers for advanced thermal interface materials. To date, graphene-filled polymers have achieved the highest overall thermal conductivity in comparable randomly filled polymer composites. However, graphene also has a high electrical conductivity, resulting composites loaded past the electrical percolation threshold exhibit strong composite electrical conductivity. This can be problematic because composites can be used in direct contact with or migrate to active circuit elements leading to damage to the device. Because the thermal conductivity of graphene composites is superior to others, it is of interest to precisely determine graphene filler loading fraction that one could use in a composite before reaching the electrical percolation threshold. This dissertation research included study of composites with a hybridized filler approach of both graphene and *h*-BN. It was found that careful selection of both the total filler level and the constituent fraction of graphene to h-BN allowed for the control of composite electrical conductivity spanning *at least* eleven orders of magnitude. Additionally, the role of filler shape to the widely reported synergistic thermal conductivity enhancement was further verified through the absence of observed synergy with the intentional use of identical filler shapes. An impressive composite thermal conductivity of 8.2 W/mK was achieved at a pure graphene filler loading level of 43.6 *vol. %*.

This dissertation research also considered the lifespan thermal performance of graphene composites, inspired by the extremely difficult environment that TIMs are subjected to. Over the course of a TIM application, the material can experience hundreds of cycles of powering on and off, each time being subjected to thermal and mechanical stresses borne from differing coefficients of thermal expansion between itself and the materials it is in contact with. The available reports on thermal cycling of TIMs with various fillers reveal substantial discrepancy. The inconsistency in published literature on this matter is primarily a result of dissimilar

accelerated aging techniques and different materials used, both in regards to the TIM itself and materials used as a junction. This dissertation covers the lifespan thermal performance of graphene composites with an intentionally simplified testing apparatus with the goal of establishing a process with greater reproducibility. It was found that the thermal conductivity of the composite increases, rather than decreases, during the course of its simulated lifespan using a custom instrument. A thermal conductivity enhancement of 17.3%, resulting in a final absolute value of 9.3 W/mK, was achieved in the 30 *vol. %* sample over the course of 400 power cycles. This increase in the intrinsic performance of the TIM was attributed to increased epoxy cross-linking density over the course of treatment.

Using the same custom instrument as in the accelerated aging study and minor alterations to its control software, equilibrium device operating temperatures for a given level of power output was studied. This work served as a practical translation between the material thermal properties and device operating temperatures. Binding a heating coil to a heat sink and measuring the temperature of the heating coil with a thermocouple served as a physical simulation of a VLSI device. Using a stock VLSI heat sink in a passive cooling configuration, relatively thick TIM application, and a heat dissipation of 13 Watts, the heating coil had an operating temperature of 118 °C using pure DGEBA and 95° C using as little as 10 wt. % graphene fillers. The results obtained in this dissertation research are important for the continued advancement of the TIM field and dependent industries.